Combined assessment of dissolution and epithelial permeability of solid oral dosage forms

Dissertation zur Erlangung des Grades
des Doktors der Naturwissenschaften
der Naturwissenschaftlich-Technischen Fakultäten
der Universität des Saarlandes

von
Stephan A. Motz

Saarbrücken
2007

Tag des Kolloquiums: 05.02.2007

Dekan: Prof. Dr. Kaspar Hegetschweiler

Mitglieder des Prüfungsausschusses:

Erstgutachter: Prof. Dr. Claus-Michael Lehr
Zweitgutachter: Prof. Dr. Hans H. Maurer
akademischer Mitarbeiter: Dr. Ulrich Schäfer

Die vorliegende Dissertation entstand auf Anregung und unter Anleitung von

Herrn Prof. Dr. Claus-Michael Lehr

am Institut für Biopharmazie und Pharmazeutische Technologie

and der

Universität des Saarlandes

Abstract:

COMBINED ASSESSMENT OF DISSOLUTION AND INTESTINAL PERMEABILITY OF SOLID ORAL DOSAGE FORMS

Assessing dissolution and Caco-2 permeability to estimate the *in vivo* performance of solid oral dosage forms is done since decades. However, permeability assays applying Caco-2 monolayers exhibit the drawback that, in contrast to dissolution testing, a complete dosage form is not eligible for conventional epithelial permeability assays. Hence, an apparatus was developed providing the possibility to assess permeability of solid oral dosage forms based on combination of a Caco-2 monolayer and a flow through dissolution cell. Combination of the dissolution and permeation module was performed using a depressurized stream splitter. Experiments with varying propranolol HCl tablets yielded plausible and conclusive results. Furthermore, data of these experiments were used to perform computational modelling of the concentration time trends within the apparatus. In order to increase throughput and to decrease manpower, the apparatus was automated by means of sequential injection technique (SIA) permitting online sampling and drug quantification. Finally, experiments with furosemide, a BCS class 4 compound, were carried out.

In summary, a novel tool for has been developed, which is able to monitor influences of excipients concomitantly on both dissolution and permeability through the small intestinal cell line Caco-2.

Kurzzusammenfassung:

KOMBINIERTE BESTIMMUNG VON AUFLÖSUNG UND EPITHELIALER PERMEABILITÄT VON FESTEN ORALEN ARZNEIFORMEN

Dissolutions- und Permeabilitäts- Tests werden seit längerem zur Abschätzung der Bioverfügbarkeit nach oraler Administration verwendet. Traditionelle, auf Caco-2 Zellmonolayern basierende Permeabilitätstest haben jedoch den Nachteil, daß man - im Gegensatz zu Dissolutionstests - nicht die komplette Arzneiform auf ihre epitheliale Permeabilität testen kann. Ausgehend davon wurde eine Testapparatur zur Permeabilitätsbestimmung fester oraler Arzneiformen entwickelt. Die Kombination Permeation- Dissolution wurde hierbei durch eine Verbindung der Module mit Hilfe eines druckfreien Stromteilers bewerkstelligt. Experimente mit verschiedenen Propranolol HCl Tabletten ergaben plausible und schlüssige Ergebnisse. Des weiteren wurden mit Hilfe der Daten aus diesen Experimenten die Konzentrations-Zeit Profile innerhalb der Testapparatur mittels eines computerbasierten Modells zu simuliert. Im Rahmen der Weiterentwicklung wurde die komplette Testapparatur automatisiert, so daß sowohl die Probennahme als auch die Arzneistoffquantifizierung programmiert ablaufen. Daneben wurden auch Experimente mit Lasix® Tabletten (40 mg Furosemid) durchgeführt.

Zusammenfassend kann die Testapparatur als neuartiges Werkzeug gesehen werden, welches die Sichtbarmachung der Einflüsse von Hilfsstoffen sowohl auf die Dissolution als auch auf die intestinale Permeation ermöglicht.

Acknowledgements

First and foremost, I would like to thank Professor Dr. Claus-Michael Lehr and Dr. Ulrich Schäfer for supervising this dissertational work and for their professional advice and encouragement.

Furthermore, I am greatly indebted to sanofi-aventis for the generous funding; especially, I would like to express my gratitude to Dr. Thomas Eichinger and Dr. Stefan Balbach and for initiating the project and for their supervising.

Additionally, I would like to express my gratitude to the technical staff of the department for their help in seeding and feeding hungry Caco-2 cells: Heike Stumpf, Petra König, Susanne Kossek, Leon Mujis, and Katja Klein.

During all steps of development, Norbert Ochs has been continuously available for technical support and precious help in constructing many parts of the apparatus.

Prof. Dr. Jennifer Dressman is thanked for helpful discussion and comments regarding the second chapter.

Jana Klimundová is thanked for teaching me the principles of sequential injection technique. It was a pleasure to work together with her. Furthermore, Prof. Petr Solich is thanked for hosting me in his lab in Hradec Kralové, Czech Republic. Also, both are thanked for their comments and discussion.

Moreover, Dr. Dirk Neumann is thanked for helpful discussion and comments, especially for his help in modeling the prototype.

Prof Dr. Chr. Weber and his team at the Department of computer aided design and manufacturing (CAD/CAM) are thanked for their support in constructing the flow through permeation cell.

For the really good working atmosphere, for the collegiality, and for the good collaboration - which is not a matter of course - my special gratitude goes to Andi, Barbara, Christiane, Eva, Frank, Javiana, Katharina, Mark, Michael, Nicole, Noah, Ping, Ruy, Sebastian, Steffi and Uli. Apart from practical support, I would like to thank them for encouragement, motivation and especially for listening.

Moreover, I would like to thank my parents and siblings for believing in me and supporting whatever I do.

Finally, I would like to thank Simone for her inestimable and precious support, for listening and for believing in me. Thank you!

Table of content

1 Introduction

Chapter 1 is forming a rationale for developing an apparatus for epithelial permeability assessment of solid oral dosage forms. Furthermore, it comprises a review of current literature of this particular area of research and reflects the state of the art. In view of the needs, the aim of the study is defined and parameters of the apparatus to be developed have been defined.

Parts of this section have been published in

Motz SA, Bur M, Schäfer UF, Lehr CM. Instrumented approaches to assess epithelia permeability of drugs from pharmaceutical formulations, Springer, Ed. Kim KJ, Ehrhardt C, 2007, Book title: “Preclinical Biopharmaceutics – In situ, *in vitro*, and in silico tools for drug absorption studies”.[1].

For most drugs, oral administration of pure active pharmaceutical ingredient (API) to patients is not feasible mainly due to low dose/mass and low compliance. To circumvent these issues, drugs are formulated in order to provide good compliance and better technical solutions for administration. Additionally, for various routes of administration, the dosage form may play a key role determining *in vivo* bioavailability. However, only few is known about interaction of cell culture based *in vitro* methods with formulated drugs.

1.1 Rationale for connecting permeation and dissolution measurement

Dissolution and subsequent permeation through intestinal epithelia are processes in oral drug absorption whereby each of those may be rate limiting. Unnumbered parameters affect both processes, such as ample wetting, appropriate swelling and disintegration of the dosage form, dissolution of the active compound within intestinal transit time depending on the surrounding microclimate pH, osmolarity, and surface tension. While sufficient disintegration and dissolution is a prerequisite for oral absorption, critical parameters can be seen in the pH in the GI-lumen and the cell covering, more acidic mucus, apical concentration and affinity to active cellular uptake or efflux systems, sink condition in the trans-mucosal receptor fluid, concomitant administration of meal and disposability of active excipients, just to mention the most important. Summarized as L and A of the LADME model, these both processes are the only being easily accessible for manipulation by researchers.

For dissolution testing, many successful efforts have been made to imitate more and more closely the physiological surrounding in the GI lumen. Variables such as temperature, osmolarity, pH, surface tension, presence of bile salts were altered and two in vitro dissolution buffers coming most closely to *in vivo* conditions were reported as FaSSIF (fasted state simulated intestinal fluid) and FeSSIF (fed state simulated intestinal fluid) by the group of Dressman et al. [2]. Dissolution testing is routinely carried out using complete dosage forms, except for assessment of intrinsic dissolution testing at very early stages in drug development. In contrast to dissolution testing, permeability testing does not allow to address the role of formulation factors and excipients. Instead, permeability is considered as an intrinsic property of a given

compound. This may be justified by some issues arising from i) the non congruency between a normal dose of a solid dosage form and permeation area of the apical volume respectively of a Caco-2 monolayers in Transwell® system potentially resulting in enormous osmotic pressure differences between apical and basolateral compartment, ii) sheer impossibility to insert a complete dosage form into a standard Transwell® device, iii) non appropriate dissolution features of the apical compartment (volume, pH, hydrodynamics, etc.). In conclusion, researchers tend to determine two related and connected things separately. However, when dissolution and permeation assays will be connected, experimental and technical efforts therefore will definitely increase. So, one might ask for the benefit of the concomitant determination of dissolution and permeation. Three main fields of interest can be seen as follows:

1.1.1 Improved in *vivo - in vitro correlation* for bioavailability screening of new API's

1.1.2 Improved formulation screening of innovative formulation approaches

1.1.3 Investigation of potential food effects on drug absorption

1.1.1 Improved in vivo - in vitro correlation for bioavailability screening of new API's

As described by Artursson at al. [3], *in vitro* permeability of drugs through Caco-2 cell monolayers are correlating well with the fraction absorbed in humans. However, pure permeation experiments disregard possible solubility issues of a compound potentially limiting absorption from the gut. By combining dissolution and permeation assay, a deeper insight into the processes happening *in vivo* in the intestine may be given, especially if one considers the clinical dose to be dissolved in the limited intestinal volumes. Furthermore, dissolution testing serves as a validated tool for generating *in vivo – in vitro* correlations (IVIVC) mainly for BCS class II and IV. However, for BCS class III (and IV), a correlation of the dissolution signal is not necessarily given since dissolution may not be rate limiting and other parameters, which are not visible in a dissolution signal, but in the permeation process may be relevant for an IVIVC.

1.1.2 Improved formulation screening of innovative formulation approaches

Considering the LADME model, liberation and absorption of drugs pose vital parameters for bioavailability after oral administration and are the only factors accessible for manipulation by designing adequate dosage forms. Evidently, detection of formulation parameters affecting dissolution processes are easier accessible than effects of the formulation on absorption processes. Dissolution studies have been shown to be a good predictor for *in vivo* performance of solid dosage forms, e.g. [2, 4, 5]. under the assumption that the more compound gets into solution within an acceptable time in a more or less physiological surrounding, the higher the bioavailability or the better the *in vivo* performance. This central paradigm of predictive dissolution testing relies on the assumption that intestinal permeation is not rate limiting and that excipients administered along with the drug do not interfere with or alter intestinal epithelia. In contrast, during the past decades, more and more drugs have been recognized as absorbed by active cellular uptake or hindered from absorption by active cellular efflux systems. Simultaneously, more and more excipients have been detected to interact with intestinal epithelia and have been discussed as intestinal absorption enhancers. The mini-review of Aungst [6] and the review of Swenson et al. [7] may serve as an overview over that particular topic. Terao et al. [8], for example, reported to increase the AUC of furosemide in rats by decreasing intra luminal pH at distal portions of the GI by means of Eudragit L100-55, a proton releasing polymers. For the influx transporter PEPT1, a proton gradient coupled oligo-peptide transporter, it is reported that lower luminal pH values increase the driving force for the uptake due to a secondary uptake coupled with a proton gradient. Accordingly, Nozawa et al. [9] found that by decreasing the pH in the lumen of rat small intestinal by means of a proton releasing polymers, the bioavailability of PEPT1 substrates such as cefadroxil and cefixime raises. Though the authors use remarkably amount of excipient (500 mg excipient per kg rat weight), a proof of principle that excipients can affect active uptake of drugs *in vivo* was performed. Beside excipients improving uptake, other excipients are existing improving oral absorption by means of interaction with tight junctions of intestinal epithelia. Lindmark et al. [10] reported to possibly enhance oral absorption by addition of medium chain fatty acids in Caco-2 cells. Medium chain fatty acids interact

with tight junction proteins such as ZO-1 and occludin and increase *in vitro* permeability of the hydrophilic marker compound fluorescein-sodium. Sakai et al. [11] supported this theory by means of confocal laser scanning microscopy (CLSM) and by increasing permeability of hydrophilic, passively permeating compounds for sodium caprate and additionally for sodium deoxycholate. Borchard et al. [12] reported that mucoadhesive polymers such as chitosan-glutamate and carbomer widen tight junction indicated by CLSM. However, only co-administration of carbomer together with chitosan-glutamate leads to significant increase of permeability. Ranaldi et al. [13] found that chitosan and other polycations decrease TEER reversibly and increase permeability for inulin through Caco-2 monolayers (for a review on that particular topic see [14]).

On the other hand, several publications are suggesting that commonly used surface active excipients affect cellular efflux systems, namely P-glycoprotein or other efflux pumps, e.g. [6, 15-21]. Many authors report increased drug fluxes from apical to basolateral and decreased fluxes in the adverse direction in presence of polyethoxylated surface active excipients such as TWEEN 80, vitamin E TPGS, pluronic block polymers, and Cremophor EL; whilst the mechanism of action is still under discussion. The application of these excipients in oral solid dosage forms affects the absorption process from the GI lumen in two ways. First, they can enhance dissolution rate by decreasing surface tension and improving wetting and by increasing solubility by means of micellar entrapment. Second, they can increase permeability through intestinal epithelia by inhibiting intestinal P-glycoprotein mediated efflux. However, these excipients can also decrease permeability since micellar entrapped active compound may no longer be thermo-dynamical active and lower fluxes may result. However, the findings reported in literature remain contradictory. Although statistical significant results in permeability assays have been found when adding such excipients in solution to the transport media, *in vivo* relevance remains questionable. Brouwers et al. [22] reported for amprenavir, being marketed as a dosage form (Agenerase®) with the P-glycoprotein inferring excipient vitamin E TPGS, a much more complicated behaviour than generally anticipated. The authors showed that increasing concentration of vitamin E TPGS leads to higher dissolution rate and solubility of amprenavir *in vivo*. The *in vitro* permeation experiment show initially increasing and subsequently decreasing apparent permeabilities for increasing vitamin E TPGS concentrations, which can be due to

micellar entrapment above the critical micellar concentration (CMC). However, at *in vivo* relevant concentration of vitamin E TPGS and amprenivir, P-glycoprotein inhibiting action of vitamin E TPGS might be made irrelevant by enormous luminal concentration of amprenavir as a result of the surface tension lowering action of vitamin TPGS. Ramsay-Olocco [23] published data on a clinical evaluation of a P-glycoprotein substrate formulated in soft capsules along with vitamin E TPGS. Although an increase of flux in presence of vitamin E TGPS in absorptive direction is found *in vitro*, no significant difference is detectable in clinical studies performed in micro pigs and humans. In contrast, Bogman et al. [24] reported for talinolol perfused intraduodenally along with vitamin E TPGS a statistically increased AUC compared to talinolol administered alone or with Poloxamer 188, a non P-glycoprotein interfering surfactant. To conclude, for formulation development, it is crucial to know the actual luminal concentration of the API and the active excipients. Beside the increase of bioavailability, researchers expect by means of these excipients to lower intersubject variability of bioavailability normally associated with low permeability and low solubility compounds. Although being potent absorption enhancer *in vivo*, the in vivo relevance of these findings remains unclear. From clinical point of view, the relative contribution of intestinal P-glycoprotein to overall drug absorption has been questioned, unless a small amount of API is administrated or dissolution and permeation rate is rather low [25]. Additionally it was doubted whether cell culture derived *in vitro* data can be directly scaled up to humans [25]. Obviously, the *in vivo* relevance of P-glycoprotein is not depending exclusively on the affinity of the API to cellular efflux systems but also on the actual luminal concentration of the API *and* excipient.

In this context, a combination of dissolution and permeation assessment may be very valuable, especially when excipients interfere at different stages in a concentration dependent manner. As shown above, a combined setup yielding physiological relevant concentrations may reveal these phenomena before testing the dosage form in animal and human studies. Additionally, a concept of combined dissolution/permeation might also be imagined to serve as a quality assurance tool for dosage forms containing active excipients.

1.1.3 Investigation of potential food effects on drug absorption

Effects of concomitant intake of food with drugs on disintegration [26] and dissolution [15, 27-31] of oral solid dosage forms are extensively described in literature. For dissolution testing, the development of biorelevant dissolution media by Galia et al. [2] simulating intestinal fluid in fed (FeSSIF) and fasted state (FaSSIF) led to a generally accepted *in vitro* method to forecast food effects in dissolution. Nevertheless, effects of food components on absorption processes is getting more and more in the focus of research [15, 32]. Wu et al. [33] suspected that concomitant intake of high fat meals with drugs are inhibiting intestinal in- and efflux drug transporters and thus may lead to decreased bioavailability of BCS class III compound; however, due to increased solubility in the intestinal lumen after fatty meals, BCS class II compounds may show an increased postprandial bioavailability. Inhibition of intestinal efflux transporters may also be mediated by flavonols in grapefruit and orange juice as stated in the review by Wagner et al. [15]. Ingels et al. [34] reported that the application of FaSSIF in Caco-2 permeability assessment does not affect permeability of passively permeating compounds. However, actively secreted compounds show a significant lower permeability in basolateral to apical direction, whereas apical to basolateral transport is not affected and thus polarity in transports diminishes. Ingels et al. suggested that the bile salts present in FaSSIF may inhibit P-glycoprotein and other efflux transporters and concluded that efflux pump interference of compound detected *in vitro* might be generally overestimated.

Consequently, an interplay between solubility and permeability with too many free variables is hindering the researcher or developer from clear statements. Interaction of food with oral absorption may happen at different stages which again can be titled as dissolution and permeation and a combined dissolution and permeation assessment might give a deeper insight in possible interaction and food effects.

To summarize there are several rational to justify the approach for permeation and dissolution testing. Nevertheless, it has to be pointed out that for BCS class I and other “unproblematic” compounds where it can be anticipated that increased luminal concentrations will lead to increased transepithelial fluxes, no significant additional information should be expected compared the conventional dissolution testing.

However, for difficult compounds mainly belonging to BCS classes III and IV, vital information about the drug in the dosage form can be obtained.

1.2 Connecting permeation and dissolution measurement assessment

1.2.1 Limitations/specifications concerning permeation/dissolution media

The choice of dissolution/permeation media is limited, mostly due to the need to maintain viability and integrity of Caco-2 cell monolayers. Main requirements of the media to be in contact with Caco-2 cells are: i) isotonic conditions (Caco-2 cell monolayers are basolaterally more sensitive to osmotic pressure than apically), ii) appropriate pH, which may be in a range from 5 to 8 (e.g. [35]), again this should be handled more restrictive basolaterally, iii) presence of calcium and magnesium ions in order to maintain monolayer integrity by stabilizing tight junctions, and iv) physiological ratio between extracellular sodium and potassium in order to warrant an appropriate potential difference across the epithelia. To circumvent these limitations, rendering dissolution media before getting into contact with Caco-2 cells may be appropriate. However, it has to be kept in mind that the original dissolution concentrations are diluted by doing so, and that the system is additionally getting more complicated. Therefore, one has to decide concerning the dissolution/permeation media between simplicity, in vivo relevance and analytical requirements. For dissolution testing, numerous media as described in literature, USP, or Ph. Eur., or other pharmacopoeias are generally accepted and mimic to some extend physiological surrounding of disintegration and dissolution processes. For permeation assessment, however, it still remains unclear which transport media generates best results. Permeability assessment though Caco-2 monolayers is routinely carried out using KRB (Krebs Ringer Buffer), KBR (Krebs Bicarbonate Ringers Buffer), or HBSS (Hanks` balanced salt solution), though those might pose too restrictive conditions for low soluble compounds due to the lack of lipids and surface active ingredients and their excessive amount of counter-ions. A shortcoming for low solubility compounds can generally be seen in the addition of either DMSO ($\leq$ 1 %) or various other solubility improving

substances (a comprehend review of applied substance together with concentrations is comprised in [36]) For more comparable *in vivo* permeation conditions in Caco-2 assays, Ingels et al. [37] recommend to employ apically FaSSIF, while basolaterally an analytically friendly buffer such as HBSS may be the best choice.

Table 1.1 summarizes the composition of the previously mentioned buffer systems. Differences among KRB, KBR, and HBSS are not that distinct and the most important difference may be seen in the absence of carbonate in KRB. Degassing procedures prior to dissolution testing may affect the carbonate concentration and thus alter the pH, and therefore, KRB appears to be most suitable for combined dissolution/permeation measurement.

Ingels et al. tested [37] FaSSIF and FeSSIF for compatibility with Caco-2 monolayer integrity, prerequisite for valid permeation experiments. Only FaSSIF turns out to maintain Caco-2 monolayer integrity throughout three hours as indicated by TEER, apparent permeability of fluorescein-sodium and by means of a MTT cytotoxicity assay. FeSSIF is immediately toxic to the cell monolayer; Ingels et al [37] attributes this to the high osmolarity (≈ 600 mOsm), low pH (5.0), and the high content of Na-taurochlate (15 mM). Additionally, the lack of glucose and especially calcium and magnesium, responsible for proper tight junction formation, may support monolayer damage. Recently, Patel et al. [38] modified FaSSIF and FeSSIF in order to obtain Caco-2 compatible *in vivo* relevant transport media. Changes of the compositions can be seen in Table 1. Briefly, Mg^{2+} and Ca^{2+} salts are added, osmolarity of FeSSIF is reduced to 330 mOsmol/kg H_2O, Na^+/K^+ ions are present in a physiological ratio, lecithin concentration in FeSSIF is doubled in order to mitigate toxicity of taurocholic acid and buffering phosphate and carbonate salts are added. Caco-2 monolayers retain their integrity throughout two hours indicated by mannitol flux and TEER. By means of scanning electron microscopy, no severe damage on the cells is detectable except a minor microvilli loss and shortening. Apparent permeability of Metoprolol is significantly reduced in the presence of FaSSIF/FeSSIF; the authors attribute that to micellar entrapment into the bile salt lecithin mixed micelles. Nevertheless, the influence of the modification of FaSSIF/FeSSIF on dissolution and solubilization properties of the media is not tested yet.

Table 1.1. Composition of various buffers possibly eligible for combined dissolution and permeation measurement. Concentrations may vary from reference to reference. Composition of FaSSIF and FeSSIF is shown as reported by Galia et al. [3]; in the meantime, several publications denoted a change from potassium to sodium as the main kation [56] or others changes. Abbreviations are given in the text body. [a]for resulting pH of 6.5: MES; for 7.4:HEPES

Compound [mM]	HBSS [36]	KRB [39]	KBR [38]	FaSSIF [4]	FeSSIF [4]	FaSSIF modified by [38]	FeSSIF modified by [38]
$CaCl_2$	1.26	1.41	1.20	--	--	1.67	1.67
Fumaric acid	--	--	5.40	--	--	--	--
KCl	5.36	3.00	4.69	103.27	203.86	5.37	5.37
$MgCl_2$	0.49	2.56	--	--	--	--	--
$MgSO_4$	0.41	--	1.20	--	--	0.81	0.81
NaCl	136.89	142.03	108.01	--	--	136.89	136.89
$NaHCO_3$	4.26	--	16.0	--	--	0.42	0.42
K_2HPO_4	--	--	0.47	--		--	--
KH_2PO_4	0.44	--	--	28.66	--	0.44	0.44
Na_2HPO_4	0.34	0.44	--	--	--	0.34	0.34
NaH_2PO_4	--	--	5.38	--	--	--	--
Na-pyruvate	--	--	4.90	--	--	--	--
D-Glu	25.00	4.00	11.50	--	--	5.55	5.55
L-Glutamine	--	--	5.67	--	--	2.00	2.00
MES/HEPES[a]	10.0/ 20.0	10.0/ 20.0	--	--	--	--	--
acetic acid	--	--	--	--	144.17	--	--
Na- TC	--	--	--	3.00	15.00	3.00	15.00
lecithin	--	--	--	0.75	3.75	0.75	7.50
NaOH	ad 7.4/6.5	ad 7.4/6.5	ad 7.4	ad 6.5	ad 5.0	ad 6.5	ad 6.0
Osmolarity [mOsm/kg H_2O]	~ 300	~ 300	~ 300	~ 300	~ 630	343	336

1.2.2 Historical evolution of combined permeation and dissolution testing

First attempts to combine both dissolution and permeation in one device have been made beginning in the mid seventies of the past century. Such typical devices employed distribution between three differently polar phases, i.e. the distribution between aqueous and lipoid and subsequent between lipoid and again aqueous phase, whereas both aqueous phases were kept apart by baffles. Thereby, a compromise that had to be accepted resulted from the fact that the "membrane" (i.e. the lipoid phase) was much thicker than the *in vivo* membranes and transport rates found *in vitro* appeared to be too strongly controlled by that. In 1969, Dibbern et al. [40, 41] circumvent this drawback by separating both aqueous acceptor and donor phase by lipoid treated polymeric membranes and thus was able to improve prediction of *in vivo* behaviour of dosage forms containing passively permeating compounds (the apparatus became commercially available under the name "Resomat" of the company Desaga). However, the validity of the obtained data was limited due to the employment of artificial lipoid membranes and thus omitted conclusions concerning actively secreted or absorbed drugs and metabolism. In 1980, Koch et al. [42] reported a simplified experimental tool ("Resotest Apparatus") again reviving the experimental determination of the partition between organic and aqueous phases. However, the apparatus was reduced to a rotating two-necked pear shaped flask containing two aqueous phases conjointly covered with a layer of suitable organic solvent. Although being a crude simplification and exhibiting non-physiologic lipoid membrane, the model made it into the textbooks; maybe because it was very easy to handle due to its simplicity. However, none of the dissolution-permeation devices were listed in the pharmacopoeias. As computing power, however, started to increase tremendously from the early 1980's and computational modelling sciences emerged, those simplified models for dissolving and passively permeating substances became obsolete.

In the meantime, dissolution testing was more and more standardized and gained enormous impact on the fields of quality assurance and drug development in

pharmaceutical industry. Several dissolution apparatus made their way into the pharmacopoeia such as the rotating paddle, rotating basket, reciprocation cylinder and the flow through cell, just to mention the most important. For comprehensive discussion on dissolution equipment, the reader is referred to books such as [43].

At the beginning of the 1990's, the general acceptance of Caco-2 cell monolayers as a model of the small intestinal mucosa caused a significant push toward

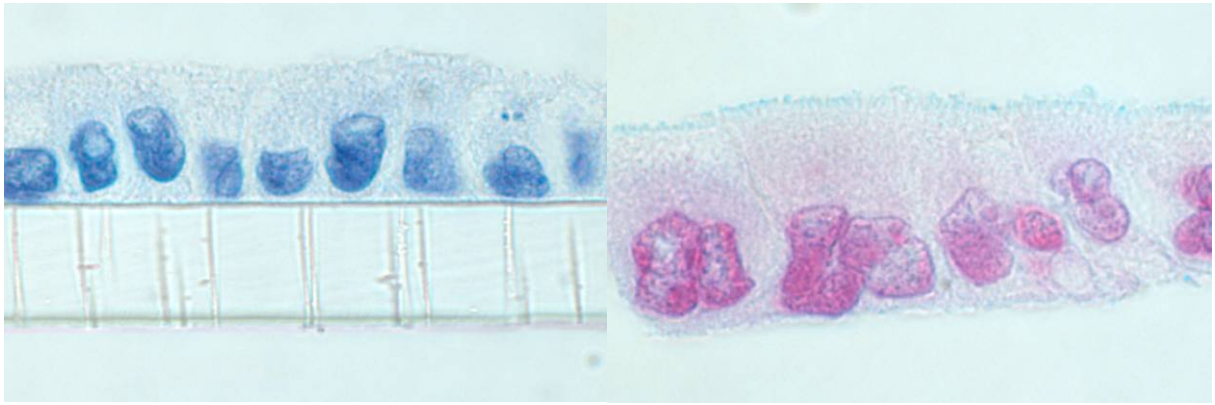

Figure 1.1. Microscopical depiction of Caco-2 cell (clone C2bB1), 21 days post seeding, 1000 fold magnification, staining left picture: haematoxylin (nuclei), right picture: alcium blue (mucus/microvili) + nuclear red (nuclei), detached from membrane.

the field of permeability testing [44, 45]. Caco-2 cells, originally derived from a colon cancer patient, differentiate spontaneously on cell culture supports to small intestinal epithelia like cells. Although lacking significant mucus production, it was found that permeability through Caco-2 cells correlates well with human intestinal permeability [3] and ultimately the Caco-2 cell line (Figure 1.1) was generally accepted as a powerful *in vitro* tool to forecast oral drug absorption. As a consequence, the pharmaceutical community became more aware that permeation through intestinal epithelia is oftentimes more than mere diffusion through a lipophilic membrane.

In 1995, Amidon et al. [46] addressed a theoretical base for a biopharmaceutic drug classification, which was also addressed in several FDA guidelines [47, 48]. The biopharmaceutical classification system (BCS) assigns drugs into classes I to IV according to their solubility and permeability properties; thus highlighting the importance of both fundamental parameters – dissolution and permeation; nowadays, the BCS has gained tremendous impact on drug development.

1.3 Published approaches for permeation and dissolution assessment

Recently, an approach mimicking the GI tract and feasible for pharmaceutical dissolution studies has been published [49]. Coming from the area of nutritional research, this approach reflects some promising aspects such as relevant luminal pH values, peristalsis, luminal bacterial colonization, and relevant volumes. However, permeation is only reflected by diffusion through hollow fiber membranes and thus is not in the scope of this chapter. Nevertheless, it will be interesting to see whether it will be possible to expand such perfect *in vitro* device with intestinal epithelia.

Several approaches combining Caco-2 permeation assessment with dissolution testing have been published. In the following, the systems are described in chronologically order of their publication.

1.3.1 Approach by Ginski and Polli [50]

In 1999, Ginski et al [50] published a continuous dissolution/Caco-2 system. Dissolution takes place in a paddle apparatus (apparatus I, USP) and Caco-2 monolayer is mounted in a side-by side diffusion cell whereas a peristaltic pump transfers media from the dissolution vessel to the permeation chamber. Dissolution and permeation media is HBSS (pH 6.8). The system (Figure 1.2) can be seen as a closed model, since no drug was allowed to leave the experimental setup.

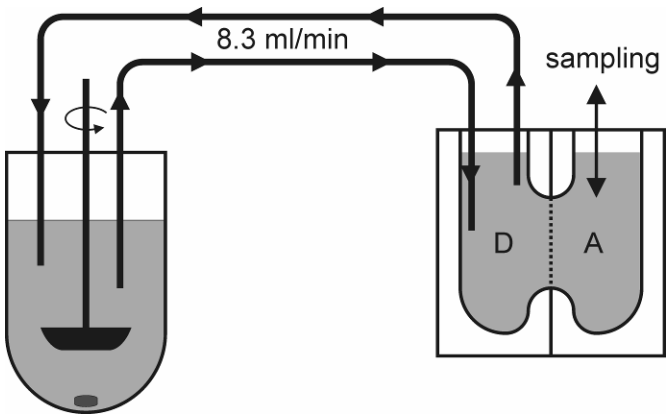

Figure 1.2. Approach of Ginski and Polli.

The study had several objectives. Main objective was to test whether the experimental data fit to the previously described mathematical model determining the dissolution/absorption relationship [50, 51]. Another objective was to detect possible effects of the formulation (disintegrating agent, solubilizers such as TWEEN 80 and cyclodextrins) on the dissolution/absorption relationship. Although being a rather simple experimental setup, the results were promising. Ginski et al. were able to confirm the validity of their setup with *in vivo* data using piroxicam and ranitidine oral solid dosage forms with varying release kinetics. The addition of croscarmellose-Na as an *in vitro* permeation enhancing agent leads to an increased permeated amount through Caco-2 cell monolayer; although *in vivo* no absorption enhancing effect of croscarmellose-Na is detected. This phenomenon is attributed to the calcium sequestering properties of croscarmellose-Na and is identified as a false positive *in vitro* finding, since complete sequestering of all extracellular calcium may not happen *in vivo*. For the variation of solubilizers the authors prove that only dissolution is altered, not permeation. Finally, the authors concluded that this continuous dissolution/Caco-2 may be a tool to forecasting formulation effects on *in vivo* dissolution and *in vivo* permeation.

1.3.2 Approach by Miyazaki et al. [52-55]

Shortly after Ginski et al., Kobayashi et al. [52] published in 2001 an open dissolution/permeation approach. A stirred glass vessel serves as a flow through dissolution device, from whose the eluted solution is pumped into second glass vessel for pH adjustment. Subsequently to neutralizing to a pH of 6.0, the eluted solution is transferred into a flow through diffusion chamber with a Caco-2 monolayer between the acceptor and donor compartment. A schematical drawing of the most recently published setup is shown in Figure 1.3. The authors routinely carry out their experiment with a HBSS like buffer, which is generated prior to contact of the buffer with the Caco-2 monolayers. The system is able to simulate various pH values acting on the drug, however, the device is not capable of changing pH acting on the drug in one experiment and thus one might argue that *in vitro,* the undissolved drug appears to stay in gastric compartment rather than being transferred to the small intestine with its increasing pH values. This issue is almost circumvented in later publications by

employing several gastric acidic models [54]. Nevertheless, the authors are able to mimic precipitation of weak bases in the “ph adjustment vessel” such as for albendazol [55]. Furthermore, the apparatus of Kobayashi et al. [52] and He at al. [53] shows a good linear relationship between the amount cumulatively permeated into the acceptor compartment and the fraction absorbed in humans although clinical doses of the drugs are disregarded. Interestingly, the authors used this system also for assessing metabolism of prodrugs to be cleaved in intestinal cells, for instance ampicillin/pivampicillin. The experiments with either rat intestine or Caco-2 monolayers indicate that pivampicillin is undergoing cleavage during the permeation through the intestinal barriers and again the obtained values correlated well with *in vivo* data.

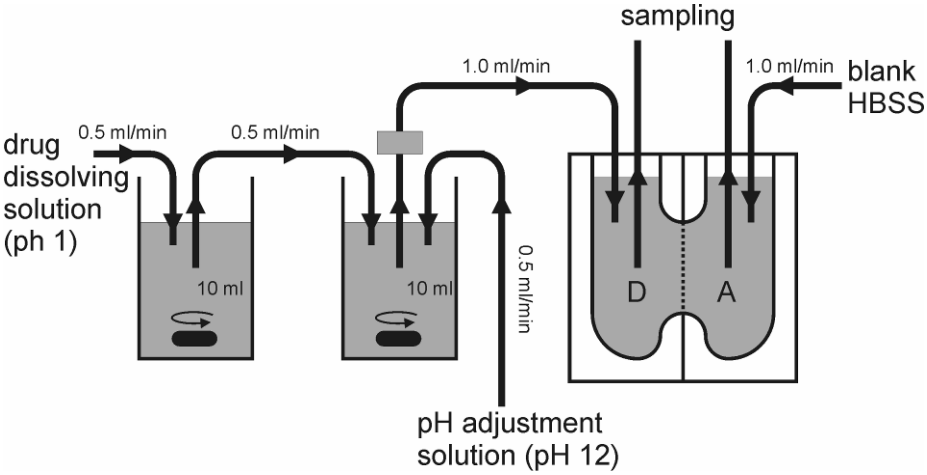

Figure 1.3. Approach of Kobayashi et al..

In comparison to the approach of Ginski et al. [50], the approach appears to be more elaborate and complex and is coming closer to *in vivo* reality. The device can simulate various effects of pH on dissolution and is, as an open system, closer to *in vivo* conditions compared to a closed one. However, it exhibits the drawback of not freely “adjustable” pH values acting on the drug. Low flow rate in the dissolution vessel may limit applications of complete dosage forms and allows predominantly only the use of granules, pellets or grinded tablets. Additionally, the application of compendial dissolution devices appears to be a more robust approach.

1.3.3 Aproach by Kataoka et al. [56, 57]

In 2003, Kataoka et al. [56] published an *in vitro* system for simultaneous evaluation of dissolution and permeation of poorly water soluble drugs. In contrast to Ginski et al. [50], this system assesses dissolution and permeation in a downsized dissolution vessel (one percent of the volume estimated *in vivo*, 8 ml) with a Caco-2 monolayer mounted between acceptor (5.5 ml) and donor compartment (Figure 1.4). When reducing the volumes to a hundredth, the dose of the drug has also to be reduced by the same scale, which may raise some balancing and handling issues when adding 0.1 mg drug or even less to the dissolution compartment. In comparison to previously published paper, the authors highlight the importance of clinical doses of the compounds tested, as also compounds are assigned into the four BCS classes [46] according to their solubility of the highest dose in 250 ml. The authors find a good correlation between the amount permeated after 120 min and the fraction absorbed in humans, whereas the 120 min time point was chosen in regard to the mean small intestinal transit time.

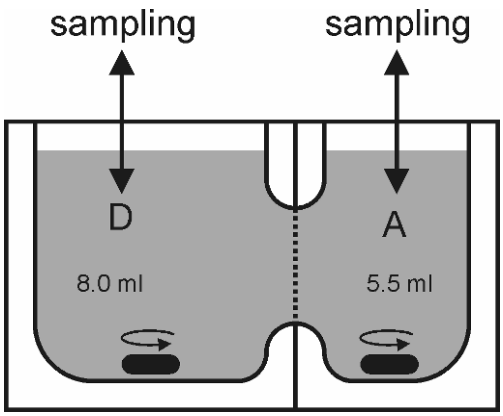

Figure 1.4. Approach of Kataoka et al..

The setup was additionally able to assign correctly all compounds into BCS classes I-III; however, the study was lacking a BCS class IV compound. Furthermore, experiments applying apically 5 mM taurocholate (ranges between FaSSIF and FeSSIF) in the dissolution compartment showed increased permeated amount for griseofulvin, mainly due to higher dissolution rate and solubility. Also the addition of 4.5 % BSA in the

acceptor compartment increased the permeation rate of griseofulvin which may be attributed to increased sink conditions. In 2006, Kataoka et al. [57] focussed on predicting effect of food intake on oral drug absorption in humans. Therefore, Kataoka and coworkers tested various kinds of simulated intestinal fluids in their dissolution/permeation setup and successfully correlated their results with human *in vivo* data. Additionally, they could visualize the interplay between food effect and formulation properties.

The approach of Kataoka et al. [56, 57] shows desirable features such as downsized, *in vivo* relevant volumes and low efforts for devices and thus low error proneness. Additionally, application of *in vivo* relevant dissolution/permeation media increased the predictive power of the dissolution/permeation system impressively. Nevertheless, the device lacks the possibility to add complete dosage forms and the use of compendial dissolution devices would be a more robust approach.

1.4 Critical evaluation of the state of the art and aims of the study

To connect two *in vitro* assays displaying fundamental processes occurring during oral absorption *in vivo*, appears to be a promising tool. Such setup allow the researcher intense comprehension of the interplay of dissolution and permeation with surrounding media and excipients. However, the following improvements would have to be made in order to improve the value of the obtained data.

In view of the published approaches, the author points out that an open dissolution system will generate concentration time trends with higher *in vivo* relevance since the drug will not accumulate at the donor site throughout the experiment (compare [50, 56, 57]). In an open system, drug concentration will reach high values and hence potentially saturate transporters or overrun efflux transporters at these concentrations. However, after the peak concentrations were reached, uptake or efflux transporter affinity is getting relevant again. In a closed system, drug concentration will increase and saturate transporters until the experiment is terminated.

A second focus of the work will be placed on the ability of the apparatus to use complete dosage forms. As already stated in section 1.1.2 (p 1-4), excipients might affect both dissolution and permeation; hence, permeability assessment should not

neglect the presence of excipients. As a consequence, the apparatus to be developed throughout this dissertational project should be capable of assessing dissolution and subsequent permeation of complete dosage forms. Although Miyazaki et al. [52-55] applied an open dissolution and permeation system, their system lacks the ability to use complete solid oral dosage forms. Furthermore, a modular, depressurized setup will allow the application of compendial dissolution pumps providing appropriate hydrodynamics for dissolution. As a consequence from the aim to use complete dosage forms, also *in vivo* relevant flow rates have to be used resulting in *in vivo* relevant dissolution volumes.

In conclusion, the aim of the study was to develop a test system with the ability to assess permeability of solid oral dosage forms in an open dissolution and permeation system. Moreover, it was intended to plan the system as a modular setup increasing the simplicity and reliability of the apparatus.

2 Proof of concept

In order to proof the concept based on the implications made in chapter 1, the apparatus has been tested using varying dosage strengths and release kinetics of propranolol HCl tablets. Propranolol HCl has been chosen as a model drug because of its high solubility and permeability. Data obtained from those tablets has been checked concerning plausibility and conclusiveness.

Parts of this section have been published in

Motz SA, Schaefer UF, Balbach S, Eichinger T, Lehr CM. Permeability assessment for solid oral drug formulations based on Caco-2 monolayer in combination with a flow through dissolution cell, Eur. J. Pharm. Biopharm. (2007), doi:10.1016/j.ejpb.2006.10.015 [39]

2.1 Introduction

Among the various setup addressed in the previous section, the most promising approaches have been combined. Hence a conventional dissolution setup was chosen according to the approach of Ginski et al.[50]. Having dynamic concentration changes on the apical surface of the Caco-2 monolayer with an open dissolution device led to the employment of the dissolution apparatus 4, USP [58]. Additionally, according to Kataoka et al., the clinical doses were taken into consideration and this also accounted for the apparatus 4 which is able to mimic physiological relevant volumes and hydrodynamics. In order to mitigate analytical issues when assessing the permeated amount, the acceptor compartment was designed to be closed.

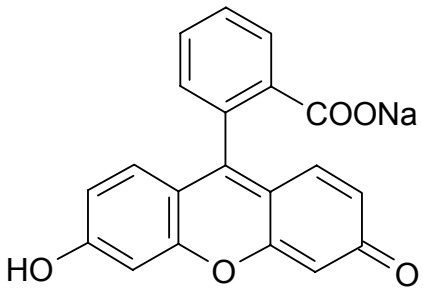

Figure 2.1. Chemical structure of fluorescein-Na

Prior to testing complete dosage forms, it was investigated if the flow through permeation cell (FTPC) provides comparable results for permeation data compared to static experiments performed in conventional Transwell® systems. For this purpose, two different compounds were tested: propranolol as a high permeability marker (marker for unstirred water layers) and fluorescein-Na as a low permeability marker (marker for barrier integrity). For the permeation module, several criteria have to be matched such as i) the integrity of the Caco-2 monolayer has to be maintained throughout the experiments and ii) conditions for permeation should be comparable to those in Transwell® systems.

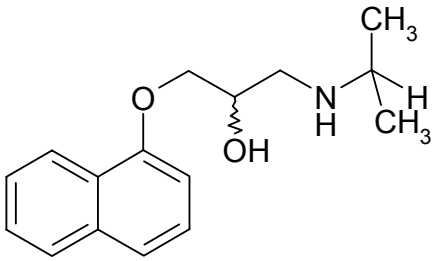

Figure 2.2. Chemical structure of propranolol

Propranolol HCl was chosen because of its biopharmaceutical properties: It shows high permeability in Caco-2 transport experiments [59] and human perfusion studies [60]. Caco-2 transport experiments indicate that propranolol is permeating mainly transcellular and neither has affinity to cellular efflux nor to influx systems [59, 61, 62]. In addition, propranolol HCl is highly soluble in aqueous buffers [59, 63] and hence is assigned to BCS class I [33, 59, 64].

In order to test and validate the newly designed combined apparatus, propranolol HCl released from a solid dosage forms at different dosage strengths was used. Beyond that, extended release propranolol HCl tablets with varying amounts of Eudragit® NE 30D as a retarding agent were produced. For propranolol, increase of dosage strength should lead to a direct proportional increase of permeation; retardation of release should lead to a direct change of the appearance rate in the trans-mucosal receptor compartment. Up to now, no other in vitro setup has been described that would allow to monitor the impact of such formulation related parameters on the intestinal permeability of a drug formulated as solid oral dosage form. Critical parameters in this “proof of concept” were i) Caco-2 cell monolayer integrity, ii) the handling, iii) reproducibility, and iv) conclusiveness and plausibility of the obtained data.

2.2 Material and Methods

2.2.1 Materials

Transwell® permeable filter inserts (pore size 0.4 μm, 1.13 cm^2, Transwell® type 3460) were purchased from Corning Incorp. Life Sciences (Acton, MA). Dulbecco’s

modified Eagle's medium (DMEM), non-essential amino acids (NeAA) and fetal bovine serum (FBS) were purchased from GIBCO (Invitrogen Corp. Carlsbad, CA). Fluorescein-Na was purchased from Sigma-Aldrich (St. Louis, MO), and propranolol HCl from Synopharm GmbH & Co KG (Barsbüttel, GE). Organic solvents were of HPLC grade. Eudragit® NE 30 D was a kind gift from Degussa. (Röhm Pharma Polymers, Darmstadt, GE). Avicel PH 102 was from Lehmann & Voss (Hamburg, GE); Lactose EP type D20 was from J. A. Meggle Milchindustrie (Reitmehring, GE); PVP insol. was from BASF (Ludwigshafen, GE); Aerosil 200 was from Degussa (Rheinfelden, GE); Mg-Stearate was from Synopharm GmbH & Co KG (Barsbüttel, GE). All tablet excipients were of Ph. Eur. grade. All salts for KRB were of cell culture tested grade and obtained from Sigma-Aldrich (St. Louis, MO).

2.2.2 Cell culture

Caco-2 cells, clone C2BBe1, were purchased at passage 60 from American Tissue Culture Collection (ATCC; Manassas, VA) and used at passages 70-92. Caco-2 cells were grown to ~90 % confluency in 75 cm^2 T-flasks with DMEM supplemented with 10% FBS and 1% non essential amino acids (NeAA). Culture medium was changed every second day. The incubator temperature was set to ~37°C in an atmosphere of ~85 % relative humidity and ~5% CO_2. After trypsinisation, cells were seeded on Transwells® at a density of 60,000 cells/cm^2. Transepithelial electrical resistance (TEER) was measured routinely (EVOM, World Precision Instruments, Berlin, Germany) and only monolayers with a TEER > 350 $\Omega \cdot cm^2$, with background for plain filters subtracted, were used for transport studies.

2.2.3 Transport assay

Caco-2 monolayers were used 21-25 days post seeding. Prior to transport experiments, DMEM with supplements was removed and KRB pH 7.4 was added to the apical and basolateral compartment.

Apparent permeability (P_{app}) was calculated according to Eq (1):

$$P_{app} = \frac{dQ}{dt} \cdot \frac{1}{A \cdot c_0} \qquad \text{Eq (1)}$$

whereas A [cm^2] is the nominal surface area of the monolayer and c_0 [μg/ml] is the donor concentration at $t = 0\ h$. The quotient dQ/dt was calculated from the slope of the linear part of the mass increase in the acceptor compartment. Concentration of propranolol HCl in the donor compartment was 30 μg/ml and 10 μg/ml for fluorescein-Na, respectively. Integrity of the Caco-2 monolayers was checked microscopically and by measuring TEER values before and after the experiments. Donor solutions were pumped into the FTPC with a flow rate of 1.0 ml/min and samples were withdrawn from the circulating basolateral compartment after 30, 60, 90, 120, 150, 180 and 210 min. Retrieved volumes were replenished with fresh KRB (n = 5 for both compounds). The retrieved amount of propranolol HCl from the basolateral compartment was taken mathematically into consideration (please see Eq(2)).

$$c_{n\,corr} = \frac{[c_1 \cdot V + c_2 \cdot V + \ldots + c_n \cdot V] + c_n \cdot V}{V_{bas}} \qquad \text{Eq (2)}$$

whereas c_n is the concentration measured at measurement time n [μg/ml], V is the sampling volume [ml], while V_{bas} is the volume of the complete basolateral compartment [ml].

2.2.4 Preparation of tablets

Immediate release tablets (IR tablets) were manufactured using direct compression (for formulation see Table 2.1). Ingredients were sieved (mesh size 315 μm), blended in an turbula mixer (TS Bachofen, Basel, Switzerland) and

subsequently compressed using a Korsch EK 01 (Berlin, GE) eccentric tablet press gaining tablet mass of 100 mg and crushing strength of 100 N (Erweka hardness tester, type TBH 30M, Erweka, Heusenstamm, GE).

Table 2.1. Composition of the immediate release propranolol HCl (IR) tablets

	5 mg	10 mg	20 mg
Avicel PH 102	70 %	70 %	70 %
Lactose EP type D20	23 %	17 %	7 %
PVP insol.	1 %	1 %	1 %
Aerosil 200	1 %	1 %	1 %
Mg- Stearate	1 %	1 %	1 %
Propranolol HCl	5 %	10 %	20 %

Extended release tablets (ER tablets) were prepared as follows (for formulation see Table 2): lactose, Avicel and propranolol HCl were granulated using a 30 % dispersion of Eudragit® NE 30D. Water was added until a capable granulate was formed. Subsequent to sieving trough a 2 mm sieve, the wet powder was dried for 1 hour

Table 2.2. Composition of the extended release propranolol HCl (ER) tablets

Eudragit® NE 30 D $^{++}$	4 %	8 %
Avicel PH 102	55 %	55 %
Lactose EP type D20	29 %	25 %
Propranolol HCl	10 %	10 %
Water	q. s.	q. s.
Aerosil 200	1%	1%
Mg- stearate	1%	1%

in an oven with circulating air at 45 °C followed by an over night drying at room temperature. Shortly before compressing, freshly sieved Aerosil 200 and Mg- stearate were added and blended for 5 min in a turbula mixer. Tablets were produced with a mass of 100 mg and a crushing strength of 100 N.

Content uniformity was determined by dissolving a tablet in 100.0 ml water by means of ultrasonic. Then, the solution was filtered through a 0.22 μm PTFE filter (Optiflow®, WiCom GmbH, GE) via a 5 ml syringe (Braun, Melsungen, GE), whereas the first eluted drops were discarded. Subsequently, the filtrated solution was diluted with water (1:20) and the concentration was assessed via HPLC. For each dosage strength and release property, ten tablets were tested.

2.2.5 Preparation of Krebs Ringer Buffer (KRB)

Krebs Ringer Buffer (KRB) was prepared by adding 1.41 mM $CaCl_2$, 2.56 mM $MgCl_2$, 142.03 mM NaCl, 0.44 mM K_2HPO_4, 4.00 mM D- Glucose and 10.0 mM HEPES to 5 liter of Millipore® water. The pH was adjusted by means of concentrated NaOH solution to 7.4 ± 0.1. Subsequently, the buffer was filtrated through a 0.22 μm filter into sterilized glass vessels in a laminar flow bench warranting sterility of the buffer. The buffer was could be used for maximum 2 weeks. Prior to experiments, the KRB was degassed by means of ultrasonic.

2.2.6 Analytics

2.2.6.1 Propranolol HCl

Quantification of propranolol HCl was performed using a Dionex HPLC system, implemented with a RP 18 (LiChroSpher® 100, Merck), 5 μm, 12,5 cm column. The HPLC system consisted of a Dionex P580 pump, a Dionex ASI 100 auto sampler, a UVD 170 S detector and a Dionex STH 585 column oven. Software was Chromeleon® 6.60, SP 1 build 9.68. Mobile phase for Propranolol quantification was 45% (v/v) water, 22% (v/v) acetonitrile, 33% (v/v) methanol, 0.033% (v/v) triethylamine and 0.044% (v/v)

phosphoric acid. Flow was 1.2 ml/min and oven temperature was 40 ± 1 °C. Detection was done with UV at 215 nm, whereas linearity (R> 0.999) was given between 30 ng/ml and 100 µg/ml. Retention time was 3.00 ± 0.15 min. It was shown that neither the excipients of the tablet nor salts of KRB interfered with the analysis.

2.2.6.2 Fluorescein-Na

Quantification of fluorescein-Na was performed using the native fluorescence in a Cytofluor II fluorescence reader (λ_{exc} = 485 nm, λ_{em} = 530 nm) with Cytofluor software version 4.2 (PerSeptive Biosystems, Wiesbaden- Norderstedt, GE). Measurement took place in a 96 well plate and was done after addition of 150 µl 10 mM NaOH to 50 µl analyte in order to assure higher fluorescence levels and to minimize pH triggered fluorescence intensity changes. Linearity (R > 0.999) was given between 5 ng/ml and 1 µg/ml.

2.2.7 Data treatment

All data is given as mean ± standard deviation. Statistical analysis has been done using Sigma Stat for Windows version 3.0.1 build 3.01.1.
Calculation of mean times for the different sampling port was done according to Eq (3) to Eq (5).

$$mean\ time\ at\ D \quad : MT_D = \frac{(t \cdot m_D) - AUC_D}{m_D} \qquad \text{Eq (3)}$$

$$mean\ time\ at\ A \quad : MT_A = \frac{(t \cdot m_A) - AUC_A}{m_A} \qquad \text{Eq (4)}$$

$$mean\ time\ at\ B \quad : MT_B = \frac{(t \cdot m_B) - AUC_B}{m_B} \qquad \text{Eq (5)}$$

t is the time duration over which dissolution or permeation was measured, m_D and m_A are the masses which cumulatively appeared at the respective sampling port after time t, m_B is the mass which permeated and was detected at sampling port B after time t. AUC_D, AUC_A, and AUC_B are the areas under the curves for the respective sampling

ports (all areas were calculated using trapezoidal rule). The withdrawn amount in the basolateral compartment was taken into consideration when calculating the permeated amount according to Eq(2). For regression, Sigma Plot 2004 for Windows Version 9.0 was used (values are given as mean ± std error).

2.3 Results

2.3.1 General consideration in respect to the apparatus

The apparatus can be divided into two modules: a flow through permeation module and a flow through dissolution module, whereas both modules are connected by means of a stream splitter (Figure 2.3, Figure 2.5). In the permeation module, flow rate was set to 1.0 ml/min and in the dissolution module to 6.5 ml/min. The flow through permeation module can be subdivided into two compartments: the open apical and the closed basolateral compartment with a Caco-2 monolayer upon a Transwell® mounted between these both compartments. Within the basolateral compartment, a magnetically stirred glass vessel was installed for sampling and for setting up a supply for KRB buffer. Sampling was performed at three different locations, designated in Figure 2.3 as

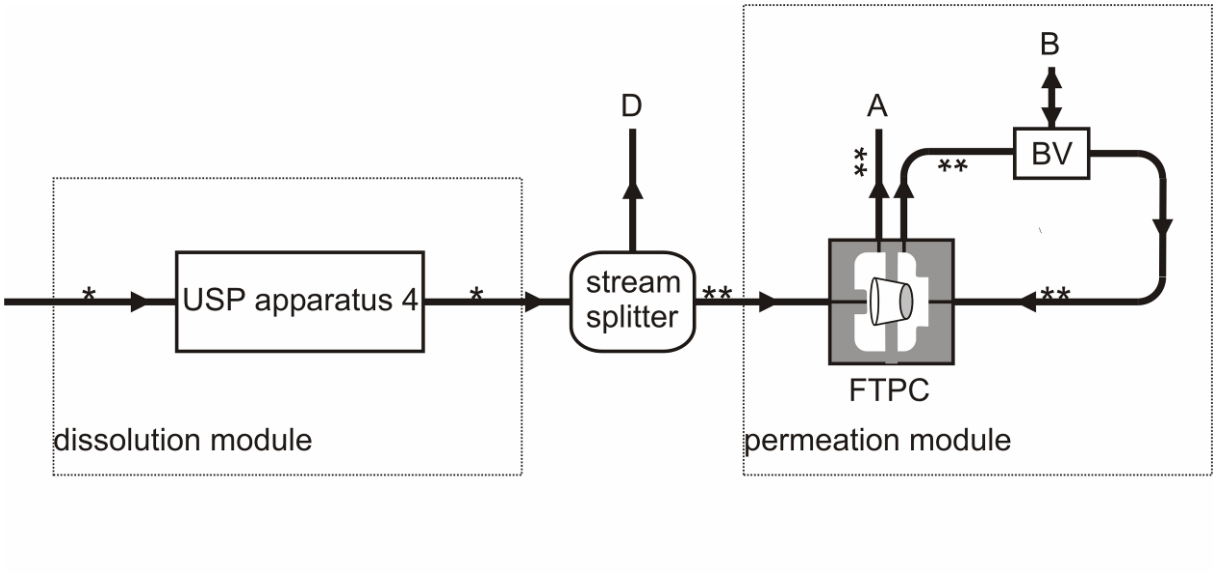

Figure 2.3. Schematical depiction of the apparatus for combined flow through measurement of dissolution and permeation (* flow = 6.5 ml/min; ** flow = 1.0 ml/min). Sampling ports are indicated with capitals: D, sampling port dissolution; A, sampling port apical, B, sampling port basolateral.

“D” – dissolution, “A” – apical, and “B” - basolateral. The flow through dissolution module consisted of the USP apparatus 4 (flow through cell, Sotax CE1, Sotax, GE) equipped with a 12 mm dissolution cell and a filter preventing undissolved solids from escaping. Tablets were placed upon small glass beads as described in <724> of USP (25). Samples taken at “D” represent the dissolution process, samples collected at “A”

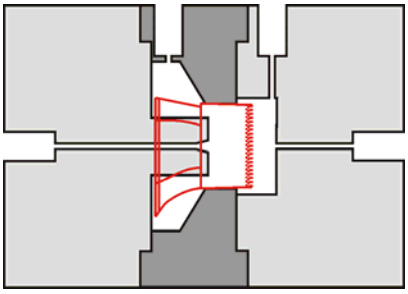

Figure 2.4. Depiction of the flow through permeation cell (FTPC) with a Transwell® inserted shown in red. The apical compartment is in the left side, whereas the basolateral compartment is in the right side.

represent the amount and extent of drug, which appeared in the apical compartment of the FTPC (Figure 2.4) being available for permeation through the Caco-2 monolayer (Sample volume at “D” was 0.5 ml, and 150 µl at “A”, resp.). Since the basolateral compartment of the permeation module is a closed compartment, the retrieved samples were replenished with blank KRB buffer (Sample volume at “B” was 150 µl). The complete volume in the basolateral compartment was calculated and experimentally confirmed as 10.5 ml. In order to avoid any issues concerning adsorption and biocompatibility, the tubing (ID 1.0 or 2.0 mm) consisted of Teflon®, and the FTPC (Figure 2.4) and the stream splitter (Figure 2.5) were made of polyetheretherketone (PEEK). All streams in the apparatus were driven by membrane dosage pumps of type Stepdos 03® (KNF Neuberger, Freiburg, GE) in combination with pulsation dampers. The apparatus 4 and the flow through permeation cell were submersed in a water bath and heated to 37.0 +/- 0.5 °C. Prior to each experiment, Caco-2 monolayers were washed twice with KRB and equilibrated in KRB for at least 30 min in an incubator. After that, transepithelial electrical resistance (TEER) was measured, the Transwell® was subsequently inserted in the FTPC, and cells were allowed to equilibrate for another 15 min with an apical and basolateral flow of each 1.0 ml/min. After the experiments, Transwells® with the Caco-2 monolayer were taken

out of the FTPC and integrity of the Caco-2 monolayer was confirmed microscopically and again by TEER measurement.

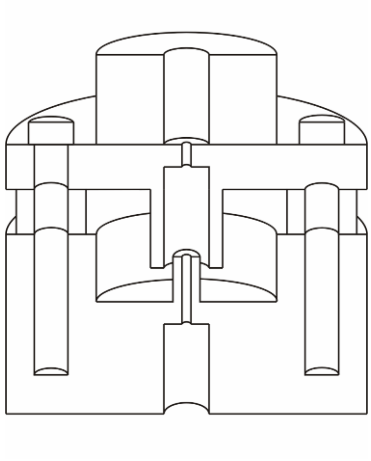

Figure 2.5. Schematical depiction of the stream splitter. The dissolution stream is led into the top of the device, whereas two pumps are aspirating the adjusted volumes per time from the underneath.

To allow the option of different media and flow rates, the dissolution and permeation module requires the use of a stream splitter (Figure 2.5) which supplies the permeation module with appropriate low flow rates to ensure viability and integrity of Caco-2 monolayers. The two modules are hydrodynamically separated, and thus can be run independently. Therefore, pressure variations in the dissolution module possibly caused by pumps and clogged filters do not carry over into the permeation module where pressure sensitive Caco-2 cell monolayers are located. Technical details of the stream splitter and the FTPC are given in Figure 8.3, Figure 8.4, Figure 8.5, and Figure 8.6, respectively. The open apical compartment of the permeation module led the stream with the dissolved drug to the waste after it has passed through the FTPC, whereas the basolateral compartment is a closed compartment. This setup entails that a peak concentration time profile generated in the dissolution module can also be detected in the apical compartment as a peak concentration profile in the permeation module. However, this peak profile is altered to a sigmoid concentration time profile in the basolateral compartment of the permeation module. The rationale to implement a circulating basolateral compartment are the higher concentrations compared to those in an open compartment, i.e. facilitating analytics of the permeated drug.

2.3.2 Effects of flow rate in the FTPC on P_{app} of propranolol and fluorescein-Na

P_{app} values of propranolol HCl and fluorescein-Na were assessed with the FTPC. For an apical flow rate of 0.75 ml/min, P_{app} of propranolol HCl was determined as $2.2 \cdot 10^{-5}$ cm/s. Apical flow rate of 1.25 ml/min led to an P_{app} of $2.9 \cdot 10^{-5}$ cm/s, flow rate of 1.00 ml/min led to an P_{app} of $2.5 \pm 0.52 \cdot 10^{-5}$ cm/s (n=4) At 1.00 ml/min, P_{app} of fluorescein-Na was $4.7 \cdot 10^{-7}$ cm/s. For the flow rates of 0.75 – 1.25 ml/min, TEER values measured after the experiments remained above 350 $\Omega \cdot cm^2$ and monolayer were microscopically intact. Flow rates above 2 ml/min showed deleterious effects on Caco-2 cell monolayers.

2.3.3 Assessment of drug permeability and dissolution at different dosage strengths

Three immediate release tablet batches with increasing amount of propranolol HCl were investigated. The concentration time profile measured at sampling port D and at A is shown in Figure 2.6. The dissolved amount after 120 min calculated by means of trapezoidal rule yielded for all three batches 90 % of the labelled amount or more (not shown). 5 and 10 mg IR propranolol HCl tablets showed a rather rapid release of propranolol and exhibited a peak concentration at approximately 10 min at sampling port D and at 15 min at sampling port A. The 20 mg immediate release propranolol HCl tablets showed a slightly delayed initial release of propranolol HCl with a shoulder and subsequently reached maximum peak concentration at about 23 min at sampling port D and approximately 30 min at sampling port A. In the lower plot of Figure 2.6, a sigmoid time curve of permeated propranolol HCl was observed. Since the volume of the basolateral compartment was experimentally determined as 10.5 ml, the permeated amount could easily be assessed from the measured concentrations. The permeated amount after 120 min was significantly different for all propranolol HCl tablets (ANOVA, Holm-Sidak test, $p < 0.001$).

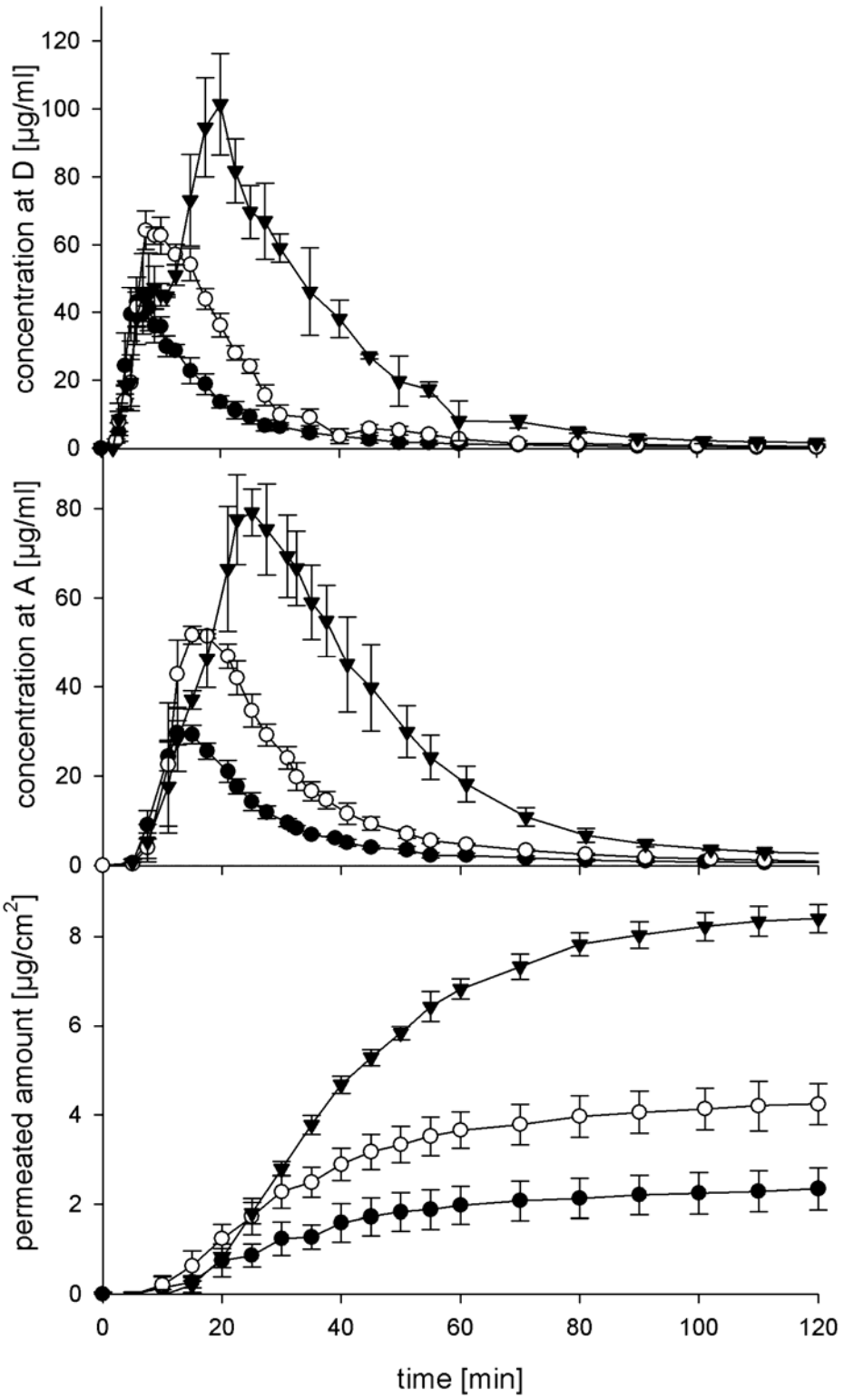

Figure 2.6. Concentration time trends for immediate release tablets at sampling port D and A (upper and middle plot). Lower plot shows the permeated amount calculated from the concentrations assessed at sampling port B. Closed circles (●) represent 5 mg, open circles (○) represent 10 mg and triangles down (▼) represent 20 mg immediate release propranolol HCl tablets (mean +/- st dev, n = 4-5 for each dosage strength).

2.3.4 Assessment of drug permeability and dissolution at different release kinetics

Three different tablet species with differently retarded 10 mg propranolol HCl were investigated. Retardation was mediated by increasing amounts of Eudragit® NE 30D. Note that sampling time was prolonged for the extended release tablets from 120 min to 180 min. The concentrations at sampling port D and A are shown in Figure 2.7. Concentration profiles of the immediate release and the two retarded tablet species can easily be distinguished from each other Figure 2.7 since retardation led to decreased maximum concentration and flattened peaks. The cumulative release after 180 minutes based on the AUC was for each, the immediate release and the 4% Eudragit® NE 30 D containing extended release tablet, greater than 90 %, whereas the 8% Eudragit® NE 30D containing extended release tablet released about 82 % of the labelled amount within the time of the experiment. In summary, the addition of Eudragit® NE 30D led to an evident, concentration dependent retardation of release of propranolol HCl. Obviously, and as expected for a highly permeable compound, the appearance of propranolol HCl in the basolateral compartment of the permeation module is governed by its concentration at the apical side of the permeation device which depends on the release rate from the dosage form (Figure 2.7, lower plot)

2.4 Discussion

2.4.1 Rationale for the particular setup and choice of media, flow rates, and formulations

To allow the option of different media and flow rates, the dissolution and permeation module requires the use of a stream splitter which supplies the permeation module with appropriate low flow rate and thus can be run independently. Therefore, pressure

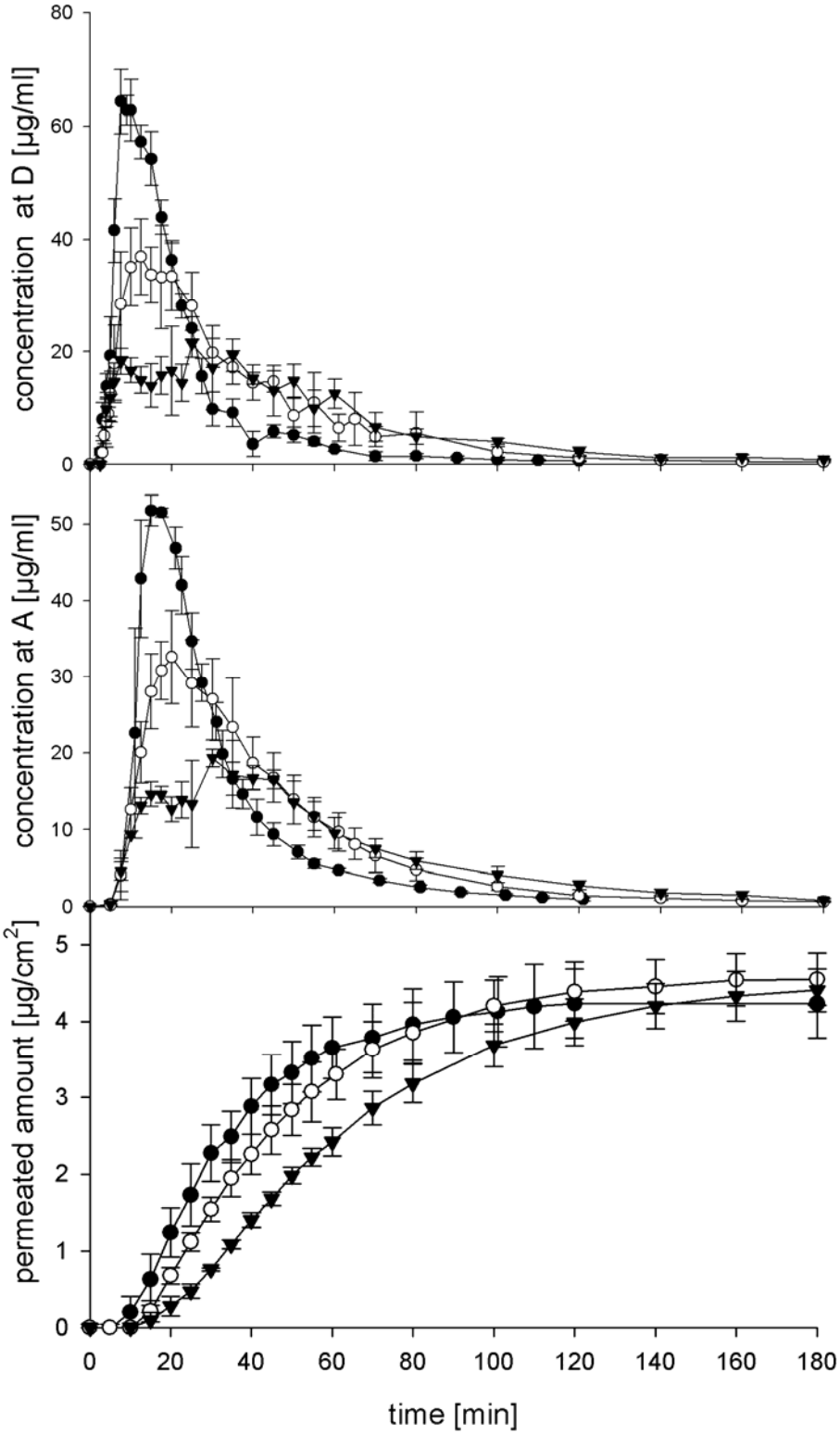

Figure 2.7. Concentration time trends for extended release tablets at sampling port D and A (upper and middle plot). Lower plot shows the permeated amount calculated from the concentrations assessed at sampling port B. Closed circles (●) represent the 10 mg propranolol HCl immediate release tablet, open circle (○) represent the 10 mg extended release tablet with 4 % Eudragit® NE 30D and triangles down (▼) represent the 10 mg extended release tablet with 8 % Eudragit® NE 30D (mean +/- st dev, n = 4-5).

variations in the dissolution module flow rates to ensure viability and integrity of Caco-2 monolayers. Since the stream splitter works depressurized, effects on the dissolution in the flow through dissolution cells are highly unlikely and have not been detected. Both modules are hydrodynamically separated, possibly caused by pumps and clogged filters do not carry over into the permeation module where pressure sensitive Caco-2 cell monolayers are located. The rationale to implement a circulating basolateral compartment are the higher concentrations compared to those in an open compartment, i.e. facilitating analytics of the permeated drug.

Working with sensitive cell culture models such as Caco-2 cell monolayers puts limitations on the use of the aqueous media to be in contact with them. Viability and integrity of a Caco-2 monolayer depends, just to mention some important parameters, on iso-osmotic pressure in combination with appropriate pH values, and thus choice of dissolution media is very limited when the liquid with the dissolved drug is directly led over the Caco-2 monolayer. Although it has been reported that HBSS like buffers tend to underestimate solubility of drugs due to its high hydrophilicity and its excessive content of possible counter-ions [37], KRB was chosen as both dissolution and permeation buffer since for the model drug propranolol HCl no solubility issues are expected. The pH for dissolution and permeation measurement was chosen to be 7.4, although pH in the small intestine is reported to be one magnitude lower. However, the authors wanted to avoid any issues arising from false efflux phenomena for weak bases as it has been described by Neuhoff et al. [35]. Moreover, applying cell culture compatible biorelevant dissolution media was beyond the scope of this first evaluation of our new apparatus.

The flow rate in the dissolution module was set to 6.5 ml/min for two reasons: first, volumes in the small intestine accessible for dissolution of orally administered drugs are generally regarded to be between 120 and 350 ml for the fasted state and up to 1600 ml for the fed state [65-67]. For the here described setup, an experiment time of 120 or 180 min combined with a flow rate in the dissolution module of 6.5 ml/min yielded total volumes of 780 or 1170 ml and are ranging within the above mentioned physiological limits. The second reason was that concentration of propranolol HCl resulted in a physiologically relevant magnitude. Assuming an administration of 10 mg of propranolol HCl dissolving in 200 to 250 ml of intestinal fluid, a concentration of 40 to

50 μg/ml would be yielded. Maximum concentrations in the apparatus for the 10 mg immediate release tablet of 50 to 60 μg/ml do fit well to the estimated values.

For selection of the flow rates in the permeation module, the determination of P_{app} was essential. For comparison, the P_{app} obtained with a flow rate of 1 ml/min in the FTPC and the P_{app} obtained with static conditions as reported in literature are shown in Table 2.3. Since permeation of highly permeable compounds, such as propranolol HCl, may be limited by stagnant water layers adhering to membrane surfaces [68], a comparable P_{app} for propranolol HCl is of vital interest in order to assure comparable hydrodynamic

	FTPC [cm/s] (n=4)	P_{app} reported in literature [cm/s]
propranolol HCl	$2.5 \pm 0.52 \cdot 10^{-5}$	1.1 ± 0.5 - $4.3 \pm 0.4 \cdot 10^{-5}$ [59]
fluorescein-Na	$4.7 \pm 0.57 \cdot 10^{-7}$	2.1 - 4.0- 5.86 - $6.23 \cdot 10^{-7}$ [10, 11, 69, 70]

Table 2.3. Comparison of apparent permeability values assessed with the FTPC and apparent permeability values reported in literature.

parameters. P_{app} for propranolol found in the FTPC ($2.5 \pm 0.52 \cdot 10^{-5}$ cm/s) nicely falls within the range reported in literature and thus suggests that both assays deliver comparable results for highly permeable compounds and both system exhibit comparable hydro dynamical properties. For low permeability compounds such as fluorescein-Na, a comparable P_{app} ($4.7 \pm 0.57 \cdot 10^{-7}$ cm/s) suggests an intact monolayer throughout 210 min. This statement is furthermore compounded by TEER values still being above 350 $\Omega \cdot cm^2$ and by microscopical observation of the monolayer. Consequently, apical and basolateral flow of 1.00 ml/min was found to be optimal for our purposes since this flow was still high enough to carry over the faster dissolution signal into the apical permeation site and maintained the barrier integrity of the Caco-2 monolayer.

The excipients for the formulation of the tablets have been chosen in order to minimize osmotic stress on the Caco-2 cell monolayer. Therefore, the fraction of soluble excipients was selected to be lower than 30 %. Considering the relative high volume in the dissolution modules, cells are highly unlikely to be negatively affected by osmotic stress due to dilution. Additionally, the excipients have been selected in order to prevent

filter clogging (e.g. no gel formation agents). Furthermore, all used excipients yet have not been reported to affect drug permeation through Caco-2 monolayers.

2.4.2 Assessment of drug permeability and dissolution at different dosage strengths

The 5 and 10 mg propranolol HCl immediate release tablets, as shown in Figure 2.6, yielded a dissolution profile as expected for immediate release tablets. Dissolution profile of the 20 mg propranolol HCl immediate release tablet showed a minor shoulder at the beginning of the experiments (at about 10 min), whereas the dissolution profile of the 5 and 10 mg propranolol HCl can be seen as almost perfectly shaped peak. The shoulder of the 20 mg dosage form could be ascribed to the high content of propranolol HCl in the tablet with a ratio of 20 % (m/m) propranolol HCl, thus dissolution properties of the tablets or slowing down disintegration of the tablet. Dissolution profiles obtained using two 10 mg propranolol HCl tablets instead of one 20 mg tablet did not show such shoulder and thus support this hypothesis (data not shown). Additionally, the saturation solubility of propranolol is reported to be approximately 100,000 μg/ml [61] and this concentration has by far never been reached. Comparing the two profiles obtained from sampling port D and A (Figure 2.6), one can see that the peaks measured at sampling port A were flattened compared to those measured at D, and additionally, a time shift of about 10 min had occurred. Both phenomena, flattening and time shift, are unwanted but inevitable in a flow through system. Undesired convection and mixing processes in the tubes, the stream splitter in the FTPC and time for physical transport from D to A could be seen as causes for that. For that reason, minimizing these influences may be an issue for further optimization of the apparatus since all the factors are affecting the original dissolution signal. Nevertheless, it can be pointed out that the shape and the character of the peaks did not change significantly. The function of the stream splitter is of vital interest for the whole apparatus Therefore, linearity of the stream splitter connecting both modules and being responsible for providing a decreased stream to the permeation module was tested. As the stream splitter divided the incoming 6.5 ml/min stream into a 1.5 ml/min and a 5.0 ml stream, the ratio between mass inserted into the dissolution module and cumulative mass measured at A should be 1/6.5 = 0.1538. Linear regression of cumulative amounts at A versus the

mass of drug in the tablet (see Table 2.4) led to a slope of 0.154 +/-0.007 ($R^2 > 0.999$) and matches quite precisely the theoretical values, thus indicating high precision and high reproducibility of the stream splitter.

	Dosage strength (n=10) [mg]	Amount appeared at A [mg]	Amount permeated [μg] after 60 min	Amount permeated [μg] after 120 min [a]	Ratio [%]
5 mg IR tablet	5.33 ± 0.21	0.68±0.03	1.98 ± 0.42	2.34 ± 0.47	0.343 ± 0.082
10 mg IR tablet	9.70 ± 0.25	1.30 ± 0.02	3.77 ± 0.50	4.23 ± 0.45	0.325 ± 0.039
20 mg IR tablet	19.23 ± 0.54	2.81 ± 0.22	6.82 ± 0.23	8.40 ± 0.32	0.292 ± 0.034
	R^2	0.9998	0.9998	<0.9999	
	Slope	0.1541	0.3462	0.4365	
10 mg ER tablet 4% Eudragit® NE 30D		1.35 ± 0.06		4.55 ± 0.34	0.336 ± 0.040
10 mg ER tablet 8% Eudragit® NE 30D		1.16 ± 0.04		4.40 ± 0.28	0.378 ± 0.037

Table 2.4. Synopsis of data for the IR and the ER tablets (mean ± stdev, n = 4-5). [a] for the extended release tablet, the amount appeared at the respective sampling port (A or B) after 180 min was taken into consideration.

Granted that also the permeation part of the system works linear, the amount which permeated after 120 min and after 60 min through the Caco-2 monolayer should be directly proportional to the dosage strength of the inserted tablet. Therefore, the permeated amounts after 60 and 120 min were correlated with the dosage strength . As it can be seen in Table 2.4, the permeated amount after 60 and 120 min nicely follows the amount of drug inserted in the dissolution module, which is expected since permeation of propranolol as a passively transported compound [62] is linear. Linearity of both regressions are described by a R^2 greater than 0.999 and indicate good reproducibility and high precision of both, the permeation and dissolution measurement. The ratio between the cumulative amount appeared at A at the end of the respective experiments and the final amount of propranolol HCl found in the

basolateral compartment are shown in Table 2.4. These ratios are consistent with data already published in literature, e. g. Miyazaki et al. [53] reported for the high permeable compound caffeine a ratio of 0.396 %.

2.4.3 Assessment of drug permeability and dissolution at different release kinetics

As mentioned before, one can detect in Figure 2.7, a flattening and broadening of the dissolution peaks throughout the passage of the apparatus. Again the shape of the peaks remained the same. Measuring permeation of prolonged release tablets raises the question for the maximum assay time. Small intestinal transit time is generally considered as 3.3 h [71] or is reported to range between 3.5 and 4.5 hours [43]. Viability of Caco-2 cells in KRB and in other HBSS-like buffers is most probably limited to approximately 5 to 7 hours, and consequently limitation in assay time might be irrelevant

Considering the appearance of propranolol HCl in the basolateral compartment, a visible delay was found for the extended release tablets. After 180 min, however, permeated amount was for all different release kinetics fairly equal. For the permeation process in an open system, two variables can be considered as rate determining for permeation in this case. First, the concentration difference according to Fick´s first law – the driving force for diffusion - and second, the contact time of propranolol HCl with the Caco-2 cells – the probability which is given for propranolol to permeate. Considering the total permeated amount, prolongation of release from propranolol HCl tablets is affecting both variables controversially. For that reason, the final mass of the three extended release tablets in the basolateral compartment seemed to be rather equal as it can be seen in Table 2.4. As the retardation increased, slightly increasing ratios were found. Since retardation of propranolol HCl release was only moderate, the differences of the quotients were statistically not significant (one way ANOVA). Higher degrees of retardation will presumably lead to more profound effects on permeation.
In order to compare the profiles of the extended release tablets, mean times for the different sampling ports were calculated according to Eq (3) to Eq (5). If MT_D is plotted against MT_A, linear regression leads to Eq (6) (graph not shown):

$$MT_A = 16.04 \pm 0.60\ min + 0.78 \pm 0.015 \cdot MT_D \qquad R^2 > 0.999 \quad \text{Eq (6)}$$

The intercept of approximately 16 min can be regarded as time for drug release added the time needed for physical transport from the dissolution vessel to the apical compartment of the FTPC. The targeted value for the slope is 1 and is not matched exactly; mixing and convection appeared to affect that value. High linearity ($R^2 > 0.999$) suggests high reproducibility for the transport throughout the apparatus. Figure 2.8 plots both, MT_D and MT_A, versus MT_B. Regression leads to Eq (6) and Eq (7):

$$MT_B = 18.01 \pm 3.50 + 0.85 \pm 0.090 \cdot MT_D \qquad R^2 > 0.99 \quad \text{Eq (7)}$$

$$MT_B = 0.62 \pm 6.28 + 1.08 \pm 0.13 \cdot MT_A \qquad R^2 > 0.99 \quad \text{Eq (8)}$$

The intercept of approximately 18 min in Eq (7) can be attributed to the time of physical transport of the drug from the dissolution vessel to the apical compartment of the FTPC and subsequent permeation. The difference between the intercept of Eq (6) and Eq (7) of approximately 2 min can roughly be estimated as time of permeation. The slope of 0.85 is close to the targeted value of 1; again, mixing and convection might have affected the signal. The intercept of Eq (8) was very small, which was expected. Physical transport can be considered as negligible, since, due to equal tubing, transport from the FTPC to both sampling ports happened within the same time. Here, the calculated slope matched precisely the targeted value of 1. For confirmation, mean time for permeation was calculated according to Eq (9):

$$mean\ time\ for\ permeation:\ MP = P_{app} \cdot monolayer\ thickness \qquad \text{Eq (9)}$$

Assuming a Caco-2 monolayer height of approximately 20-30 μm [72] and a P_{app} of $2.5\ 10^{-5}$ cm/s, MP can roughly be estimated as 80 to 120 s. This value apparently corresponds well with the intercept of Eq (8) and the difference of the intercepts of Eq (6) to Eq (7). In summary, it can be pointed out that using a mean time approach consistent and plausible explanation for the different concentration time profiles were found.

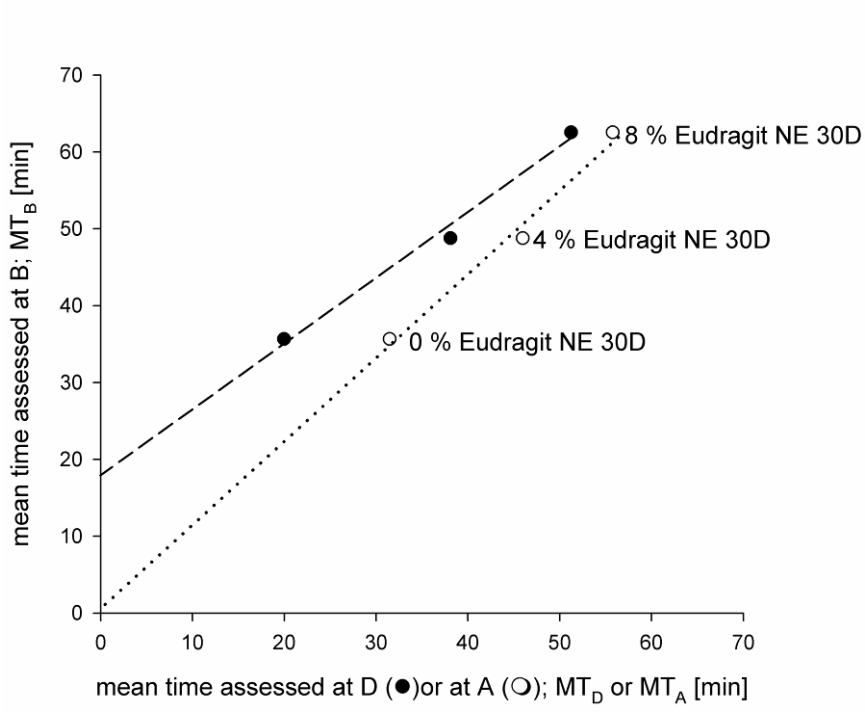

Figure 2.8. Mean times of the three differently retarded tablets assessed from sampling port B are plotted i) against mean times assessed from sampling port D (●) and ii) against mean time assessed from sampling port A (○). R2 < 0.99 for both regression lines.

In contrast to previously published setup, the here described apparatus facilitates the use of complete oral dosage forms with physiologically relevant volumes and drug concentrations. Beyond that, the use of a commonly accepted and extensively described compendial dissolution device entails the advantage of comparability and reliability. A further advantage is obviously the installation of the stream splitter dividing the dissolution and permeation system into two hydrodynamically independent subunits. This facilitates, in comparison to previous setup, the application of pumps in the dissolution module as they are generally recommended for flow though dissolution cells. Thorough drug quantification at various sampling port facilitates a better tracing of drug in the apparatus. Nevertheless, the here described apparatus is lacking a unit mimicking the gastrointestinal pH gradient. Additionally, efforts for performing experiments have been increased.

After all, it is worth to mention that is was not intended to mimic perfectly *in-vivo* dissolution and permeation conditions. Although, it was possible to simulate the estimated volumes of liquid accessible for dissolution and intestinal concentrations, it is up to now not possible to simulate the area accessible for permeation and present *in-*

vivo, which would be deductive for permeation when mimicking the volumes in the gastrointestinal tract. It remains, however, unclear whether results from such perfect *in-vivo* apparatus will achieve adequate results when comparing to the financial efforts which have to be made therefore.

Summarizing these experimental results, one can conclude that our new apparatus was able to monitor permeation through a Caco-2 monolayer of drugs formulated as a solid dosage form. The apparatus showed linear behaviour for increasing dosage strengths of propranolol HCl immediate release tablets and also linear behaviour in terms of retardation of release.

2.5 Conclusion

A successful installation of a promising novel apparatus for the assessment of intestinal permeability of drugs formulated as solid oral dosage forms was realized by combining a flow through Caco-2 permeation cell with a compendial flow though dissolution cell (USP apparatus 4). This combination of established, but so far only separately used research tools yields plausible data, not only for immediate but also for extended release tablets of the BCS class I compound propranolol HCl. Problems arising from applying compendial flow through dissolution devices were adequately solved by a stream splitter. The above shown data provides the basis for more advanced studies on the influence of dosage form, excipients and other factors on the permeation as well as the dissolution process.

3 Computational modeling of the prototype

In order to improve the understanding of flow dynamics, mass transport and permeation processes, concentration time profiles at the various sampling ports have been modeled computationally. The hereby developed program is able to simulate the behavior of drug/solid dosage forms in the apparatus and is a tool for estimating dissolution and permeability *in silico* for the here described apparatus.

The work for this section has been performed in collaboration with the Center of Bioinformatics, Saarland University and is part of the bachelor thesis of Thomas Schackmann. Dr. Dirk Neumann was co-supervisor of this work at the Center of Bioinformatics.

3.1 Introduction

Computational methods are evolving more and more to valuable tools in pharmaceutical sciences. *In silico* modeling of experiments enables the researcher to improve experimental planning and thus to decrease the number of failed experiments. Furthermore, computational modeling allows optimization of experimental conditions with low application of lab resources.

For the here described setup assessing permeability of solid dosage forms, a modeling of the apparatus would specifically facilitate following features: i) detect influences of tubing/hydrodynamical properties on dissolution and permeation signals and hence improve and speed up rational optimization of these parameters, ii) objective classification of drugs into categories such as high and low soluble or high and low permeable, and iii) check plausibility of experimental results.

For the computational simulation, a compartmental model has been defined as shown in Figure 3.1. Drug release and flow rate in the flow through dissolution cell determine the velocity of drug leaving this compartment towards the stream splitter. In the stream splitter, drug molecules have either the possibility to be led to the waster or to be led to the flow through permeation cell (FTPC), whereas the ratio between the flow rates in the flow through dissolution cell and the flow through permeation cell determines this probability. As the drug enters the FTPC, the drug may permeate into the basolateral compartment of the FTPC or if not may be led to the waste.

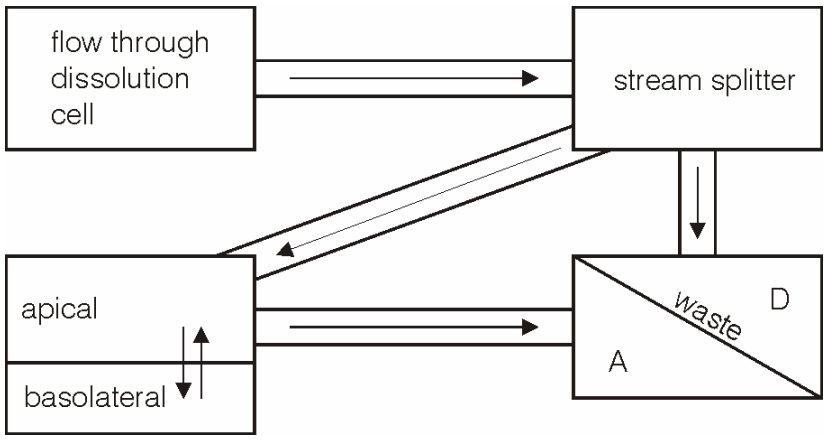

Figure 3.1. Compartmental basic model for the simulation of the apparatus for permeability assessment of solid oral dosage forms.

3.2 Material and methods

In the following, several putative approaches for simulating mass transport and concentrations at the various sampling ports are described.

3.2.1 Basic model of a compartment

A putative approach to model mass transport is to divide the apparatus into several compartments and to monitor the concentration in those compartments. A compartment describes a balanced region in which system parameters are constant or change only insignificantly. The volume flows are calculated by means of mass balance, density distribution and the actual flow rates. Consequently, a compartment is characterized by its volume *V* and the number of molecules/particles inside the compartment resulting in the concentration of molecules/particles in the compartment (Figure 3.2).

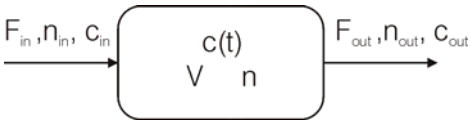

Figure 3.2. Basic model of a compartment. Explanation is in the text body.

Flow rate into the compartment (F_{in}), the amount of molecules/particles entering the compartment (n_{in}), and accordingly the concentration of molecules/particles entering the compartment (c_{in}) and their contrariwise parameters F_{out}, n_{out}, and c_{out} are characterizing the compartment.

3.2.2 Random walk

In order to mimic the broadening of peaks in the apparatus, the *random walk* may be a valuable tool. The basis for the *random walk* can be seen in the area of the Monte Carlo simulation. The one dimensional *random walk* is considered to be a Bernoulli process; more exactly, a series of independent Bernoulli experiments leading to a binomial distribution. A particle allowed to move accordingly in one dimension has the probability to do one step forward of p, whilst the probability to do one step back is $q = 1-p$. When $q = 1/2 = p$, no predominant direction is given. Consequently, the

probability that a particle has made after n steps the way *X* can be calculated according to Eq (10).

$$P(X)=\binom{n}{k} p^k q^{n-k} \qquad \text{Eq (10)}$$

As a consequence, when a particle is allowed to diffuse freely, the mean square distance between the place of origin of the particle and the actual localization is growing proportionally to the time (compare Higuchi square root law for diffusional processes). Particles obeying the rules of a two dimensional *random walk* are allowed to change their location to a new field once per time step as indicated in Figure 3.3.

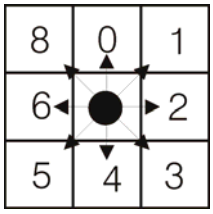

Figure 3.3. Degrees of freedom for a particle in a random walk

Depending on following conditions, the *random walk* of a particle is obeying the following rules.

1.) If the place to be occupied with the next step is free, the move will be allowed and the particle is placed on the desired position.

2.) If the place to be occupied with the next step is already occupied, the move will not be allowed.

3.) If a particle moves to a field named as "leak site", the particle is removed from the matrix. Consequently, the particle is allowed to participate the subsequent transport or other processes.

The above addressed type of random walk is applied for particles exhibiting a certain size and thus demanding a certain unoccupied place to move to. For the modeling of diffusional processes in diluted solutions, case 2.) can be neglected. Case 3 has been implemented in order to simulate the outflow of substance from a compartment, in which the apparatus is segmented. A visual explanation of the *random walk* is illustrated in Figure 3.4. The left depiction shows the start configuration at time zero. The leak site is indicated by the grey fields. The configuration after *n* steps is shown on the left side.

Two particles have already left the matrix, one particle will be removed from the matrix within the next step, and six particles will remain in the matrix at the next step.

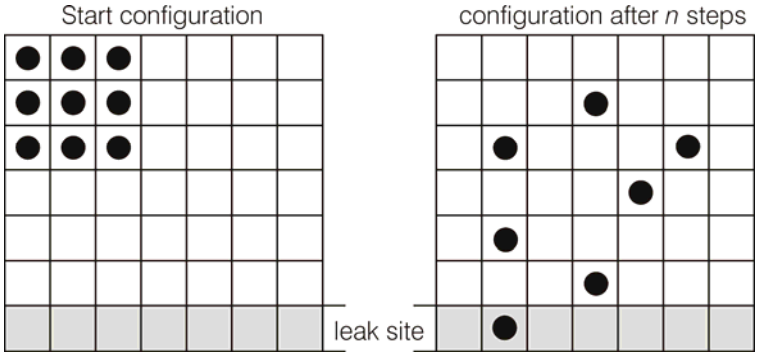

Figure 3.4. Illustration of a two dimensional random walk. Explanation is given in the text body.

3.2.3 Dynamics of flow

A suitable model to describe the behavior of a liquid streaming through a cylindrical tube can be illustrated as follows:

A liquid with a dynamic viscosity η is seeped through tubing with the radius R by a pressure gradient Δp. The cylinder of liquid with radius r and length l experiences at its superficies the frictional force F_R as described by Eq (11),

$$F_R = 2\pi r\, l\, \eta \frac{dv}{dr} \qquad \text{Eq (11)}$$

and at its top surface the pressure force F_P (Eq (12))

$$F_P = \pi r^2 (p_1 - p_2) \qquad \text{Eq (12)}$$

In the steady state, pressure force and frictional force are equalizing each other and from $F_P = F_R$ follows:

$$2\pi r\, l\, \eta \frac{dv}{dr} = \pi r^2 (p_1 - p_2) \Leftrightarrow \frac{dv}{dr} = \frac{\pi r^2 (p_1 - p_2)}{2\pi r\, l\, \eta} \Leftrightarrow \frac{dv}{dr} = \frac{p_1 - p_2}{2\eta\, l} \cdot r \qquad \text{Eq (13)}$$

resulting in a parabolic flow profile according to Figure 3.5.

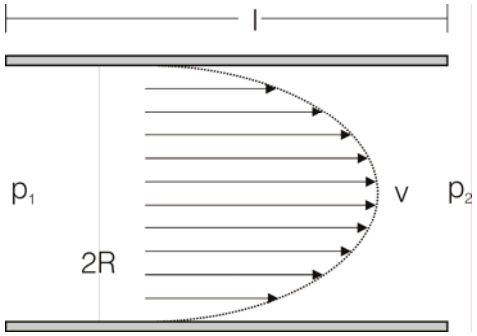

Figure 3.5. Parabolic flow profile through a cylindrical tube.

$$v=v_o-\frac{p_1-p_2}{4\eta l}r^2, \text{ if } v_0=\frac{p_1-p_2}{4\eta l}R^2 \qquad \text{Eq (14)}$$

Through the hollow cylinder between r and $r + dr$, a volume flow dV is streaming

$$dV = 2\pi r\, v(r)dv \qquad \text{Eq (15)}$$

and through the complete tubing

$$dV = \int_0^R 2\pi r\, v(r)dr = \frac{\pi(p_2-p_1)}{8\eta l}R^4 \qquad \text{Eq (16)}$$

, which is known as the law of Hagen-Poiseuille or law of Ohm for voluminal laminar stationary flow of incompressible uniform viscous liquids (Newtonian liquids).

Consequently, the median fluid velocity along the length of the tube v can be calculated as

$$v = \frac{V}{\pi R^2} = \frac{1}{2}v_0 \qquad \text{Eq (17)}$$

Since neither Δp nor η are know parameters of the apparatus, the above described equation has to be converted as follows summarizing both parameters to a simplifying constant c, which can be calculated using the known parameters R, l, and V:

$$V = \frac{\pi\Delta p}{8\eta l}R^4 \Leftrightarrow V = \frac{\Delta p}{\eta}\cdot\frac{\pi R^4}{8l} \Leftrightarrow \frac{\Delta p}{\eta} = \frac{V8l}{\pi R^4} = c \qquad \text{Eq (18)}$$

If a particle is placed in such cylindrical tubing, one can calculate its velocity v_i by means of the distance r_i of the particle from the central point of the cylindrical tubing.

$$v_i = v_o - c\cdot r_i^2 \text{ with } c = \frac{c}{4l} = \frac{\Delta p}{4\eta l} = \frac{2V}{\pi R^4} \qquad \text{Eq (19)}$$

In the following, the dynamic viscosity at 20 °C is considered to be 0.001 Pa/s.

3.2.4 Generation of the dissolution profile

A mathematical function displaying the input of mass/particles into the apparatus is needed. Drug dissolution from solid dosage forms can be described by kinetic models in which the dissolved amount of drug (Q) is a function of the test time, t or Q=f(t). Some analytical definitions of the Q(t) function are commonly used, such as zero order, first order, Hixson-Crowell, Weibull, Higuchi, Baker-Lonsdale, Korsmeyer-Peppas and Hopfenberg models among others. For a comprehensive review on this topic please refer to [73]. Two models are described here.

3.2.4.1 Higuchi model

Higuchi developed in 1961 [74] a model to describe the release from semisolid and solid dosage forms. When assuming a planar and homogenous matrix releasing a drug, Eq (20) can be used to describe the release.

$$f_t = Q = \sqrt{D(2c\text{-}c_s)c_s t} \qquad \text{Eq (20)}$$

, whereas Q is the amount of drug released at time t, c is the initial concentration, c_s is the saturation concentration in the release media, and D displays the diffusions constant according to Einstein of the drug molecule in the matrix. For spherical matrices, Higuchi described drug release as shown in Eq (21).

$$f_t = Q = K_H \cdot t^{\frac{1}{2}} \qquad \text{Eq (21)}$$

, while K_H is the considered as the Higuchi dissolution constant.

3.2.4.2 Weibull model

The empirical exponential equation described by Waloddi Weibull (1887-1979) Eq (22) can be applied to almost all dissolution curves.

$$\frac{M_t}{M_\infty} = M_\infty \cdot [\, 1 - e^{-a \cdot (t-T_i)^b}] \qquad \text{Eq (22)}$$

, whereas M_t is the cumulative amount of drug in solution at time t. T_i describes the delay of release and this case considered to be zero. For $b = 1$, an exponential shaped

curve is yielded; for $b > 1$, a sigmoid shaped curve. For a more detailed study on this particular topic, the author refers to Costa et al. [73].

3.2.4.3 Applying the Weibull function to simulate drug release

The Weibull function was used to calculate the released amount of drug per time step. Prior to the modeling, the cumulative concentration time plots at sampling port D of the 5, 10, and 20 mg immediate release tablets were compared to the Weibull function. If a proper correlation was achieved, an appropriate description of the drug release in the flow through dissolution cell would be highly likely. Figure 3.6 plots both experimental and fitted data. Table 3.1 summarized the respective parameters.

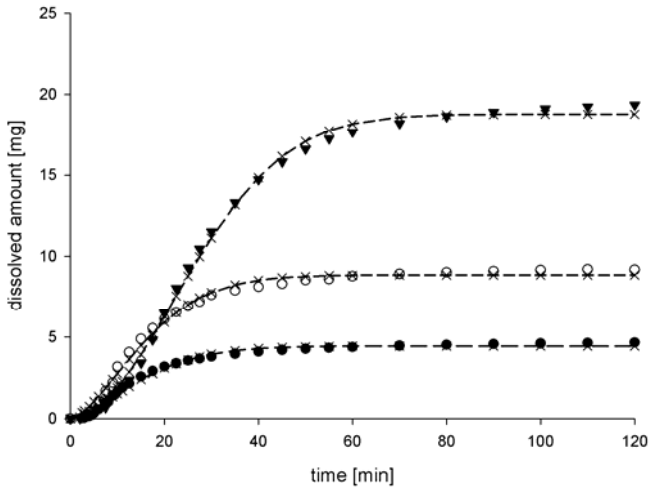

Figure 3.6. Cumulative amount of propranolol HCl detected at sampling port D for the 5 mg (●), 10 mg (○), and the 20 mg (▼) immediate release tablet. Weibull function is indicated by dotted line and thin X. Fitting parameters are summarized in Table 3.1.

The low RMSD and high R^2 in Table 3.1 as well as the obvious good correlation in Figure 3.6 suggests that the Weibull function can be used in this case for modeling the drug release in the flow through dissolution cell.

Table 3.1. Parameters obtained from non linear fitting of the cumulative amount of propranolol HCl detected at sampling port D for the 5 mg, 10 mg, and the 20 mg immediate release tablet against a Weibull function (Eq. (22))

Parameter:	M_∞	a	b	RMSD	R^2
5 mg	4.45	0.0132	1.501	0.156	0.991
10 mg	8.84	0.0101	1.570	0.307	0.993
20 mg	18.78	0.00124	1.936	0.342	0.935

3.2.5 Positioning of the particles in the tubing

When a particle is allowed to leave a compartment into a tubing, they are randomly positioned on various sectors as indicated in Figure 3.7. In the next modeling step, particles closer located to the center are subjected to a faster flow than particles which are more remote from the center (law of Hagen-Poiseuille). As a consequence, this model is used to simulate peak broadening and flattening throughout the passage of the apparatus.

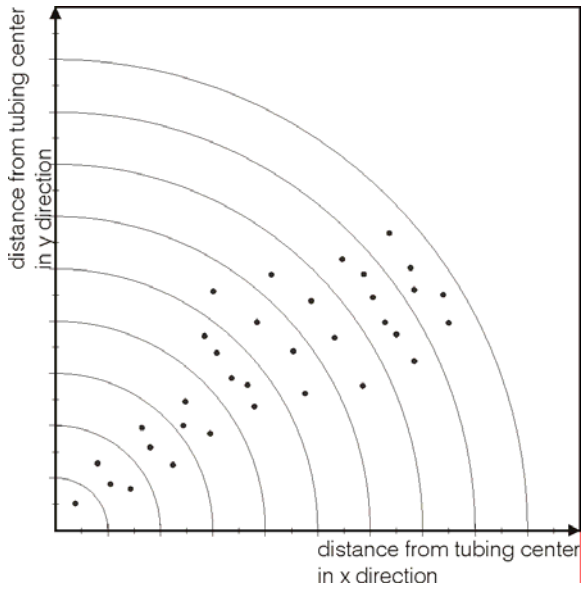

Figure 3.7. Schematical depiction of the particle positioning on the various sectors of a tubing. Black dot indicate randomly placed particles.

3.2.6 Optimizing the computational model

In order to optimize and to calibrate the computational model, a solution with a known volume and concentration was inserted into the flow through dissolution cell and concentration were assessed at sampling ports D and A. Concentration of the solution was 20 μg/ml, volume was 5 ml, so that in total 100 μg propranolol HCl were inserted into the apparatus. The concentration time trends are as shown in Figure 3.8. At sampling port D, 98.53 % of the inserted amount of drug was found, i.e. 98.53 μg. After 60 min, 14.01 % of the initial amount was detected at sampling port A, which is close to the targeted value of 15.38 % when assuming a split ratio of 1 ml/6.5 ml = 15.38 %. To

conclude, a valid data set is with a known dissolution, namely no dissolution since a solution was inserted, was found facilitating proper optimization.

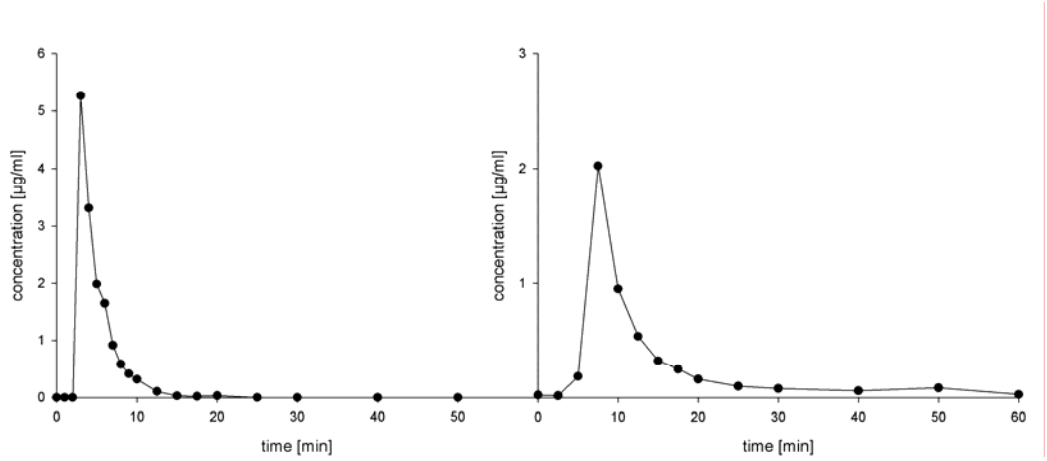

Figure 3.8. Concentration time trends for 5 ml of 20 μg/ml propranolol HCl solution in KRB 7.4 for sampling port D (left plot) and sampling port A (right plot).

As one can see in Figure 3.9, data obtained from the simulation (○) fits nicely to the experimental values (●). Although some differences can be observed, especially around the peak concentrations and at the increasing part of the peak, the simulated data describes the experiment sufficiently. By applying this approach, validity and exactness of the model can be evaluated.

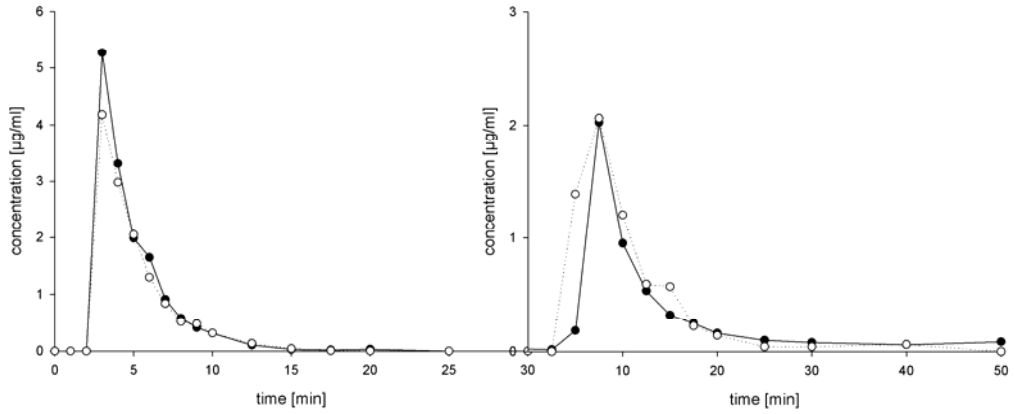

Figure 3.9. Both experimental (○) and simulated (●) data for the 20 μg/ml solution is plotted.

3.2.7 Error function

In order to facilitate comparison of modeled concentrations with measured concentrations at any time point, an error function had to be found. The optimal error function for the 5, 10, and 20 mg immediate release tablet was determined as Eq. (23).

$$f(x) = a \cdot \frac{1}{1+e^{-\frac{x-x_0+b/2}{c}}} \cdot \left[1-\frac{1}{1+e^{-\frac{x-x_0-b/2}{d}}}\right] \qquad \text{Eq (23)}$$

In order to estimate the quality of correlation, the root mean square deviation has been calculated according to Eq. (24)

$$RMSD = \sqrt{\frac{1}{N}\sum_{i=1}^{i=N} e_i^2} \qquad \text{Eq (24)}$$

, whereas N is the number of compared pairs and e_i^2 is the squared error of a pair. Correlation coefficient *R* was calculated according to Bravais-Pearson and squared:

$$R = \frac{\frac{1}{n}\sum_{i=1}^{n}(x_i-x)(y_i-y)}{\sqrt{\frac{1}{n}\sum_{i=1}^{n}(x_i-x)^2} \cdot \sqrt{\frac{1}{n}\sum_{i=1}^{n}(y_i-y)^2}} \qquad \text{Eq (25)}$$

whereas $x = \frac{1}{n}\sum_{i=1}^{n} x_i$ and . $y = \frac{1}{n}\sum_{i=1}^{n} y_i$.

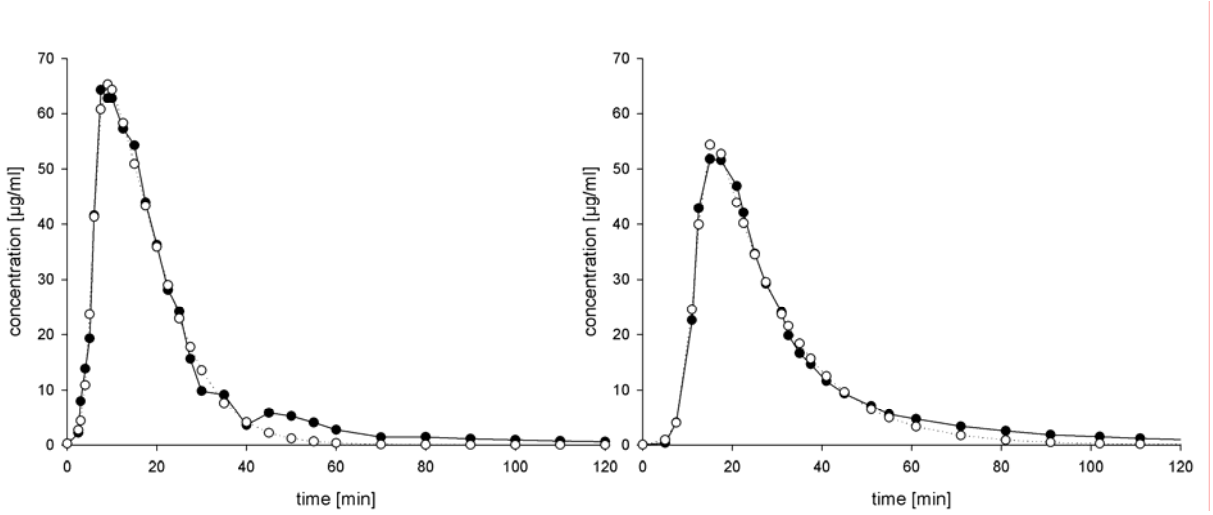

Figure 3.10. Error function (○) and experimental data (●) are plotted exemplarily against time for the 10 mg immediate release tablet for sampling port D (left plot) and sampling port A (right plot).

Figure 3.10 shows exemplarily experimental data and data obtained from Eq (23) with parameters as shown in Table 3.2. In summary, an appropriate equation with sufficient accuracy indicated by low root mean square deviation (RMSD) was found.

Table 3.2. Summary of the parameters for the error function for the sampling port D and A using Eq (22). Route mean square deviation (RMSD) is given in the last column.

	100 µg solution		5 mg IR tablet		10 mg IR tablet		20 mg IR tablet	
	D	A	D	A	D	A	D	A
a	13.91	6.56	131.97	231.57	94.24	447.58	9.46	875.22
b	1.44	96.35	- 5.03	- 20.13	10.46	- 24.36	- 28.07	- 38.34
c	1.15×10^{-8}	2.52×10^{-3}	0.52	1.59	0.98	1.50	0.41	3.77
d	1.83	185.81	10.24	13.23	7.71	1.498	16.63	20.90
x_0	2.72	348.18	1.56	3.70×10^{-4}	11.01	2.01×10^{-4}	-8.84×10^{-11}	3.98×10^{-10}
RMSD	--	--	6.83	2.02	2.26	1.45	1.07	0.82

3.2.8 Modeling the flow through dissolution cell

The flow through cell has been modeled as follows: It consists of one compartment with an exit to a tubing compartment. Within the compartment, a certain number of particles are located and a certain number is allowed to leave the compartment into the tubing compartment per time step. Here, a particle is randomly placed on a sector of the tubing as shown in Figure 3.6 (p. 3-51). For the simulation of dissolution, a Weibull function as addressed in 3.2.4.2 (p 3-49) displayed the best choice and was applied. For future application, dissolution function can be changed in respect to the releasing kinetic of the dosage form.

3.2.9 Modeling the stream splitter

In the simulation, the stream splitter comprises a single compartment and deviates in its properties from the basic compartment model as stated in 3.2.1 (p. 3-45) as follows: The compartment possesses two outlets (F_{waste} and F_{apical}). In the experiments, the 6.5 ml/min stream from the dissolution cell is divided into a 5.5 ml/min stream for the waste and a 1.0 ml/min stream for the apical compartment. For simulation, a random number $p \in [0; 6.5]$ is determined for each particle currently located in the stream splitter and for $p \leq 1$, the particle is allowed to proceed to the permeation cell. For r $1 < p \leq 6.5$, the particle is removed from the simulation. The stream splitter is moreover simulated as space and the movement of particle within this space is modeled by means of a random walk (section 3.2.2, p. 3-45)

3.3 Results and discussion

Hitherto, simulated concentrations time profiles will be exemplarily shown for the 20 mg immediate release propranolol HCl tablet. Since this project of modeling the prototype is still ongoing, data shown is considered to be preliminary.

In Figure 3.11, simulated data for sampling port D is compared to experimental data by plotting both in one graph. The simulated data describes properly the time of the maximum concentration, whereas the peak height is in the simulation with 80 μg/ml too low. However, taking the standard deviation of the experimental data into account, the simulation only slightly failed. The rise to the peak and the time shift is predicted correctly. The shoulder in the experimental data is not predicted, since the shoulder can be regarded as an experimental artifact as already stated in 2.4.2 (p 2-36 and ff.) and

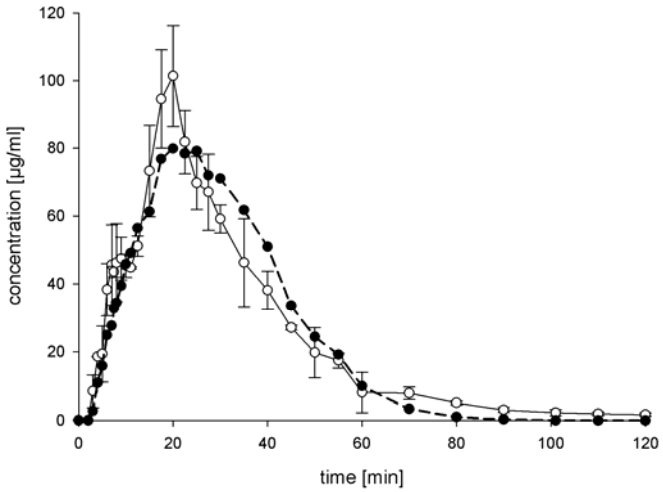

Figure 3.11. Experimental data from sampling port D of a 20 mg immediate release tablet (○) and simulated data (●, dashed line) is plotted against time.

prediction by a computational model is highly not expected. The concentration decrease at sampling port D is simulated to be slightly slower; however, simulated data keeps always close to the experimental data with respect to the error bars. The terminal part of both concentrations time trends are rather similar. In order to provide objective comparison between the calculated and the experimental data set, Figure 3.12 plots them against each other. Non linear regression led to the following equation: (mean ± standard error)

$$c_{\text{sim data}} = (0.9296 \pm 0.0550) \cdot c_{\text{exp data}} + (0.2460 \pm 2.5097) \; ; \; R^2 = 0.96$$

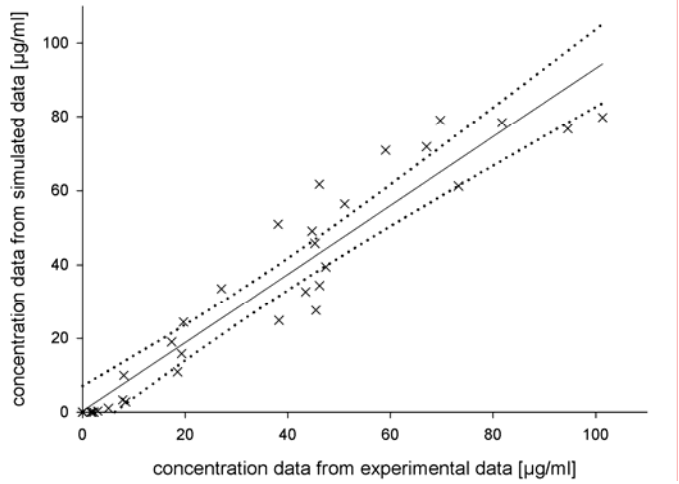

Figure 3.12. Simulated data is plotted pairwisely versus experimental data for sampling port **D**. Correlation coefficient of the linear regression line was calculated as 0.96. Dotted lines indicate the 99 % confidence interval.

RMSD was calculated as 9.167. Slope of the regression line is close to one. Apparently, data points scatter randomly around the regression and no systematic error is visible suggesting that the simulation is able to calculate the concentration time trends for sampling port D for the 20 mg immediate release tablet correctly.

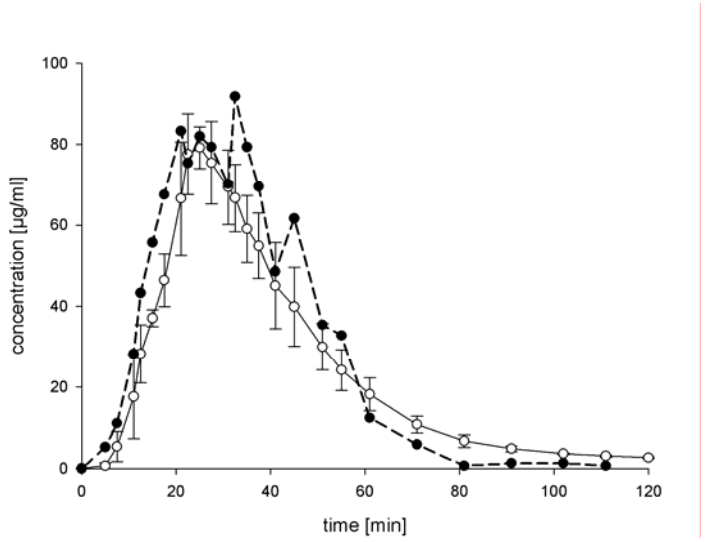

Figure 3.13. Experimental data from sampling port **A** of a 20 mg immediate release tablet (○) and simulated data (●, dashed line) is plotted against time.

The calculation of concentration time trends at sampling port A is considered to be more difficult. Not only drug release from the dosage form and the escape of drug out of the flow through dissolution cell has to taken into consideration, but also the stream splitter and peak broadening and flattening as a function of tubing length and diameter are affecting the shape of the peak. Figure 3.13 plots experimental and

calculated concentration in one plot. It is clearly visible that the simulated concentrations show some scattering between 30 to 60 min. This, however, is attributed to the lack of a smoothing algorithm in the simulation. This may be a subject of optimization in the future. Nevertheless, the shape of the peak is described correctly, peak concentrations are both at the same time and at the same concentration of approximately 80 μg/ml.

Figure 3.14 plots both data sets as pairs against each other. Non linear regression led to the following equation:

$$c_{\text{sim data}} = (1.1478 \pm 0.0671) \cdot c_{\text{exp data}} + (1.7207 \pm 2.9532)\ ;\ R^2 = 0.97$$

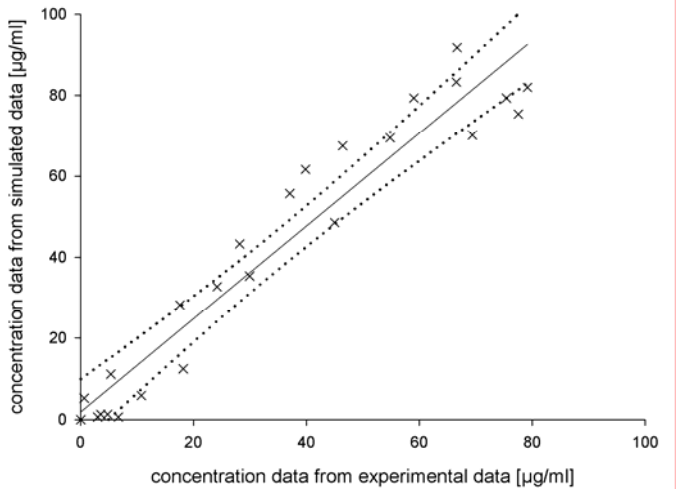

Figure 3.14. Simulated data is plotted pairwisely versus experimental data for sampling port A. Correlation coefficient of the linear regression line was calculated as 0.97. Dotted lines indicate the 99 % confidence interval.

RMSD was calculated as 11.753 and is slightly higher than for sampling port D. Also, slope of the regression is not that close than for sampling port D. Nevertheless, the data points appear to scatter randomly around the regression line indicating the lack of a systematic error.

Data for sampling port B representing the permeation process is yet not available. However, after having made the important milestone with the successful calculation of the concentration time profile at sampling port D and A, simulating sampling port B will be straightforward since no convectional processes have to be considered. It is planned to give a *in silico* particle located in the apical compartment of the flow through permeation cell a probability to enter the basolateral compartment, i.e.

to permeate, or the leave the FTPC into the waste, while the probability will be calculated according to the Caco-2 permeability of the compound.

3.4 Conclusion

From the above shown data, one can conclude that a promising first step for a computational modeling of the dissolution - permeation prototype has been done. The concentration time trends at two sampling ports have been calculated correctly and also peak broadening and flattening from sampling port D to A have been calculated correctly.

The next step of this project will be to implement a permeation step into the simulator and to test weather the simulator is predicting the concentration time trends and permeation of the propranolol HCl extended release tablets.

4 Automation

One major conclusion of the proof of concept study in chapter 2 was to automate sampling and quantification at the various sampling ports in order to increase throughput and to decrease manpower consumption. Sequential injection technique was found to be an optimal tool because of its simplicity, versatility, and robustness.

Parts of this section have been published in

Motz SA, Klimundová J, Schäfer U, Balbach S, Eichinger T, Solich P, Lehr CM. Automated measurement of dissolution and permeation of propranolol HCl tablets using sequential injection analysis, Analytica Chimica Acta, Acta 581 (2007) pp. 174–180, [75].

4.1 Introduction

Several apparatus for simultaneous measurement of dissolution and permeation through Caco-2 have been established in the past years [39, 50, 52-55], and auspicious results were obtained. Combining two *in vitro*- methods to forecast behavior of solid oral dosage forms when administered *in vivo* appears to be a promising tool to obtain more vital information of the *in vivo*- performance compared to deploying both assays separately. Generally speaking, these apparatuses can be divided into two classes. Ginski et al. [76] and Kataoka et al. [56] reported on a closed dissolution and permeation system, either using the USP apparatus 2 or a specially designed dissolution vessel. In contrast, Miyazaki et al. [52-55] and our group are using open systems for dissolution and permeation assessment. Whereas Miyazaki et al. is using glass or plastic vessels of different sizes, our group applies the USP apparatus 4 for dissolution measurement. However, simultaneous analysis of dissolution and permeation remains tedious and labor consumptive; not only the use of viable cells but also manual sampling and analysis with HPLC definitely limits the throughput. HPLC based quantification can be considered as time consumptive and also as money consumptive, since expensive mobile phase, vials and further equipment have to be used. In addition, organic solvents wastage bears issues concerning environmental pollution. In most cases, however, selectivity provided by HPLC is not necessary if only one active pharmaceutical ingredient (API) is used and if sensitive and/or selective UV or fluorimetric detection are possible.

Sequential injection analysis (SIA) and its predecessor flow injection analysis (FIA), which has been developed in 1975 [77], have been continuously applied in pharmaceutical sciences and further improved [78-80]. SIA facilitates fast and reproducible on-line sample handling such as sample aspiration, sample dilution, solid phase extraction and many other applications [81]. Additionally, SIA permits - in combination with fluorescence or UV-detectors - fast and reliable quantification of many pharmaceutically applied compounds [78, 79]. Beyond that, SIA is described to be a flexible, robust and a highly versatile tool for automating sampling and sample treating. For these reasons, sequential injection analysis appears to be an ideal solution for our purposes, especially when high sampling frequency and rapid online quantification is of

vital interest. Several groups reported to employ SIA for automating dissolution systems using both fluorimetric [82-84] and UV [85-87] detection. The detection limit of fluorimetric quantification was comparable to quantification limits provided by HPLC based methods (30 ng ml^{-1} for ergotamine tartrate [83] and 50 ng ml^{-1} for acetylsalicylic acid [82]).

Test substance for combined measurement of dissolution and permeation was propranolol HCl. It was chosen because of its favorable biopharmaceutical properties exhibiting high solubility and high permeability [59] and is therefore assigned to the biopharmaceutical classification system class 1 [46]. Beyond that, quantification of propranolol HCl is easily accessible using either HPLC method with UV detection or fluorescence detection. Taking into account that for combined measurement of dissolution and permeation relatively high concentrations in the dissolution part and relatively low concentration in the permeation part have to be measured, fluorimetric detection would be an appropriate way to quantify in a SIA based system dissolved and permeated propranolol HCl in the matrix Krebs-Ringer Buffer.

Not only the usually rather time consumptive manual sampling procedure was subjected to optimization, but also lag time and dead volumes were found to be still rather large in the apparatus described previously in Section 0. In order to minimize those issues, inner diameters of all tubing were chosen to be as minimal as possible. In addition, the volume of the acceptor compartment was decreased. Changes related to these modifications will be discussed subsequently.

4.2 Materials and Methods

4.2.1 Methods

Cell culture conditions were the same as described in 2.2.2. 10 mg immediate release test tablets were as described in 2.2.4. KRB was prepared according to 2.2.5.

4.2.2 SIA system

The SIA system consisted of the FIAlab 3500 (FIAlab instruments, WA, USA) implemented with a 2.5 ml piston pump, a peristaltic pump and an eight port multiposition valve. Standards were aspirated by means of an autosampler (Cetac ASX 260, NE, USA). Fluorimetric detection was performed with the FIAlab fluorescence detector PMT-FL. Integration time was set to 100 msec, scan rate was adjusted to 2.0 Hz. An UV light source was purchased from Mikropack (type D-2000, Ostfildern, GE), and the light source was linked with the fluorescence detector with a fiber optic cable. An excitation filter (λ_{exc} = 260 nm, 10 nm full width half maximum, Andover Corporation, NH, USA) and no emission filter was used. Software was FIAlab for Windows® version 5.9.192. The program codes for the respective sampling ports are given in section 8.3.1 (main), 8.3.2 (D), 8.3.3 (A), and 8.3.4 (B) (pages 8-111 - 8-114). The configuration of the autosampler for the aspiration of standard solution from the standard tray was as given in Table 8.1.

4.2.3 The automated apparatus for combined dissolution and permeation measurement

The automated apparatus is schematically depicted in Figure 4.1, and a photograph is shown in Figure 4.2. The apparatus for combined measurement of dissolution and permeation can be divided into two modules: on the left the dissolution module with the flow through dissolution cell (USP apparatus 4, Sotax CE1, Sotax,

Lörrach, GE) and on the lower right side the permeation module with the flow through permeation cell, whereas both modules are connected by

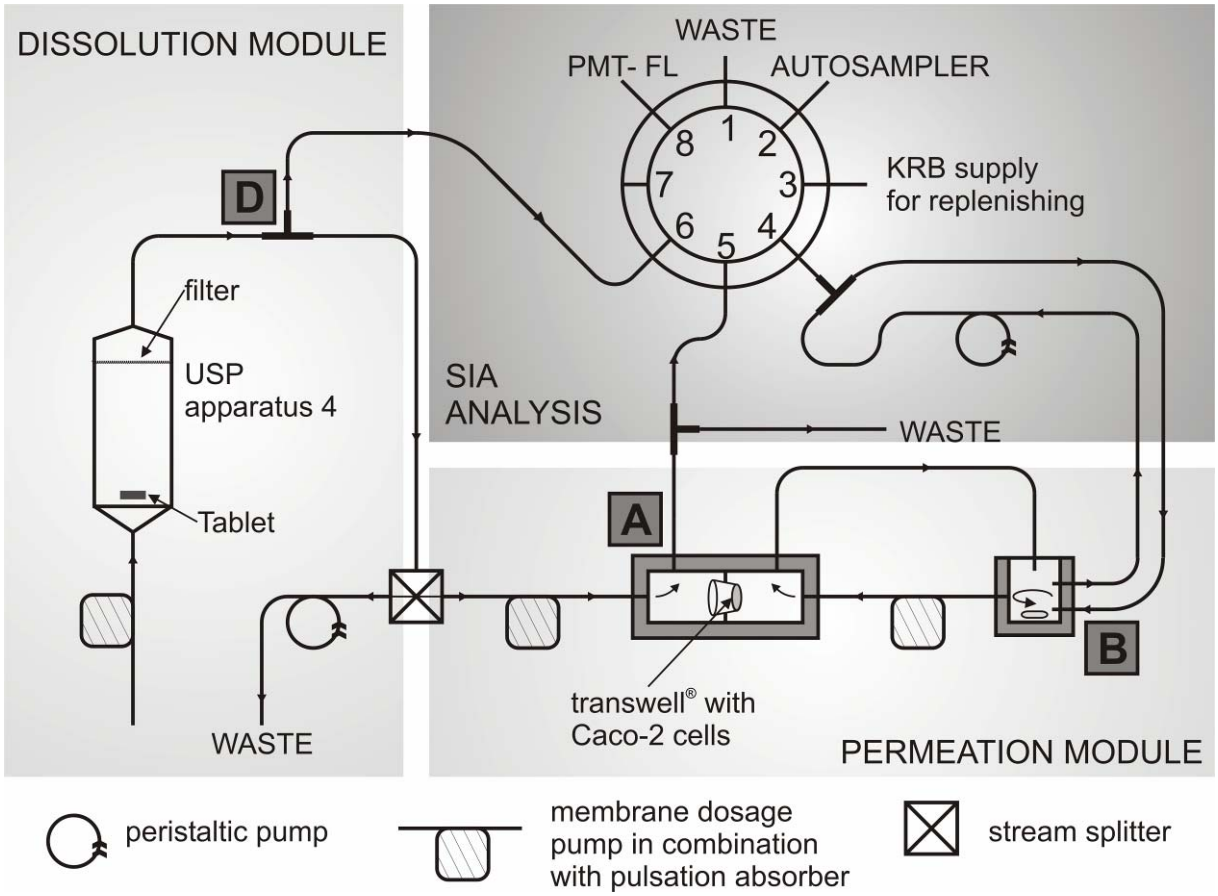

Figure 4.1. Schematic depiction of the automated apparatus for simultaneous measurement of dissolution and permeation. Sampling ports are indicated with capital letter, D for **D**issolution, A for **A**pical and B for **B**asolateral. The multipositional valve and its port assignment was as follows. Port 1 was connected with the waste; port 2 with the autosampler for aspirating the standards solutions; port 3 was connected to the KRB supply for replenishing the volumes taken from the basolateral compartment. Port 8 was connected to the fluorescence detector PMT-FL and ports 4, 5 and 6 are assigned to sampling ports B, A and D, respectively.

means of a stream splitter providing appropriate low flow rates for the permeation module. The permeation module can be subdivided into two compartments: the open apical and the closed, circulating basolateral compartment, which comprises a stirred reservoir with a volume of 1.0 ml KRB and a measurement loop to the multipositional valve. Flow rate in the dissolution module was adjusted to 6.5 ml min^{-1} and to 1.0 ml min^{-1} in the permeation module, respectively. Three points of sampling within the apparatus are indicated in Figure 4.1 with the capital letters D, A and B. Samples taken at sampling port D, directly after the flow through dissolution cell, are providing the

original dissolution signal. Concentrations at sampling port A, located at the apical part of the permeation module, exhibit the concentration in contact with the apical side of the Caco-2 monolayer. Concentrations measured at sampling port B allow the calculation of the amount permeated to the basolateral side of the Caco-2 monolayer (volume of the complete basolateral module 5.25 ml).

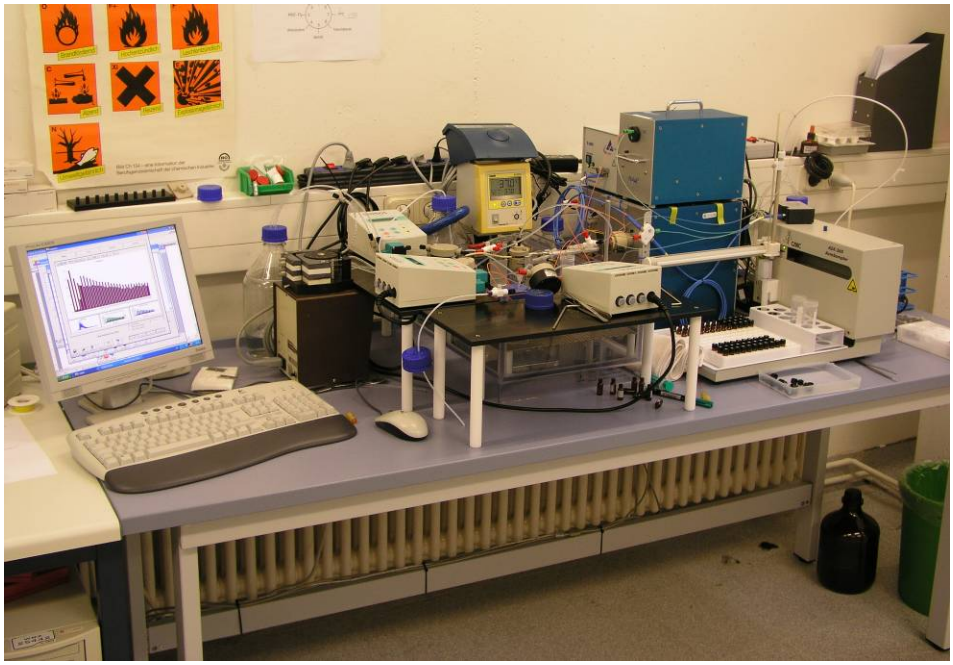

Figure 4.2. Photograph of the automated setup. The SIA devices are placed on the right side, the water bath in the middle, and the controlling computer on the left side.

The interface between the apparatus for combined dissolution/permeation apparatus measurement and the SIA system was as follows. At sampling port D and A, a tubing was used to directly connect the stream containing the dissolved drug with the multiposition valve. Volumes of the connecting tubing were 15 μl for D and 60 μl for A. In order to assure that correct concentrations were assessed, this connection was washed prior to each real measurement at sampling port D by aspirating 50 μl, and at sampling port A by aspirating 100 μl, respectively. Since the aspirated volumes compared to the flow rate at D (6.5 ml·min^{-1}) are sufficiently low, no replenishment of the withdrawn sample was necessary. Also, at sampling port A, no replenishment was required since the stream is subsequently going to waste. The basolateral vessel posing the reservoir for the closed basolateral compartment was connected to the multiposition valve by means of a measurement circuit driven by the peristaltic pump of

the FIAlab 3500 system (flow = 0.9 ml·min^{-1}). The dead volume of the connection between the measurement circuit and the multipositional valve was approximately 6 µl. Prior to aspiration of the real sample, 25 µl were aspirated in order to wash the T-connector and were subsequently discarded. Post washing, 50 µl were aspirated for the fluorimetric analysis, and afterwards 75 µl of KRB were dispensed back into the measurement circuit.

All tubing of the apparatus for combined measurement of dissolution and permeation and the SIA system were made of Teflon® to minimize adsorption; inner diameter of tubing in the dissolution module was 1.55 mm and 1.0 mm in the permeation module (Upchurch, WA, USA). Connection tubing to the multipositional valve had an inner diameter of 0.50 mm. The flow through dissolution cell was equipped with filters (type GF/D, Whatman International Ltd, Maidstone, UK) preventing undissolved drug and excipients from leaving the dissolution module. The flow through permeation cell was the same as described in section 1. The basolateral reservoir vessel was made of Polyetheretherketone (PEEK) (for details see Figure 8.6). The basolateral vessel was magnetically stirred (MINI 07, H+P, Oberschleißheim, GE). Prior to each experiment, all media were properly degassed by stirring 10 minutes under reduced air pressure. Before inserting in the apparatus, Caco-2 cells were washed twice with KRB and were allowed to equilibrate for at least 30 min in KRB at 37 °C. Then, TEER was measured and the Transwell® with a cell monolayer exceeding 350 Ω·cm^2 was inserted into the flow through permeation cell. Subsequently, the flow was adjusted to 1.0 ml·min^{-1} and cells were equilibrated for another 10 min before the experiment was started.

Cumulative amount appeared at sampling port D and A has been calculated from the measured concentrations using Eq (26), which is derived from the trapezoidal rule:

$$cumulative\ amount = \sum_{i=1}^{n-1} [\frac{c(t_{i+1})+ct_i}{2} \cdot (t_{i+1}-t_i)] \cdot FLOW \qquad \text{Eq (26)}$$

whereas $c(t)$ is the concentration [µg ml^{-1}] measured at time t [min] and $c(t_{i+1})$ is the concentration measured at time t_{i+1}. FLOW designates the flow rate [ml·min^{-1}] in the respective module.

As the apparent permeability (P_{app}) is generally defined as flux over donor concentration, apparent permeability was calculated from the concentrations assessed at sampling port A and at B. Flux was estimated by interpolation using Eq (27).

$$Flux\ at\ measurement\ point\ n:\ Flux_n = \frac{mass_{n+1}\text{-}mass_{n-1}}{t_{n+1}\text{-}t_{n-1}} \qquad \text{Eq (27)}$$

$Mass_{n+1}$ is the mass permeated at measurement point $n+1$ and t_{n+1} is the time of the measurement point $n+1$. $Mass_{n-1}$ is the mass of the measurement before n, t is the time of the measurement point before n. The apical concentration at the respective time points were calculated using linear regression between two measurement points at A.

4.3 Results and discussion

4.3.1 Calibration

Signal of native fluorescence of propranolol HCl was sufficiently strong for direct detection in the matrix KRB. Experiments with placebo tablets (the API propranolol HCl was replaced by lactose) led to signals comparable to those obtained from blank KRB, thus indicating that no interference of excipients with the analysis occurred. Standards were provided by aspiration from the autosampler, and peak height was correlated with standard concentrations. Flow rate of the analyte through in the PMT-FL was found to be ideal in terms of reproducibility and signal height at 50 μl s^{-1}. Since concentrations at sampling ports D, A and B differ strongly, different aspiration volumes were found to be optimal. Sampling port D and A exhibiting sampling ports with the highest concentration had an aspiration volume of 25 μl; however, sample aspiration volume at port B, where only low concentration are expected, was increased to 50 μl to assure sufficient sensitivity at low concentrations. The lower aspiration volume was shown to yield lower fluorescent signals combined with an increased linear part of the regression line. Consequently, higher aspiration volumes caused higher fluorescent signals and led to earlier non linear behavior. Nevertheless, it was not feasible by decreasing the

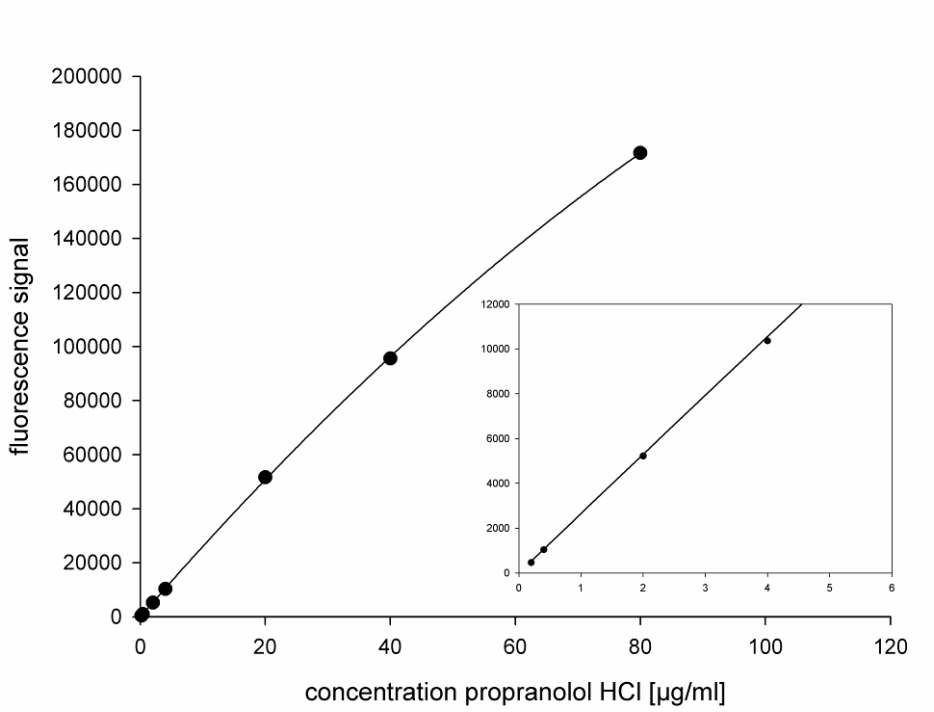

Figure 4.3. First order calibration of propranolol with fluorescence detection using the PMT-FL. The smaller graph shows the regression for the lower standards.

aspiration volume to 25 µl to fit the calibration curve to a straight line as it can straight line as it can be seen in Figure 4.3, and thus calibration for sampling port D and A was performed with an first order polynomial equation. For 50 µl injection, calibration was performed with five standard solutions and for 25 µl injection with seven standards. Standard concentration for 50 µl injection were 0.05, 0.2, 0.4, 2.0, 4.0 µg ml^{-1} of propranolol HCl. Standards concentrations for 25 µl injection were 0.2, 0.4, 2.0, 4.0, 20, 40, 80 µg ml^{-1} of propranolol HCl. All standards were measured in sextuple. Prior to regression, blank values obtained injecting KRB were subtracted. Relative standard deviation for the 50 µl injection at the lowest standard was 2.35 % (n = 6) and at the highest standard 1.63 % (n = 6). Linear regression led to the following equation: $y = 4246.8 \cdot c - 44.9$ (y = fluorescence signal, c = concentration [µg ml^{-1}], $R^2 > 0.999$). Limit of quantification was calculated as 0.04 µg ml^{-1} (10σ); limit of detection 0.02 µg ml^{-1} (3σ). Relative standard deviation at the lowest standard concentration for 25 µl injection was 2.82 % (n = 6) and for the highest standard concentration 3.09 % (n = 6). Regression led to a first order polynomial equation (see Figure 4.3): $y = - 6.55 \cdot c^2 + 2669.1 \cdot c - 18.7$ (y = fluorescence signal, c = concentration [µg ml^{-1}], $R^2 > 0.9999$). The values for quantification and detection limit are consistent with values

found for comparable substances in literature [82, 83]. In conclusion, it can be pointed out that an accurate and sensitive quantification method for propranolol HCl was found and no interference with excipients occurred.

4.3.2 Automated measurement of dissolution and permeation

Sampling and analysis were performed alternating at sampling port D and A, intermitted by a measurement at sampling port B after every third loop of measurement at D and A. Sampling together with quantification took 0.7 min at sampling port D, 0.9 min at A and 1.3 min at B. Time for sampling at port B lasted longer because of the time needed for replenishing KRB. Sampling frequency of approximately 60 h^{-1}

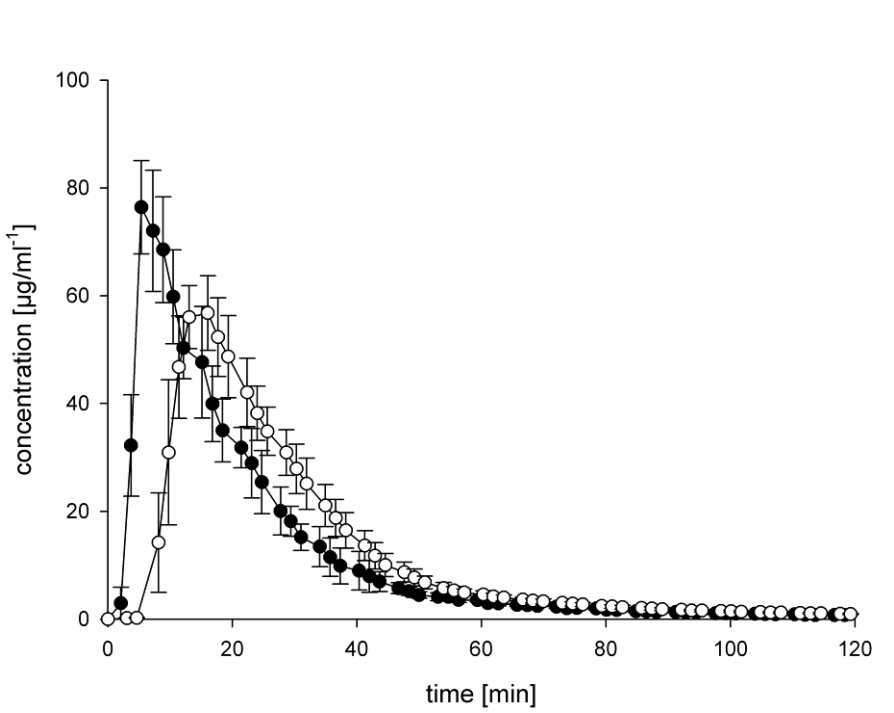

Figure 4.4. Closed circles (●) represent the propranolol HCl concentrations measured at sampling port D and open circles (○) the concentration assessed at A for a 10 mg immediate release tablet (n = 7, all values as mean ± stdev).

60 h^{-1} was found to be sufficiently high, although more measurement point at early time points of the experiments might be desirable. Figure 4.4 plots the concentration measured at sampling port D and sampling port A against time. Concentration

assessed at sampling port D yielded higher concentrations than at sampling port A since convectional mixing and dilution throughout the passage of the apparatus broadened the peak and decreased peak height. In addition, a time shift between the peak maxima at D and at A of approximately 7.5 min was detected.

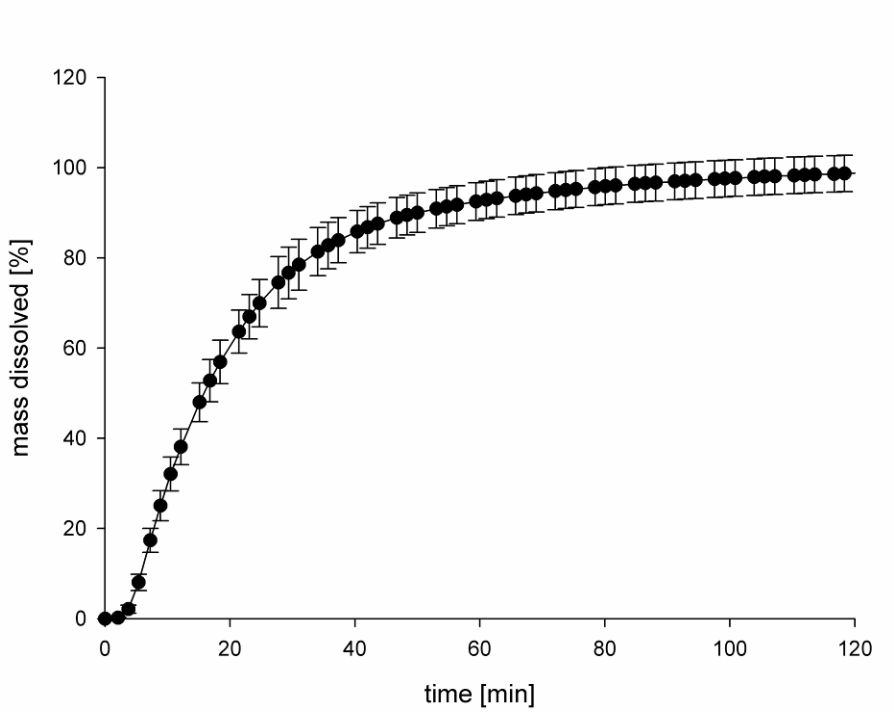

Figure 4.5. Cumulative mass of propranolol HCl calculated according to Eq (26) from the concentration obtained at sampling port D is plotted vs. time. After 120 min tablets released 98.7 ± 4.0 % mg of the labelled amount (n = 7, all values as mean ± stdev)

Figure 4.5 plots the percentage of released propranolol HCl calculated according to Eq (22) against time. An almost complete release of 98.7 ± 4.0 % of the labeled amount of propranolol HCl could be detected, thus being a strong indicator for correct calibration. Cumulative amount appeared at A yielded a mass of 1.48 mg at 120 min (curve not shown). Since the stream splitter is dividing the incoming 6.5 ml min^{-1} stream from the dissolution device into an 1.0 ml min^{-1} for the apical compartment and a waste stream, the mass appeared at A should be 1 / 6.5 = 15.4 % of the amount appeared at D. The observed value of 15.5 % matched sufficiently precise the targeted value, indicating that flow rates were adjusted correctly and that the stream splitter worked properly. Figure 4.6 shows on the primary ordinate the concentration measured at sampling port A vs. time, hence the concentration which was led over the Caco-2 monolayer. The amount of propranolol HCl measured in the basolateral compartment

against time is plotted on the secondary axis. It is evident that the greatest increase of propranolol HCl in the basolateral compartment is accompanied with the maximum peak concentrations at sampling port A.

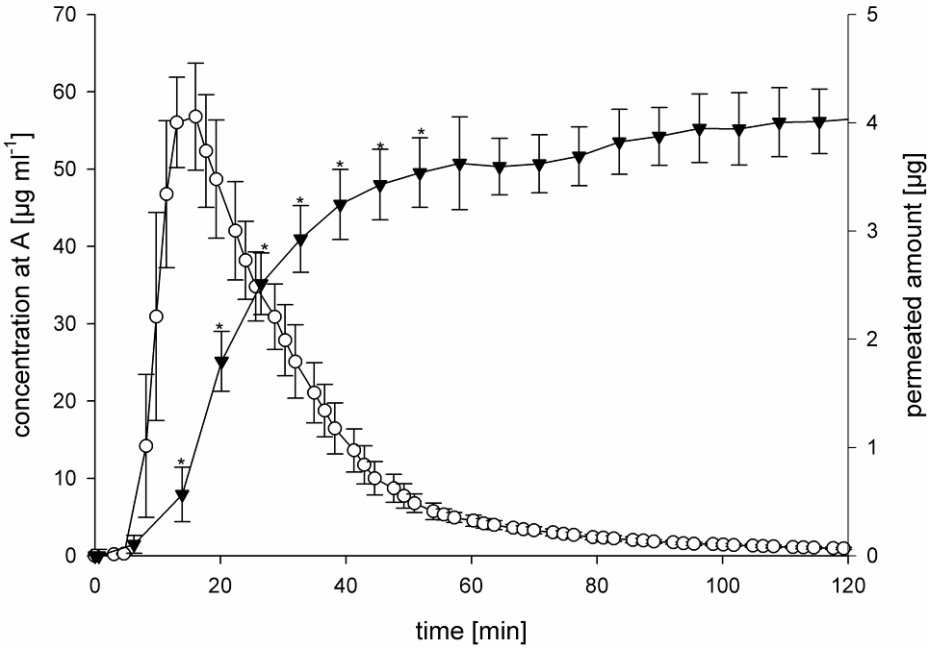

Figure 4.6. Open circles (○) represent the concentration measured at A (primary ordinate), triangles down (▼) represent the permeated amount of propranolol HCl derived from concentration measured in the basolateral compartment (secondary ordinate). Asterisks indicate the values from the P_{app} value was calculated (n = 7, all values as mean ± stdev).

After 120 min, a total amount of propranolol of 4.07 ± 0.37 μg (n = 7) was detected in the basolateral compartment. When forming the ratio between the amount which permeated and the cumulative amount appeared at A, a value of 0.275 % is found. This value is comparable with values found in literature for high permeability compounds [53]. According to Eq (27), apparent permeability (P_{app}) was calculated from seven time points as indicated with asterisks in Figure 4.6. P_{app} was estimated as $2.61 \pm 0.63\ 10^{-5}$ cm·s^{-1} (mean of 7 independent calculations). Vogelpoel et al. [59] stated that P_{app} values for propranolol HCl through Caco-2 cell monolayers are reported in literature to be in a range of $1.12 \pm 0.05 \cdot 10^{-5}$ to $4.30 \pm 0.36 \cdot 10^{-5}$ cm·s^{-1}. Therefore, it can be pointed out that the value found with the here described apparatus is consistent, either with previous experiments of the authors [39] and with literature.

Caco-2 monolayers retained their integrity throughout the experiments indicated by a TEER before and after each experiment being above 350 $\Omega \cdot cm^2$ with blank filter subtracted.

4.3.3 Comparison between manual sampling and automated sampling

Synopses of data obtained from manual sampling with quantification by HPLC as described in [39] and data obtained from the above described SIA method are graphically juxtaposed in Figure 4.7. The same propranolol HCl 10 mg immediate release tablets of the same batch were used for both sets of experiments. Before interpreting the data, it is worth to mention that aside from automation the apparatus for combined measurement of dissolution and permeation underwent some further changes compared to the one previously described. The inner diameter of the tubing and the length of the tubing were decreased wherever feasible since lag time and time shift were found to be improvable. In addition, the volume of the basolateral compartment was decreased in order to be able to measure higher concentrations. As it can be seen in Figure 4.7, concentration trends at sampling port A and B obtained from either manual or automated sample processing appear to be comparable. The optimized and automated setup yielded at sampling port D higher peak maximum concentrations of approximately 75 $\mu g\ ml^{-1}$ vs. 65 $\mu g\ ml^{-1}$ of the previously described apparatus. This may be contributed to the shorter and thinner tubing and to higher resolution due to more sampling points. Maximum concentrations derived from sampling port A behave similar (57 $\mu g\ ml^{-1}$ vs. 50 $\mu g\ ml^{-1}$). Standard deviation of the automated apparatus seemed to increase slightly. This phenomenon might be due to the higher sampling volumes of the not automated apparatus where 500 μl of sample were withdrawn and analyzed (compared to 25 μl at the SIA). Sampling higher volumes will average the concentration variation within this volume and thus apparently decrease variation of concentrations. Aside from that, peak shape was not significantly affected. By means of the automation, sampling frequency was increased nearly by the factor two compared to manual sampling. At the peak concentrations, however, higher

sampling frequency for the SIA system would be appreciated. This might be subject for

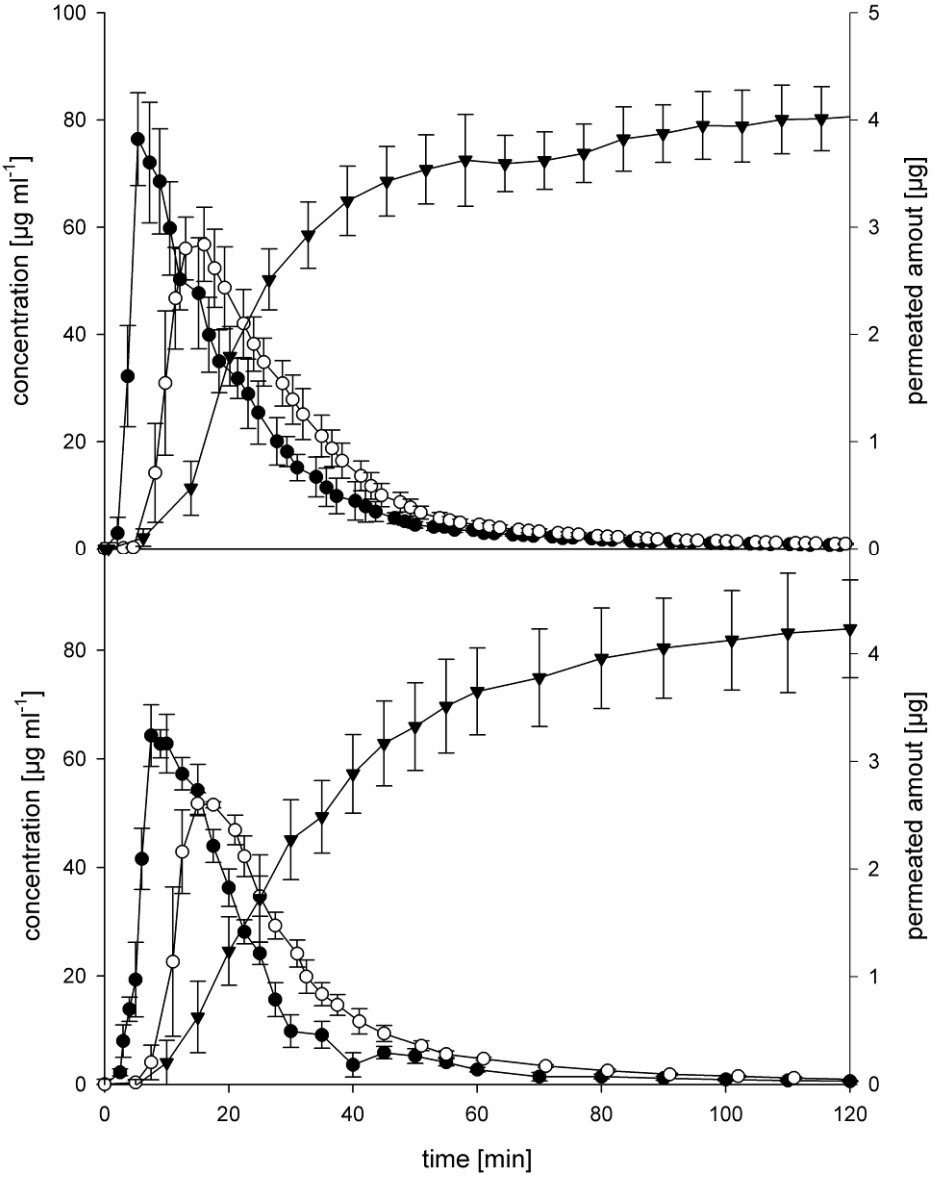

Figure 4.7. Comparison between manual sampling and analysis via HPLC (lower diagram) (n=5) and automated sampling and fluorescence detection using SIA (upper diagram) (n=7). Closed circles (●) represent the concentrations at D, open circles (○) the concentration measured at A (both primary ordinate) and triangles down (▼) represent the permeated amount of propranolol HCl (secondary ordinate).

further optimization. The concentration trend measured in the basolateral compartment changed only slightly. It appears that for the newer setup a plateau is reached earlier (Figure 4.7). The reason for that might be – additionally to shorter tubing – the decreased volumes in the basolateral compartment (5.25 ml compared to 10.5 ml). However, after 120 min, a comparable amount of propranolol HCl in the basolateral compartment was detected (4.07 ± 0.37 μg for SIA vs. 4.23 ± 0.45 μg for manually and

HPLC treated samples, respectively). Additionally, decreased standard deviations of the concentrations for the automated setup were found for concentrations measured at B; however sample number is too small to generalize this finding. Table 4.1 shows in summary the mean times at the different sampling ports D, A and B calculated according to Eq (3) to Eq (5). Generally speaking, a trend to shorter mean times at the different sampling ports can be seen for the automated and optimized apparatus.

Table 4.1. Mean times calculated according to Eq (2), Eq (3) and Eq (4) in comparison (n = 5 for manual sampling according to data in [39] and n = 7 for SIA analysis)

	Manual sampling followed by HPLC analysis	Automated sampling and analysis by SIA
MT_D [min]	23.45 ± 0.96	22.32 ± 2.32
MT_A [min]	31.37 ± 1.12	30.35 ± 1.56
MT_B [min]	34.98 ± 2.27	30.02 ± 2.56

Since sampling port D is located very early within the apparatus, only a minor decrease of the MT_D is be detected. A similar behavior can be observed for sampling port A, where the MD_A time was slightly decreased in the automated setup. A more pronounced effect could be detected for the MT_B, which has been calculated from the mass increase in the basolateral compartment. Here, the MT_B shifted distinctively for approximately 5 min. Since the mean times for sampling port D and A did not change significantly, the change of the MT_B can exclusively be assigned to changed setup. This entails that a small change in tubing and dead volumes can greatly effect the concentration trends and intends for future studies that comparing results from different apparatus for combined measurement of dissolution and permeation is difficult if even impossible.

4.4 Conclusion

It was possible to automate the apparatus for combined measurement of dissolution and permeation of solid dosage forms by means of sequential injection analysis. Two limitations of SIA are set concerning sampling frequency and selectivity. Analysis, filling and washing requires time and restrict sampling frequency to maximum 60-80 measurements per hour. In addition, not every API is accessible selectively and sensitively via fluorescence, hence forcing the researcher to search for alternative solutions for detection. Many aspects of sequential injection analysis supported this successful attempt for automation. Flexibility and versatility facilitated rapid sampling from different sampling ports with varying washing steps, varying aspiration volumes and in case of sampling from sampling port B automated replenishing of the withdrawn buffer. Detection with fluorescence permitted sensitive and selective online determination and quantification of propranolol HCl in KRB. In addition, online measurement could reduce issues when working with unstable compounds. Furthermore, automation decreased labor intensive manual sampling and dramatically dropped the costs for HPLC accessories.

5 Test with a BCS class 4 compound: furosemide

Subsequent to the basic testing of the apparatus using a unproblematic compound propranolol HCl, the focus of interest was shifted to more sophisticated drug such as furosemide, a BCS class 4 compound. Prior to testing permeability of the dosage form Lasix®, efforts have been made in order to establish an analytic basis for the experiments. Subsequently, experiments with the tablets have been done.

5.1 Introduction

In previous chapters, propranolol HCl served as an uncomplicated model drug for testing the basic parameters of the apparatus such as cell monolayer integrity, leak tightness of the tubing, and the eligibility of automation. However, as discussed in section 1.1.2 (pp. 1-4 to 1-7), the here described apparatus is intended to be used - among other reasons - for advanced formulation screening for solid oral dosage forms. Therefore, the apparatus has to be tested using compounds from more demanding BCS classes. As a first step, quantification and automation has to be extended to low permeability compounds, especially with a focus on concentration assessment at the sampling port B. In order to determine the permeated amount of low permeability compounds, HPLC would be the most appropriate since it is a routine method in most laboratories and since it exhibits lower LOQ/LOD compared to SIA and allows separation prior to quantification. As a model compound for this objective, furosemide (frusemide) was chosen showing sufficient UV/VIS absorbance for the assessment of concentration at the sampling ports D and A. At sampling port B, however, online quantification by means of UV/VIS is not feasible since furosemide does not exhibit significant fluorescence in KRB. Prior to testing furosemide by means of combined dissolution and permeation assessment, transport experiments in Transwells® were performed in order to verify effects of excipients on permeation.

5.1.1 Furosemide as a model substance; biopharmaceutical classification

Furosemid is assigned to BCS class 4 [64], since it shows low permeability in Caco-2 permeability assays and low solubility in aqueous buffer systems. Solubility is depending strongly on pH as furosemide is a monovalent acid with a pK_a of 3.9 [88].

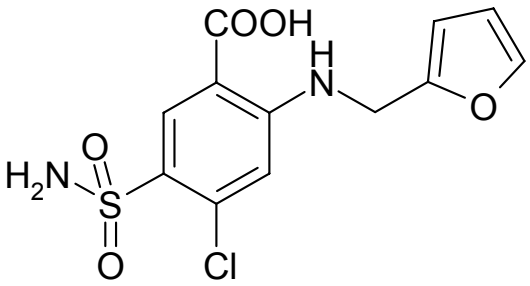

Figure 5.1. Chemical structure of Furosemide.

Therefore, declining pH values decrease solubility of furosemide as it can be seen in Figure 5.2. Equilibrium solubility of furosemide in KRB at pH 7.4 was determined as approximately 1900 µg/ml, while equilibrium solubility at pH 6.5 is 1500 µg/ml and further decreases to 330 µg/ml at pH 5.0 (all values for 24 h stirring at 37 °C of an excessive amount of furosemide, values found are correlating well with data reported in literature [61]).

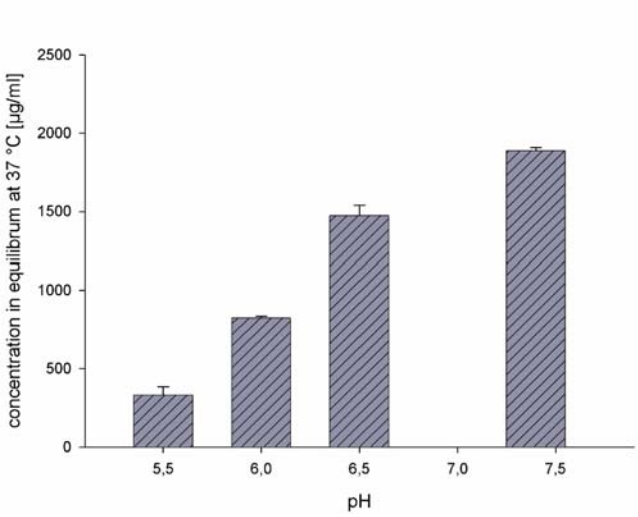

Figure 5.2. Solubility of furosemide in KRB is depending in the pH. Note that the experiments have been performed with MES for pH values lower than 7 and with HEPES for higher pH values (n = 3 for each pH).

In Caco-2 permeability assays, furosemide shows low permeability as well as an asymmetric transport [61, 89, 90]. Experiments in our laboratory applying a proton gradient between the apical and the basolateral compartment (pH 6.5 apical and pH 7.4 basolateral) led to the following P_{app} values: $P_{app}(A\text{-}B)$ $2.12 \pm 0.70 \cdot 10^{-7}$ cm/s and $P_{app}(B\text{-}A)$ $1.04 \pm 0.068 \cdot 10^{-5}$ cm/s (Figure 5.3); resulting in a high flux-efflux ratio of approximately 50. Values reported in literature are in the same magnitude: Pade et al. [61] reported a $P_{app}(A\text{-}B)$ of $1.20 \pm 0.10 \cdot 10^{-7}$ cm/s and a $P_{app}(B\text{-}A)$ of $2.74 \pm 0.02 \cdot 10^{-6}$ cm/s; Rege et al. [89] reported a $P_{app}(A\text{-}B)$ of $4.66 \pm 0.29 \cdot 10^{-7}$ cm/s

and a P_{app}*(B-A)* of 6.46 ± 0.12·10^{-6} cm/s; Hilgendorf at al. [90] reported a P_{app}*(A-B)* of 2.9 ± 0.1·10^{-7} cm/s. Interestingly, P_{app}*(B-A)* was in our lab two to three fold greater compared to literature. This might be attributed to the applied proton gradient and to different experimental protocols and putatively also to varying Caco-2 clones.

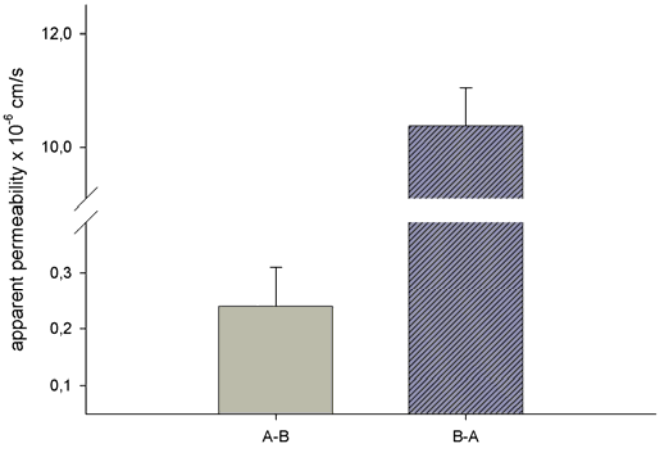

Figure 5.3 Apparent permeability (P_{app}) of furosemide through Caco-2 monolayer, either in absorptive (A-B) or in secretory direction (B-A) (n = 12 for each bar). Flux efflux ratio is calculated as approximately 50.

In summary, furosemide can be assigned to BCS class 1 [64], showing low solubility especially at low pH values and low permeability in Caco-2 monolayer permeability assay. Consequently, furosemide shows poor [88, 91] oral bioavailability of 50% [61] or 37-51 % [92].

5.2 Materials and methods

5.2.1 Materials

Transwell® permeable filter inserts (pore size 0.4 μm, 1.13 cm2, Transwell® type 3460) were purchased from Corning Incorp. Life Sciences (Acton, MA). Dulbecco's modified Eagle's medium (DMEM), non-essential amino acids (NeAA) and fetal bovine serum (FBS) were purchased from GIBCO (Invitrogen Corp. Carlsbad, CA). Furosemide (batch 0405A074) was bought from Synopharm GmbH & Co KG (Barsbüttel, Germany). Organic solvents were of HPLC grade. Composition of Krebs-Ringer Buffer (KRB) buffer was as follows: 1.41 mM CaCl2, 3.00 mM KCl, 2.56 mM MgCl2, 142.03 mM NaCl, 0.44

mM K2HPO4, 4.00 mM D- Glucose and 10.0 mM HEPES if pH 7.4 or 10.0 mM MES if pH 6.5. KRB was adjusted to pH 7.4 or 6.5 by means of NaOH. All salts for KRB were of cell culture tested grade and obtained from Sigma-Aldrich (St. Louis, MO).

5.2.2 Test tablets

Test tablet were: Lasix® 40 mg. According to the package insert, the ingredients of a tablet were except furosemide: lactose, corn starch, pre-pasted corn starch, talcum, silicon dioxide, and magnesium stearate. Batch number was 40E200.

5.2.3 Cell culture

Caco-2 cultivation has been done as described in section 2.2.2 (p 2-22).

5.2.4 Transport experiments

Transport experiments have been performed using the Transwell® system. Donor concentration of furosemide was 20 μg/ml. Transport medium was KRB, whereas the apical pH was adjusted to pH 6.5 (MES) and the basolateral pH to 7.5 (HEPES). The donor solution was added to the respective compartment (apical 500 μl; basolateral 1500 μl), and 100 μl samples have been collected hourly for five hours. The withdrawn amount was replaced by the respective KRB solution and has been mathematically taken in account (Eq (2)). Samples have been analyzed by HPLC and mass increase in the acceptor compartment was used to calculate the drug flux across the Caco-2 monolayer. Then, P_{app} was calculated by correlation of the flux with the donor concentration according to Eq (1).

5.2.5 Apparatus for permeability assessment of complete dosage forms

Basically, the apparatus for combined measurement of dissolution and permeation of complete solid oral dosage was used as reported in section 2-4 [39, 75]. Compared to the setup reported in [39, 75] some changes have been made. Firstly, the pump in front of the flow dissolution cell was changed to a pump as claimed by USP and Ph. Eur. generating a sinusoidal flow profile (type CE1, Sotax, Lörrach, Germany). Secondly, the flow rate in the dissolution module was changed since furosemide shows under the more stressing hydrodynamics rather fast and complete dissolution in pH 6.5 KRB. Therefore, in order to assure correct measurement of the concentrations, the flow rate was reduced to 4.5 ml/min. Moreover, the basolateral compartment was changed as follows: Since the temporal resolution of the permeated amount was too poor due to insufficiently slow mixing in the basolateral compartment. A putative solution might be to increase the flow rate in the basolateral compartment to ensure proper mixing; however, this might entail problems with the monolayer integrity or evoke other, new problems. Therefore, in order to circumvent this issue, the basolateral compartment was designed to be open, and drug concentration in the outflow of the basolateral part of the FTPC was monitored in the same manner as for sampling port A. All other settings have not been changed.

5.2.6 Drug quantification

5.2.6.1 Quantification of furosemide via HPLC

Quantification of Propranolol HCl was performed using a Dionex HPLC system, implemented with a RP 18 (LiChroSpher® 100, Merck), 5 μm, 12.5 cm column.

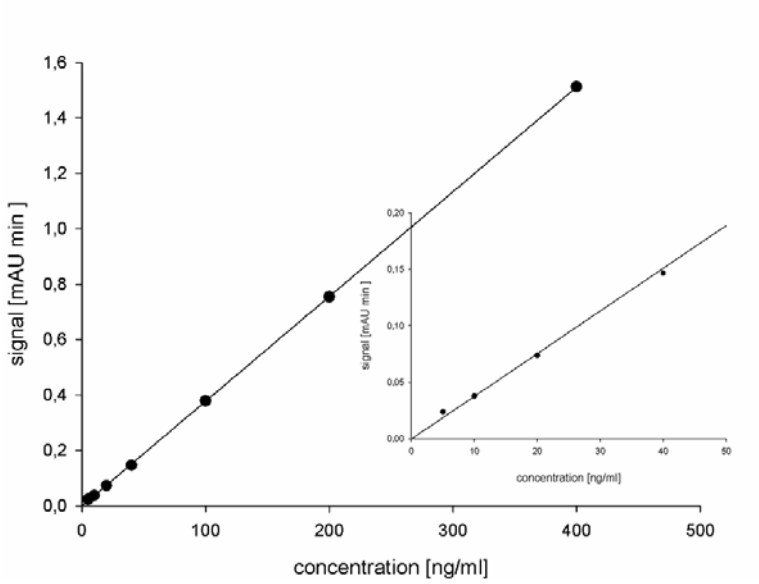

Figure 5.4. Calibration line for furosemide in HPLC applying the above described HPLC method: peak area is plotted against the furosemide standard concentration. The extract shows a magnification for the lower standards (5, 10, 20, and 50 ng/ml).

The HPLC system consisted of a Dionex P580 pump, a Dionex ASI 100 auto sampler, a UVD 170 S detector and a Dionex STH 585 column oven. Software was Chromeleon® 6.60, SP 1 build 9.68. Mobile phase was 60% (v/v) water, 20% (v/v) acetonitrile, 10% (v/v) methanol, 0.033% (v/v) triethylamine and 0.044% (v/v) phosphoric acid. Flow was 1.2 ml/min and oven temperature was 40 ± 1 °C. Detection was done with UV at 235 nm, whereas linearity ($R^2 > 0.999$) was given between 5 ng/ml and 20 μg/ml. Retention time was 3.10 ± 0.10 min. It was shown that none of the excipients interfered with the analysis.

5.2.6.2 Automated SIA procedure for furosemide quantification

The SIA system consisted of the FIAlab 3500 (FIAlab instruments, WA, USA) implemented with a 2.5 ml piston pump, a peristaltic pump and an eight port multiposition valve. Software was FIAlab for Windows® version 5.9.192. Standards were aspirated by means of an autosampler (Cetac ASX 260, NE, USA). A rack (material polyoxymethylene, POM) for the HPLC vials has been custom made (Figure 8.7, Figure 8.8). UV light source was purchased from Mikropack (type D-2000, Ostfildern, Germany), and was linked with the spectrometer (USB2000, Ocean Optics, Dunedin, FL, USA) by means of a fiber optic cable, whereas a FIAlab SMA-Z Flow Cell (Teflon®) for absorbance measurements (optical path length 5 mm) was inserted between the

light source and spectrometer. Spectrometer setting was as shown in Table 8.3. The programs codes for the automated measurement at the respective sampling ports are given in sections 8.4.1 (main), 8.4.2 (dissolution), 8.4.3 (apical), 8.4.4 (basolateral) (pp. 8-115 to 8-118). Port allocation was as given in Table 8.5 (p. 8-121). At D and at A, the connecting tubing was washed prior to the analysis by aspiration. Then, for quantification, 100 µl at D and at A were aspirated (15 µl/s) and were pushed through the detector with a velocity of 30 µl/s, which was found to be the optimal pump rate in terms of reproducibility and peak height. For quantification, peak height was correlated with furosemide standard concentration.

For sampling port B, a filling routine was developed since, due to its low concentrations, furosemide is not directly quantifiable by means of UV. Consequently, the SIA apparatus was used to bottle automatically samples from the basolateral sampling port into HPLC (200 µl inserts). The following procedure was shown to be superior in terms of recovery and reproducibility among others tested: Prior to aspirating the sample, 100 µl of air are aspirated into the coil between the syringe pump and the eight port multiposition pump, then 100 µl sample are aspirated and subsequently again 100 µl of air are aspirated. In the mean time, the autosampler washes its tip and subsequently moves to the waste position. After dispensing 210 µl (which is the volume between the multiposition valve and the tip of the autosampler) into the waste (50 µl/s), the autosampler tip moves to the respective HPLC vial and dispenses 110 µl sample into a vial (25 µl/s). Subsequently, the tip moves again to the waste position and discards the remaining volume in the tubing (250 µl/s). In order to check recovery and reproducibility, original and "bottled" standards have been quantified by HPLC (n = 3). In Figure 5.5, peak area of the original standards is plotted against the area of the "bottled" standards. Linear regression leads to the Eq (28).

$$y = 0.85579 \pm 0.0014\,x + 0.00014 \pm 0.0008 \quad \text{(value} \pm \text{std. error)} \qquad \text{Eq (28)}$$

The slope of 0.85579 can be interpreted as a recovery of 85.58 %, whereas the standard error is less than 0.2 %. The tiny offset of 0.00014 suggests low tendency for carry over effects or other irregularities.

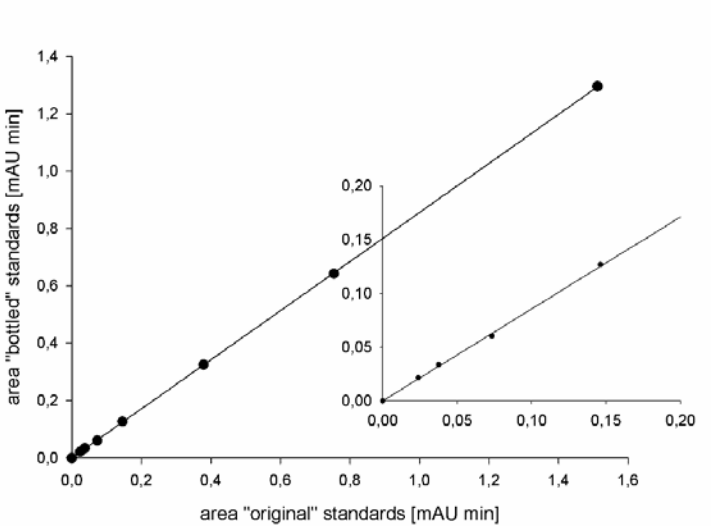

Figure 5.5. Comparison of the peak area of original standards and standards which have been treated according to the procedure given in section 8.4.4 ($R^2 > 0.9999$). The extract shows a magnification for the lower standards (0, 5, 10, 20, and 50 ng/ml)

5.2.6.3 Calibration of furosemide measured by means of SIA

Furosemide exhibits three UV absorbance maxima (235, 275, 344 nm). However, due to the measurement in KRB showing significant UV-absorbance up to 250 to 260 nm, only the area above 270 nm is directly accessible with SIA analysis. Since the concentration to be measured throughout the analysis do span over three decades (approx. 1 to 1000 µg/ml), three wavelengths have been applied for quantification. Absorption at 275 nm was used for the lowest concentrations down to 3.2 µg/ml, absorption at 344 nm was applied for concentrations in a range of 30 to 150 µg/ml, and absorption at 360 nm was used for the highest concentration up to 800 µg/ml furosemide in KRB.

Table 5.1. Calibration parameters for various wavelength of furosemide in KRB. The calibration follows a linear equation $y = ax+b$ [µg/ml].

wavelength	a	b	R^2	range [µg/ml]
275 nm	0.0344	-0.0329	> 0.9999	3.2 - 32
344 nm	0.00619	-0.0197	> 0.9999	32 - 160
360 nm	0.00149	-0.00024	0.99976	160 - 800

Standards have been prepared at the following concentrations: 0, 3.2, 8, 16, 32, 80, 160, 320, and 800 µg/ml; each standard has been measured ten times. A typical calibration for these three wavelengths is shown in Figure 5.6, Figure 5.7, Figure 5.8.

Calibration factors are summarized in Table 5.1. Limit of quantification for the calibration at 275 nm was calculated as 1 μg/ml (10σ)

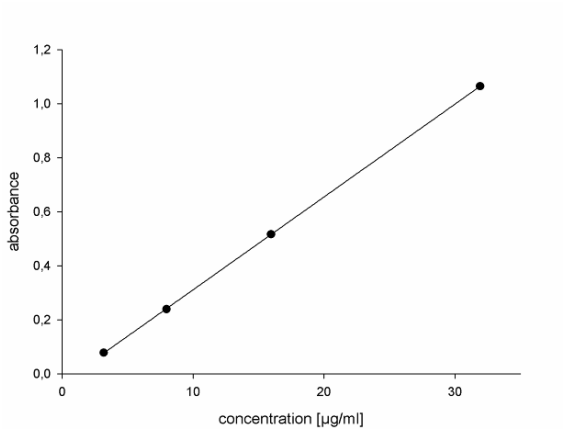

Figure 5.6. Calibration for 275 nm for furosemide in KRB ($R^2 > 0.9999$).

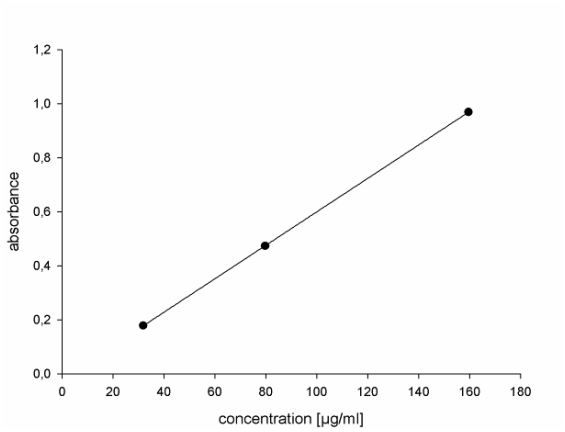

Figure 5.7. Calibration for 344 nm for furosemide in KRB ($R^2 > 0.9999$).

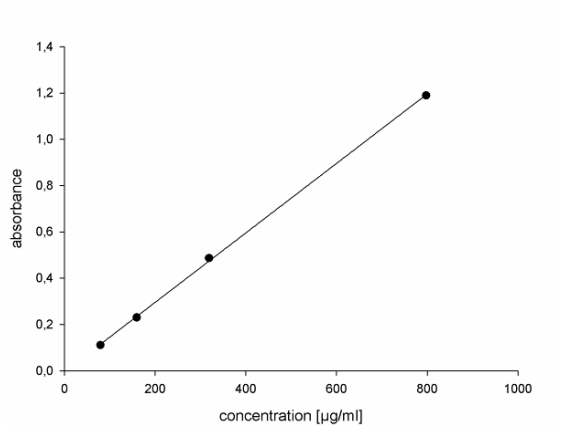

Figure 5.8. Calibration for 360 nm for furosemide in KRB ($R^2 = 0.9976$)

Relative standard deviation (s_{rel}) for the lowest standard (3.2 μg/ml) was 2.31 % and for the highest standard 0.82 % (n = 10). For all other standards in between s_{rel} never exceeded 2.4 % (n = 10).

5.2.7 Data treatment

Concentration time trends at the sampling ports have been fitted to Eq (29)

$$c = k \cdot \frac{a}{b-a} \cdot (e^{-a \cdot x} - e^{-b \cdot x}) \qquad \text{Eq (29)}$$

using SigmaPlot 2004 for windows version 9.0 (bateman equation). For the fitting a kinetic model for a exponential invasion of furosemide into a assumed compartment and an exponential elimination out of the compartment. For sampling ports A and B, a time shift was taken into consideration. The cumulative amount at sampling port D has been calculated according to Eq (26). Mean times for the various sampling ports have been calculated according to Eq (3) to Eq. (5).

All values are denoted as mean ± standard deviation if not denoted different.

5.3 Results and Discussion

5.3.1 Furosemide in Caco-2 transport experiments – impact of excipients

It has been reported that apparent permeability of furosemide can be affected by the presence TWEEN 80 (Figure 5.10). Rege et al. [89] reported to increase the absorptive P_{app}*(A-B)* from $4.66 \pm 0.29 \cdot 10^{-7}$ cm/s to $3.49 \pm 0.35 \cdot 10^{-6}$ in presence of 1.8 mg/ml TWEEN 80 and hence to neutralize the asymmetry in transport without toxic effects on Caco-2 cell monolayers. Preliminary studies in order to confirm these results have been done using vitamin E TPGS (Figure 5.9) and TWEEN 80 (Figure 5.10) at various concentrations.

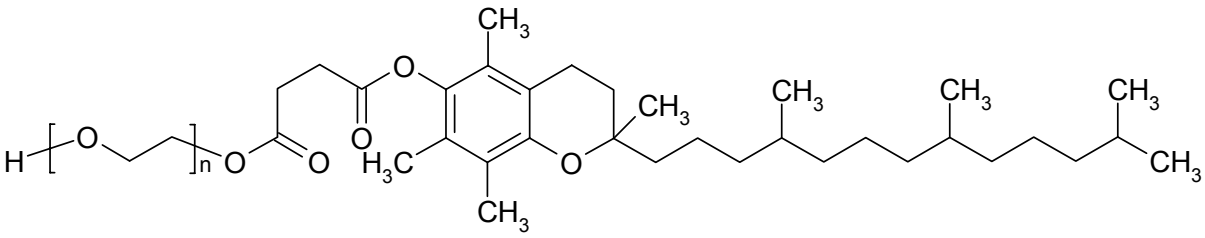

Figure 5.9. Chemical structure of vitamin E TPGS (d-alpha-tocopheryl poly(ethylene glycol) 1000 succinate), a polyethoxylated (n = 23) vitamin E derivative with a succinic acid linker.

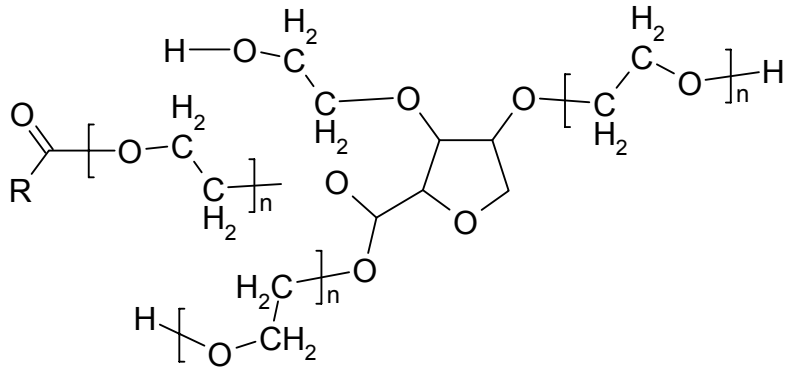

Figure 5.10. Chemical structure of TWEEN 80, a polyethoxylated fatty sorbitan acid ester, R = oleic acid.

5.3.1.1 Impact of vitamin E TPGS

Vitamin TPGS was tested at two concentrations: 33 μM and 100 μM. (CMC of vitamin E TPGS approx. 100 μM). A 33 μM vitamin E TPGS solution exhibited maximum inhibitory effects on P-gp as stated by Collnot et al. [17] and equalized apical to basolateral and basolateral to apical transport of rhodamine 123. For furosemide, however, a complete depletion of polarity in transport could not be achieved by means of vitamin E TPGS. Results are visualized in Figure 5.11. $P_{app}(A\text{-}B)$ was increased from $2.12 \pm 0.70 \cdot 10^{-7}$ cm/s to $3.59 \pm 0.33 \cdot 10^{-7}$ cm/s in presence of 33 μm vitamin E TPGS and to $3.46 \pm 0.35 \cdot 10^{-7}$ cm/s in presence of 100 μM vitamin E TPGS. Differences in A to B transport were statistically different. (t-test, $p < 0.001$). $P_{app}(B\text{-}A)$ was reduced by 33 μM vitamin E TPGS from $10.4 \pm 0.68 \cdot 10^{-6}$ cm/s to $8.78 \pm 0.31 \cdot 10^{-6}$ cm/s and for the 100 μM solution to $6.68 \pm 0.16 \cdot 10^{-6}$ cm/s. Again, a statistical difference could be found (t-test, $p < 0.001$).

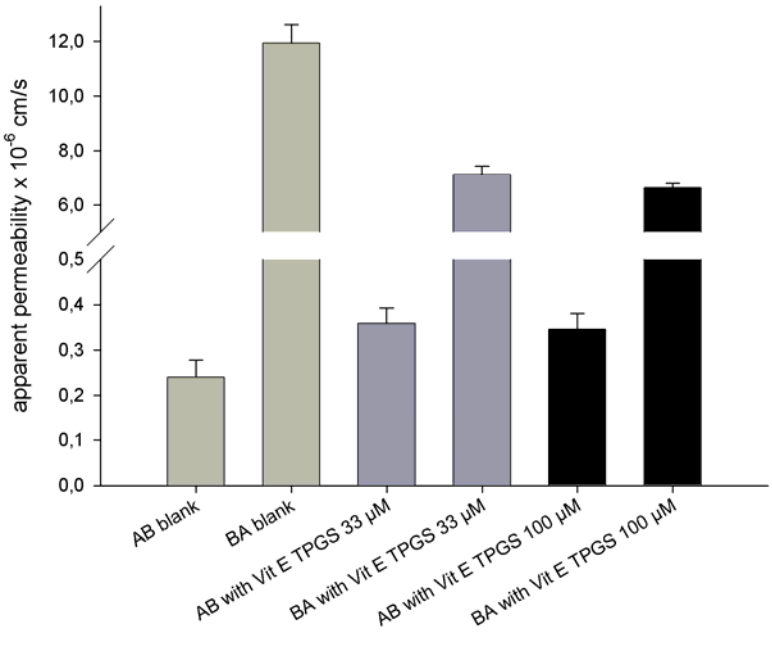

Figure 5.11. Impact of Vitamin E TPGS on furosemide transport in secretory (BA) and absorptive (AB) direction (n = 5-6 for each column).

5.3.1.2 Impact of TWEEN 80

TWEEN 80 was added in three concentrations: 1.0 mM, 1.5 mM, and 2.0 mM which correspond to 1.31 g/l, 1.965 g/l, and 2.620 g/l. Rege et al. [89] proposed to

apply a 1,8 g/l TWEEN 80 solution for Caco-2 experiments in order to simulate physiologic conditions and relevant concentrations. Application of TWEEN 80 increased apical to basolateral and decreased basolateral to apical permeability suggesting that TWEEN 80 interferes with cellular efflux systems (results are summarized in Figure 5.12. P_{app}*(A-B)* was statistically significantly ($p < 0.001$, Holm Sidak, one way ANOVA) increased to $6.18 \pm 0.30 \cdot 10^{-7}$ cm/s (1.0 mM), to $6.57 \pm 0.16 \cdot 10^{-7}$ cm/s (1.5 mM), and to $9.32 \pm 0.45 \cdot 10^{-7}$ cm/s (2.0 mM). P_{app}*(B-A)* was statistically significantly decreased from $10.4 \pm 0.68 \cdot 10^{-6}$ cm/s to $5.76 \pm 0.17 \cdot 10^{-6}$ cm/s (1.0 mM), $5.47 \pm 0.20 \cdot 10^{-6}$ cm/s (1.5 mM), $5.38 \pm 0.43 \cdot 10^{-6}$ cm/s (2.0 mM). Accordingly, the flux efflux ratio was decreased from 50 to 9.3, 8.33, and 5.8, respectively. In contrast to the findings of Rege et al [89], no complete neutralization of the flux efflux ratio was found. Nevertheless, a similar trend has been observed. Putatively, varying batch to batch quality of TWEEN 80 might lead to scattering results. Also, Caoc-2 cells used by Rege et al. [89] might have had different expression pattern of the efflux protein.

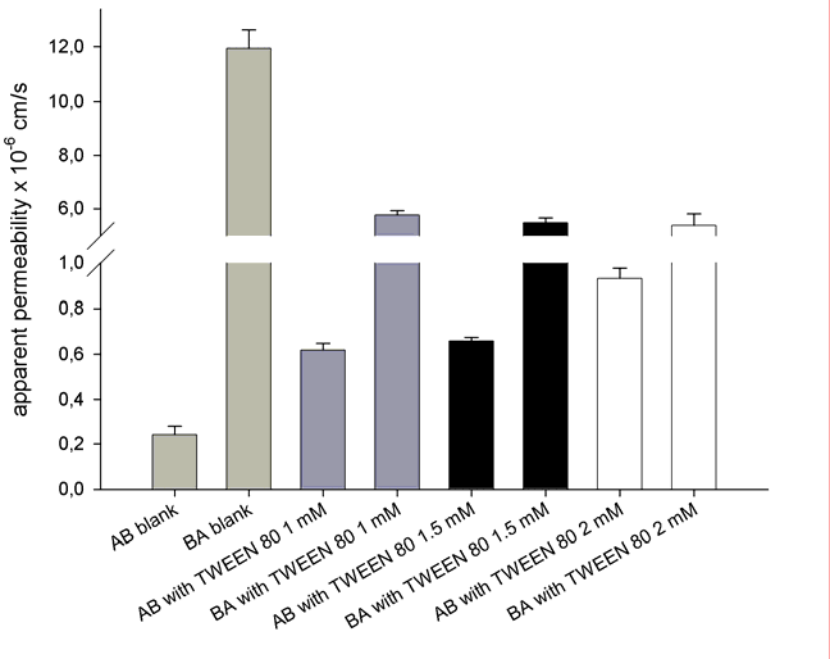

Figure 5.12. Impact of TWEEN 80 at various concentrations on furosemide transport in secretory (BA) and absorptive (AB) direction (n = 5-6 for each bar).

5.3.2 Combined measurement of dissolution and permeation of Lasix® tablets

5.3.2.1 Concentration time trend at sampling port D

Sampling port D is located directly after the flow through dissolution cell and is delivering dissolution signals which are almost not affected by mixing and convectional processes. The right plot in Figure 5.13 plots the concentrations assessed at sampling port D against time.

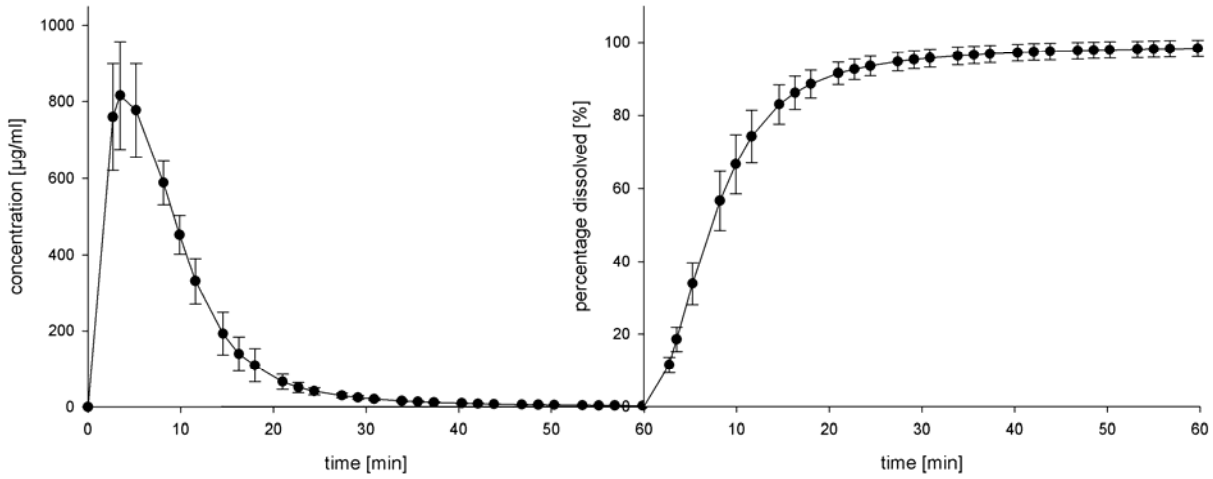

Figure 5.13. Left plot: concentration time trend at sampling port D for Lasix® tablet containing 40 mg furosemide. Right plot: cumulative amount of furosemide assessed at sampling port D (n = 6)

Maximum concentrations were reached at approximately 3.5 min. The cumulative amount has been calculated according to Eq (26), and percentage dissolved and detected is plotted against time in Figure 5.13. After 60 min, a cumulative amount of 99.03 ± 1.95 %, i.e. 39.61 ± 0.78 mg, of the declared amount (40 mg) were detected. When applying Eq (28) to the data shown above, a nice correlation of the fitting is observed as illustrated in Figure 5.14 (R^2 = 0.9986). The variables obtained from linear regression are summarized in Table 5.2. Mean time assessed with Eq (3) is given in Table 5.3.

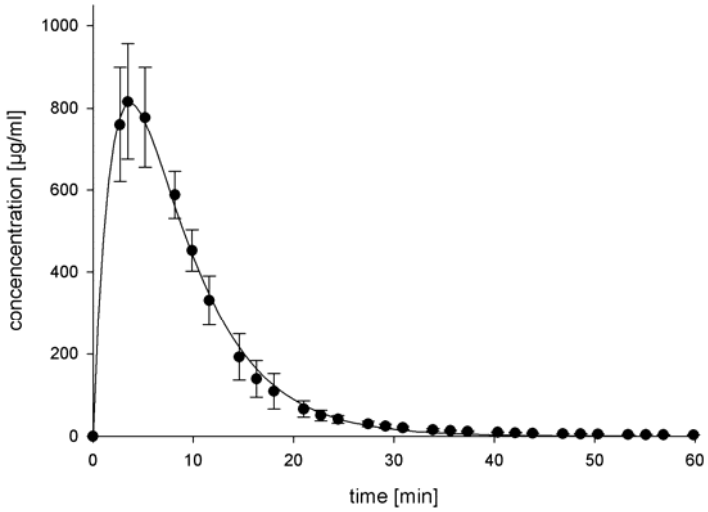

Figure 5.14. Concentrations of furosemide at sampling port D fitted to a bateman equation according to Eq (12); $R^2 = 0.9986$.

5.3.2.2 Concentration time trend at sampling port A

Concentration assessed at sampling port A are plotted against time in Figure 5.15. A time shift of approximately 9 min is observed (peak to peak difference).

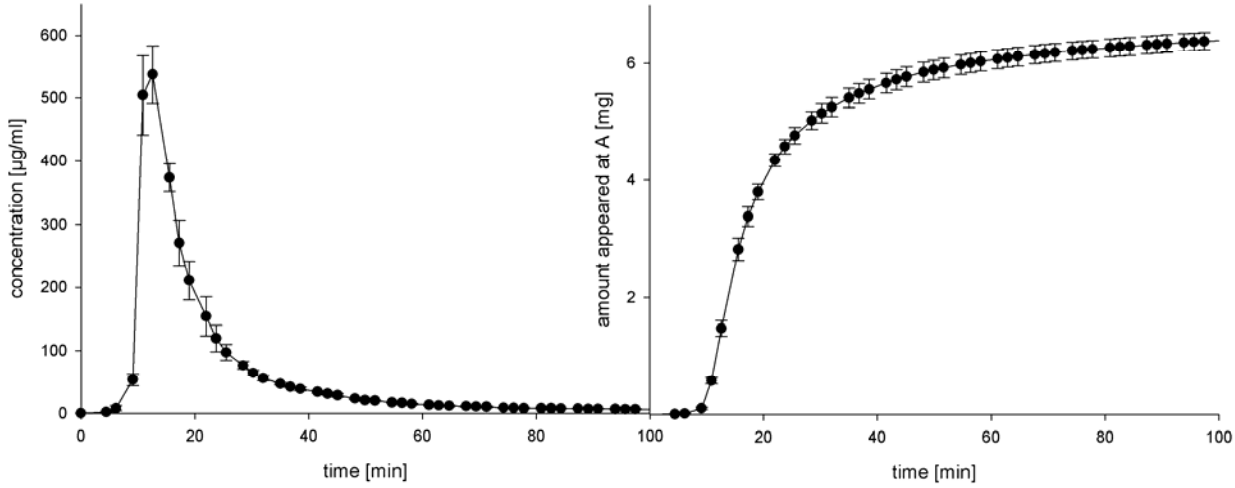

Figure 5.15. Left plot: concentration time trend at sampling port D for Lasix® tablet containing 40 mg furosemide. Right plot: cumulative amount of furosemide assessed at sampling port D (n = 6)

Furthermore, the peak appears to be flattened and stretched. Maximum concentrations were reached at 12.5 min post experiment beginning. In order to fit the curve at A to Eq (25), the peak was shifted for 12.5-3.5 min = 9 min to the left in order to assure that

the peak is going through the origin (Figure 5.16). Fit parameters are summarized in Table 5.2.

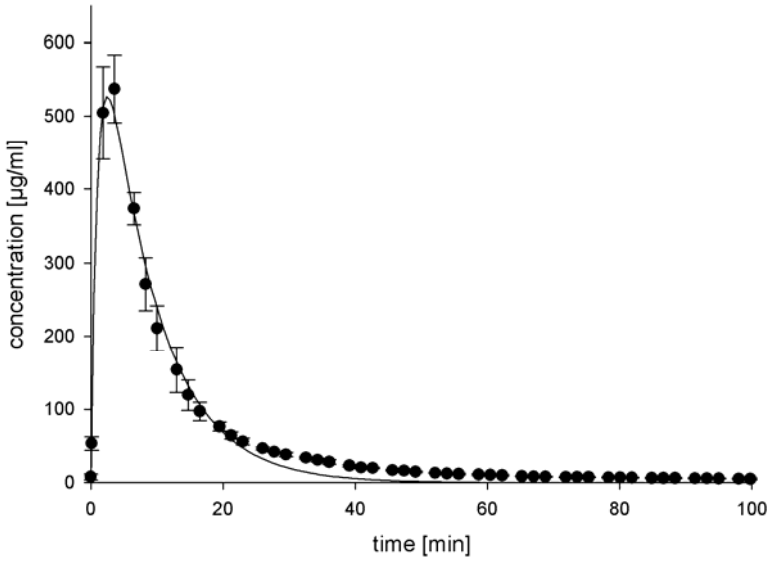

Figure 5.16. Concentrations of furosemide at sampling port A fitted to a bateman equation according to to Eq (12); $R^2 = 0.9899$.

5.3.2.3 Concentration time trend at sampling port B

The concentrations at sampling port B are assessed according to the previously described filling procedure and HPLC method. The concentrations are corrected for the

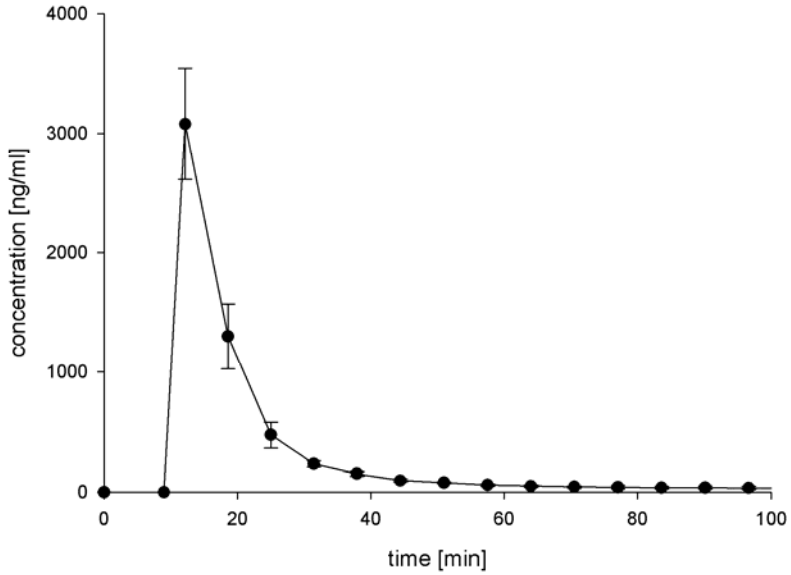

Figure 5.17. Concentration of furosemide in the outflow of the FTPC is plotted against time (n = 6).

loss of substance during the filling procedure and are plotted against time in Figure 5.17. Evidently, highest concentrations in the outflow are accompanied with the peak concentrations at sampling port A. TEER remained above 500 $\Omega \cdot cm^2$ during all experiments. For fitting, the curve was also shifted to the left by 9 min as described above. (Figure 5.18). Mean times for sampling port B are given in Table 5.3.

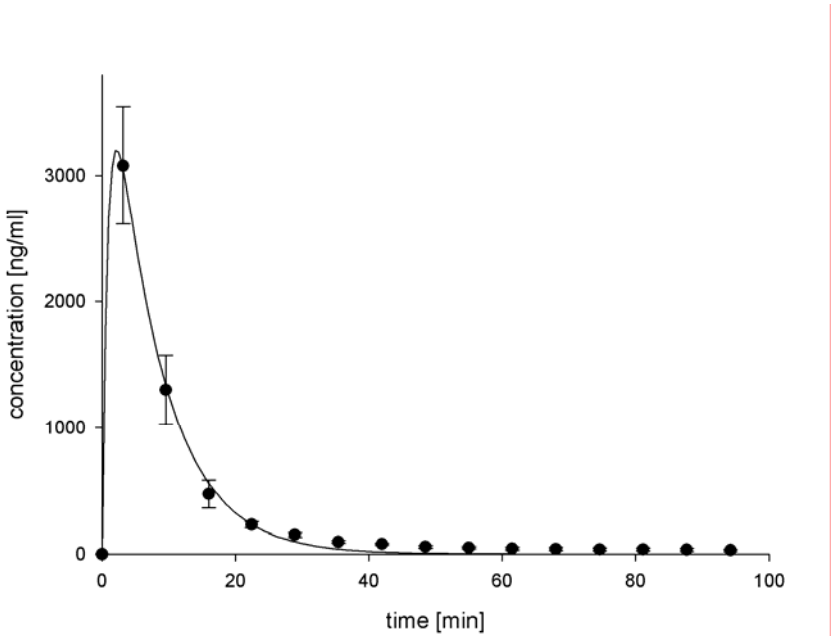

Figure 5.18. Concentrations of furosemide at sampling port B fitted to a bateman equation according to Eq (12); $R^2 = 0.9970$.

The cumulatively permeated amount was calculated as 38.06 ± 5.89 μg according to Eq (23). In comparison to the amount cumulatively appeared at sampling port A (6,591.36 ± 132.46 μg), a ratio of 0.577 % was able to permeate.

Table 5.2. Parameter obtained from linear regression according to Eq. (25)

sampling port	time shift [min]	k	a	b	R^2
D	0	3681.59	0.1677	0.4082	0.9986
A	9	5312.66	0.1247	0.9189	0.9899
B	9	38686.0	0.1359	1.2168	0.9970

Table 5.3. Mean times for sampling ports D, A, and B.

	at D: MT_D	at A: MT_A	at MT_B
mean time	10.15 ± 1.00	24.74 ± 0.39	21.97 ±1.75

5.3.2.4 Discussion of the furosemide/Lasix® results

Preliminary tests using membrane dosage pumps in the dissolution module as done in previous sections yielded unsatisfactory results concerning the dissolution process. It appeared as if low hydrodynamic stress in the flow through dissolution cell led to irreproducible, incomplete, and delayed dissolution behavior of the tablets. By contrast, the application of a compendial dissolution pump generating a sinusoidal flow profile and resulting in higher hydrodynamic stress on the dosage form led to rather fast dissolution. Release of 40 mg furosemide was completed within 30 min resulting a MD_D of ~10 min, which is much lower than the MD_D for propranolol HCl with ~22 min (compare Table 4.1, p 4-73). Maximum concentrations assessed at sampling port D were in mean 800 µg/ml and were close to maximum solubility of furosemide in pH 6.5 KRB. Although furosemide powder shows severe wetting problems in KRB pH 6.5, the tablet showed no wetting issues and behaved concerning its dissolution properties more or less as an immediate release dosage form. This might be attributed to furosemide highly dispersed within the insoluble corn starch. The cumulative amount at sampling D of 99.03 ± 1.95 % indicates proper calibration and correct adjustment of the flow rate.

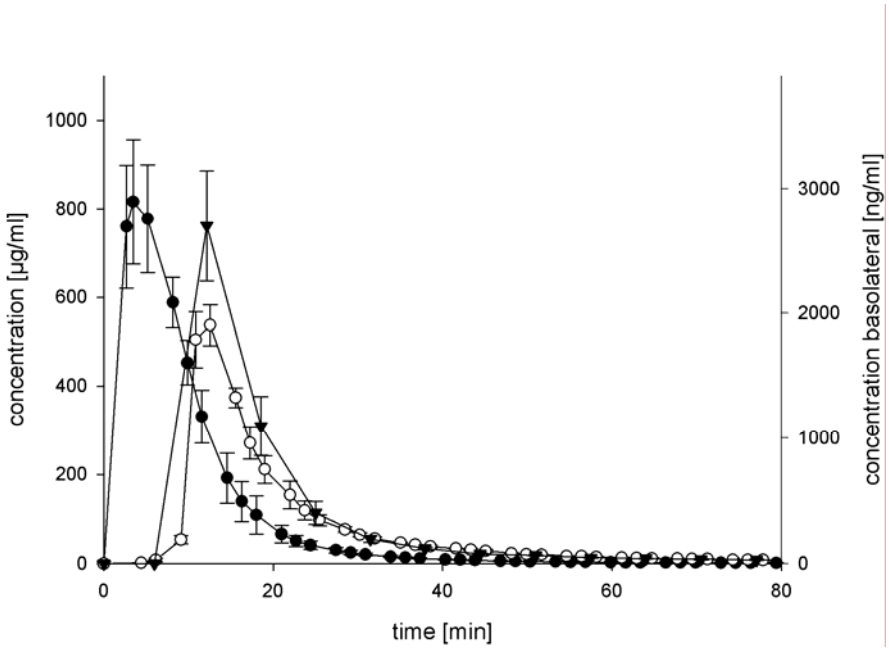

Figure 5.19. Graphical summary of Lasix® 40 mg furosemide tablets. Closed circles (●) represent the concentration time trend at sampling port D, open circles (○) at sampling port A, and triangles down (▼) at sampling port B.

Number of data points of this sampling port can be considered as sufficiently high. At sampling port A, a similar peak shaped concentration time profile can be observed. Maximum peak time shifted from 3.5 min to 12.5 min and the peak height was declined from ~800 µg/ml at D to ~500 µg/ml at A. Accordingly, mean time at A was greater than mean time at D. Though the peak to peak time difference was 9 min, the mean time are differing by ~15 min. This might be explained by the stronger 'tailing' of the peak at sampling port A apparently increasing the mean time at sampling port A.

Concentrations at sampling port B resulted also in a peak shaped curve (Figure 5.17). The setup has been altered to an open compartment since mixing in the basolateral compartment was insufficient. The cumulative amount of permeated furosemide was rather high (0.577%) and exceeded the permeated amount of propranolol HCl (~0.35%, compare Table 2.4). Several reasons may be accounted for that: First, a leakage in the FTPC may lead to high permeated amounts. Second, the cell monolayer is disrupted by the analysis, or third, high concentrations saturate efflux transporters. The first possibility can clearly be excluded since in not even one past experiment, a leakage in the FTPC has been detected. The second possibility may be rebutted since the cell monolayer showed high TEER values after the experiments and were microscopically intact. Potentially, high concentrations of furosemide and lactose might affect with their osmolarity cell monolayer integrity. At the peak concentrations, for example, 500 µg/ml furosemide are adding another 15.2 mOsmol/kg to the osmolarity of KRB of approximately 300 mOsmol/kg; for lactose no numbers can be given, since the amount of lactose per tablet is unknown. However, the osmotic effects remains unclear since Caco-2 cells are generally not that sensitive, if the osmotic stress persists only for a short time. The third possibility is still to be clarified with static transport experiments at higher concentrations.

In summary, a method for assessing reproducibly dissolution process with the apparatus for permeability assessment of drug formulated in solid dosage forms has successfully described. For the permeation process, however, a deeper study to reveal the processes happening on the permeation stage has to be done in the future.

5.4 Conclusion

Transport experiments revealed the impact of TWEEN 80 and vitamin E TPGS on the barrier properties of Caco-2 cell monolayers. Both surfactant were shown to increase P_{app}(A-B) and to decrease P_{app}(B-A). Hence, a suitable candidate was found for elucidation dissolution and permeation processes with the newly setup apparatus.

The automated analytic has been expanded to UV VIS measurement, and a filling routine for offline HPLC analysis has been successfully implemented; thus, allowing to measure compounds with the apparatus lacking significant fluorescence in KRB.

Furthermore, the apparatus for permeability assessment of solid oral dosage formulations was successfully used for measuring a marketed product containing 40 mg furosemide. Concentrations assessed at sampling port D and A were reproducible, plausible and recovery was satisfactory. Fitting the concentration time profiles at all sampling ports to a bateman equation led to high coefficients of determination in comparison to previous experiments with propranolol HCl. This might be attributed to improved hydrodynamics within the apparatus. Concentrations assessed at sampling port B were indeed reproducible but the permeated amount was too high for a BCS class 4 compound, although the monolayer retained its integrity. A putative reason for that might be the tremendously high donor concentrations (500 μg/ml) affecting reversibly Caco-2 monolayer integrity and allowing high amounts of furosemide to permeate. This phenomenon poses an urgent field of research for future studies.

6 Summary

Determination of *in vivo* performance of solid oral dosage forms is mainly based on two *in vitro* assays: *in vitro* dissolution testing applying *in vivo* relevant dissolution parameters, and cell culture based *in vitro* permeability assays employing monolayers of the small intestinal cell line Caco-2. Both assays have been evolved since decades; nevertheless, they exhibit some major drawbacks. Permeability testing in Transwell® systems determines intrinsic permeability of pure compounds and thus questions discriminatory power: first, the presence of endogenous (e.g. bile salts) or exogenous (e.g. dosage form excipients, food) substances affecting permeation processes is often neglected. Second, donor concentrations tend to be arbitrarily chosen and are assumed to be constant over time in contrast to *in vivo*. Therefore, it appears cumbersome to determine two processes happening *in vivo* concomitantly in an *in vitro* assay separately. Hence, the aim of this work was to connect both assays in one apparatus and to develop an assay eligible to determine *in vitro* permeability of solid dosage forms.

The recently setup prototype consists of two modules: a dissolution and a permeation module (Figure 6.1). In order to connect both, a stream splitter providing appropriate low flow rates for the sheer stress sensitive Caco-2 monolayer was installed.

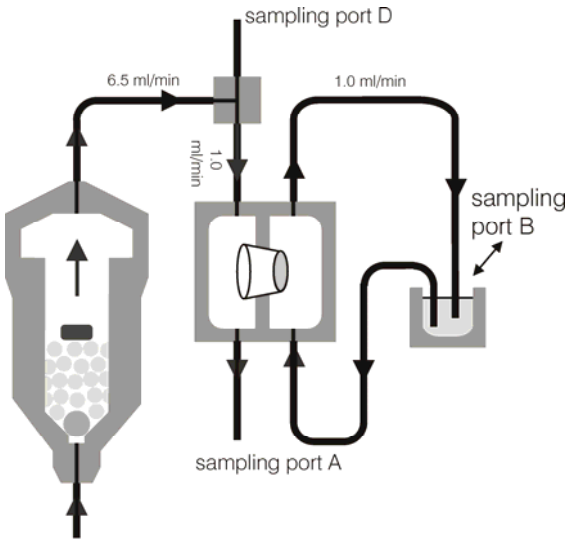

Figure 6.1. Schematical depiction of the apparatus for permeability assessment of solid dosage forms. Sampling ports are indicated with capital letter: D (dissolution), A (apical), B (basolateral).

The dissolution module was open, whereas the transmucosal receptor compartment was closed. Several sampling ports were implemented to monitor thoroughly dissolution and permeation: sampling port D (dissolution), shortly after the USP apparatus 4, sampling port A (apical), after the stream splitter and after passage through the flow through permeation cell (FTPC) and finally sampling port B (basolateral), in the acceptor compartment. For test purposes, several propranolol HCl immediate release tablets with increasing dosage strength and two different propranolol HCl extended release tablets were manufactured. For those tablets, experiments showed that the permeated amount is linear dependent on the dosage strength as for the passively permeating compound expected. For the extended release tablets, a delay in release of propranolol HCl from the solid dosage form was visible in the permeation profile; nevertheless, the cumulatively permeated amount was not statistically different among the differently releasing tablets. Mean time approach for the different sampling ports D, A, and B yielded plausible and conclusive results for this setup. Also, the stream splitter was found to work reliable. Advantage of such setup can be seen in the hydrodynamically separated modular setup providing the possibility to employ the dissolution module with compendial, sinusoidal flow profile generating pumps. A major improvement may be seen in the possibility to use complete solid dosage forms together with physiological flow rates/volumes in the dissolution module; and thus, facilitating the application of relevant concentrations. In addition, three sampling ports are allowing thorough monitoring of both dissolution and permeation.

In order to improve the understanding of the processes occurring in the apparatus, it was attempted to describe concentration time trends at the three sampling ports by computational simulation. The *in silico* model based on several hypotheses. The apparatus was separated into several compartments such as the flow through dissolution cell, the stream splitter, and the apical compartment in the flow through permeation cell. Consequently, the tubing in between and connecting those compartments were modeled according their actual inner diameter and length. In order to model the peak broadening, the stream in the tubing was described by the law of Hagen Poisseuille, which characterizes a parabolic flow profile in the tubing. The release of drug from the dosage form was described by means of a Weibull distribution. In order to calibrate the *in silico* model, the concentration time trend of a propranolol

HCl solution applied into the flow through dissolution cell was modeled and parameters such as flow rate, compartment size, and other variable have been optimized. Subsequent to calibration, the concentration time trends for the various propranolol HCl tablets with varying content and release kinetics were successfully simulated. (...)

Subsequent to the early testing of the prototype, work time for sampling and drug quantification was found to be suboptimal. Therefore, the system was automated by means of sequential injection technique (SIA). Quantification at the three sampling ports was done in this first study via fluorescence measurement. An appropriate volume of sample was aspirated from the respective sampling port, and subsequently, the sample volume was processed and finally pushed through the flow through fluorescence detector. Signal height was then correlated with standards concentrations, and a good correlation was found for the sample analyzed at sampling port B showing the lowest concentration to be assessed. In order the quantify propranolol HCl at sampling ports D and A, where comparatively high concentration appear, the injection volume was decreased to extend linearity of the calibration function. Nevertheless, it was not possible for sampling D and A to fit the calibration function to a straight line, and an appropriate calibration was done by means of a first order polynomial equation. Automation almost doubled sampling frequency and decreased error probability possibly caused by manual sampling. A comparison of the results obtained with the automated setup revealed similar results to those from the manual. The automated apparatus allows online measurement at the three different sampling ports D, A, and B or partially online analysis in combination with HPLC. For the future, the automation facilitates more and faster experiments as well as higher reproducibility of the measurement due to less error sources.

After this extensive testing and development of the apparatus, the next target was to be able to measure more sophisticated compounds, and a suitable candidate for further studies was chosen as furosemide. Furosemide shows low intrinsic permeability through Caco-2 monolayers and is apparently subjected to a cellular efflux pump. Apical to basolateral and basolateral to apical permeability can be influenced in presence of surface active excipients such as TWEEN 80 and vitamin E TPGS.

For the assessment of permeability from solid dosage forms, a marketed tablet (Lasix®) was used. Prior to this analysis, a quantification method for the SIA analysis

had to be developed. Since furosemide shows almost no fluorescence signal in aqueous media, quantification has been done via UV/VIS at sampling ports D and A and at sampling port B via HPLC. For sampling port B, an automated bottling procedure was successfully developed. Dissolution of 40 mg furosemide in pH 6.5 KRB was rather fast; however, the concentration time trends at sampling ports D and A were measured correctly. Nevertheless, at sampling port B, more data points would be desired. Recovery of furosemide at sampling port D was sufficiently high (~98 %), the permeated mass, however, was estimated as too high for a low permeability compound. Still, it remains unclear whether those high permeated amount is a consequence from efflux saturation or from osmotic cytotoxicity.

In the future, the system may be enhanced in order to simulate the pH gradient a drug undergoes after oral administration. Furthermore, the media for permeation/dissolution testing has to be refined so that results with higher *in vivo* relevance may be obtained. However, it has to be kept in mind that improving the apparatus in such way, entails that also the complicity of the system and efforts for the experiments are increasing.

In summary, a versatile tool for assessing drug permeability of solid dosage forms has been developed. Flow rates in the dissolution module are easily and freely adjustable, and also the type of dissolution pump is interchangeable. Depending on the desired temporal resolution of the permeation process, the basolateral compartment can be open or closed. Consequently, the automation was attempted to be versatile and flexible, too. Drug quantification at the respective sampling ports can be performed with either fluorescence, UV/VIS - both as online analysis -, or with an offline HPLC analysis. Combining all these properties, a rather unique tool to estimate dosage form interference with biological systems has been developed.

7 Zusammenfassung

Prädiktive Urteile zum *in vivo*- Verhalten fester oraler Arzneiformen nach ihrer Applikation basieren hauptsächlich auf Ergebnissen zweier Methoden: Zum einen auf *in vitro* Dissolutionversuchen und zum anderen auf *in vitro* Permeationsversuchen, welche meist eine zellkulturbasierte Permeabilitätsanalyse zu Hilfe ziehen. Beide Methoden werden seit Jahrzehnten weiterentwickelt und eingesetzt. Nichtsdestotrotz beinhalten diese entscheidende Nachteile: Mit Hilfe von Permeabilitätsanalysen in sogenannten Transwell® Systemen wird die intrinsische Permeabilität reiner Substanzenlösungen bestimmt, was die prädiktive Aussagekraft solcher Versuche in Frage stellt: Zum einen werden die gleichzeitige Anwesenheit und somit die möglichen positiven oder negativen Einflüsse von endogenen (z.B. Gallensalze) oder exogenen (z.B. Hilfsstoffe) Substanzen auf die Permeabilität vernachlässigt. Zum anderen scheint die Donorkonzentration beliebig und eher nach analytischen Aspekten gewählt als nach *in vivo* Relevanz. Aus diesem Grund erscheint es dingend angebracht, beide Prozesse - Permeation und Dissolution - gemeinsam in einer Prüfungsanrodnung zu bestimmen. Ziel dieser Arbeit war es, beide Methoden in einer Apparatur für feste orale Arzneiformen zu kombinieren.

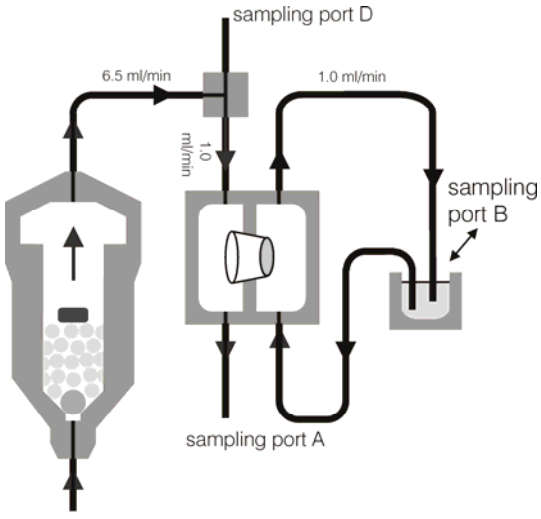

Figure 7.1. Schematischer Aufbau der Apparatur zur Permeabilitätsbestimmung von Arzneistoffen aus festen oralen Arzneiformen. Die Probennahmepunkte sind mit den Großbuchstaben D (dissolution), A (apikal) und B (basolateral) gekennzeichnet.

Die hierbei entwickelte Apparatur besteht sinngemäß aus zwei Modulen (Figure 7.1): einem Dissolution und einem Permeationsmodul, wobei ein Stromteiler die beiden

Module miteinander verbindet. Ein Stromteiler ist notwendig, da das Permeationsmodul auf Grund der dort vorhandenen Zellschichten im Vergleich zum Dissolutionsmodul einen geringeren Flüssigkeitsbedarf benötigt. Die Testapparatur wurde offen geplant, sodass ein An- und Abfluten des Arzneistoffes beobachtet werden kann; das basolaterale Kompartment im Permeationsmodul wurde jedoch geschlossen geplant. Verschiedene Probennahmepunkte wurden installiert um die Konzentrations-Zeitverläufe gründlich zu überwachen. Probennahmepunkt D (Dissolution) wurde kurz nach der Durchflussdissolutionszelle installiert, Probennahmepunkt A (apikal) wurde am Ausfluß der Durchflusspermeationszelle eingefügt. Letztendlich wurde der Probennahmepunkt B (basolateral) eingerichtet, welcher die Menge an permeierter Substanz im basolateral Kompartment zu bestimmen erlaubt.

Um die Testapparatur zu testen, wurden verschieden schnellfreisetzende Propranolol HCl Tabletten mit ansteigendem Gehalt sowie zwei modifiziert freisetzende Propranolol HCl Tabletten produziert und vermessen. Es zeigte sich, daß mit ansteigendem Gehalt an Propranolol HCl pro Tablette die permeierte Menge proportional ansteigt, was mit den Erwartungen für eine passiv permeierende Substanz übereinstimmt. Für die verschieden schnellfreisetzenden Tabletten ergab sich, daß das Ausmaß der Verzögerung der Freisetzung in gleichem Verhältnis im Permeationsprozess wieder sichtbar ist, wobei sich die kumulativ permeierte Menge zwischen den verschieden freisetzenden Tabletten nicht statistisch signifikant unterscheidet. Weiterhin ergab die Zuhilfenahme des so genannten Ansatzes der "mittleren Dissolution- und Permeationszeit" für die Testapparatur plausible und schlüssige Ergebnisse. Ebenso konnte die exakte Arbeitsweise des drucklosen Stromteilers bewiesen werden.

Abgesehen von der Verwendung kompletter Arzneiformen zur Permeabiltätsbestimmung durch Caco-2 Zellen ist der Vorteil der hier aufgestellten Apparatur insbesondere in ihrem modularen Aufbau sowie in ihrer daraus resultierenden Vielseitigkeit und Flexibilität zu sehen. Durch die hydrodynamische Trennung von Dissolutions- und Permeationsmodul können vom Arzneibuch geforderte Dissolutionspumpen verwendet werden, welche ein sinusoidales Flußprofil erzeugen und somit prinzipiell inkompatibel mit druckschwankungssensitiven Caco-2 Zellmonolayer sind. Des weiteren können die Flußraten in beiden Modulen in gewissen Grenzen unabhängig voneinander verändert werden, was die Methodenentwicklung für

die Dissolutionsmessung erheblich erleichtert und es somit ermöglicht, Konzentrationen im Permeationsmodul mit *in vivo* Relevanz zu erzeugen.

In einem weiteren Teilprojekt wurde anschließend versucht, ausgehend von den erzeugten Daten die Konzentrations-Zeit Verläufe an den verschiedene Probennahmepunkte D, A und B zu modellieren. Motivation hierfür war, das Verständnis für die Apparatur zu verbessern und künftig Experimente auf ihre Schlüssigkeit mit einem Computermodell überprüfen zu können. Das der Modellierung zu Grunde liegende Modell läßt sich folgendermaßen beschreiben: Die Apparatur wurde in verschiedene Kompartimente geteilt, so die Durchflussdissolutionszelle, der Probenteiler und die apikale Seite der Durchflusspermeationszelle. Die so erzeugten Kompartimente wurden mit den tatsächlichen Ausmaßen entsprechenden Leitungen verbunden. In diesen Leitungen wurde die Fortbewegung von Substanzteilchen mit Hilfe eines parabolischen Flussprofiles nach den Vorgaben des Gesetzes nach Hagen-Poiseuille beschrieben. Die Freisetzung aus der Arzneiform wurde mit Hilfe einer Weibull-Verteilung dargestellt. Um das so aufgestellte Model und seine Parameter, wie - beispielsweise Flußverhältnis - zu kalibrieren und zu validieren, wurden die Konzentrations-Zeit Verläufe einer in die Durchflussdissolutionszelle eingebrachten Propranolol HCl Lösung modelliert. Nach der Kalibrierung wurden die Konzentrations-Zeit Verläufe für die verschiedenen Propranolol HCl Tabletten berechnet und mit den experimentellen Daten verglichen.

Nach ersten erfolgreichen Tests der Apparatur stellte sich die Frage nach einer Automatisierung. Manuelle Probennahme und -analytik schienen zu zeitaufwendig und behinderten ein weiteres schnelles Vorankommen. Von den verschiedenen möglichen Automatisierungsstrategien erschien die sequentielle Injektionsanalyse (SIA) am erfolgversprechendsten. Für die Quantifizierung in den ersten Studien wurde die Fluoreszenz von Propranolol HCl in KRB verwendet. Hierfür wurde an den verschiedenen Probennahmepunkten ein geeignetes Probenvolumen automatisiert in die Halteschleife aspiriert, um anschließend diese Probe durch den Fluoreszenzdetektor zu schieben. Die hierbei erhaltene Peakhöhe würde mit Propranolol HCl Standardkonzentrationen korreliert.

Im Rahmen der Automatisierung erwies vor allem die große Bandbreite an zu messenden Konzentrationen als Herausforderung. Aus diesem Grund wurden für die

Probennahmepunkte D und A geringere Probenvolumen in den Detektor injiziert, um den linearen Bereich zu erweitern. Gleichzeitig wurde für den Probennahmepunkt B ein größeres Volumen verwendet. Nach erfolgter Kalibration wurden 10 mg Propranolol HCl Tabletten mit der automatisierten Testapparatur erfolgreich vermessen. Mit Hilfe der Automatisierung konnte die Probennahme- und Analysenfrequenz im Vergleich zum manuellen Ansatz nahezu verdoppelt werden. Gleichzeitig wurde es ermöglicht, die Apparatur ohne Aufsicht zu betreiben, was den Durchsatz erheblich erhöhte.

Nach diesem ausführlichen Testen und Entwickeln der Apparatur gerieten Arzneistoffe aus problematischeren BCS Klassen in den Fokus des Interesses. hierbei wurde insbesondere Furosemid (Lasix®) wurde hierbei als möglicher Kandidat in Erwägung gezogen. Der Arzneistoff weist eine niedrige intrinsische Permeabilität durch Caco-2 Zellmonolayer auf, und sein Transport unterliegt einer ausgeprägten Polarität. Weiter läßt sich die Polarität des Transportes durch Zugabe geeigneter Hilfsstoffe wie TWEEN 80 oder Vitamin E TPGS beeinflussen. Vor der eigentlichen Messung der Lasix® Tabletten mußte jedoch die Analytik auf die neuen Bedürfnisse angepaßt werden. Furosemid zeigt keine Fluoreszenz in salzhaltigen, wäßrigen Medien und ist deshalb an den Probennahmepunkten D und A nur per UV-Messung zugänglich. Auf Grund der niedrigen Konzentration im basolateralen Probennahmepunkt wurde weiterhin eine Methode entwickelt, um Proben automatisch in HPLC Probenbehälter abzufüllen und anschließend offline per HPLC zu analysieren.

Die Freisetzung von Furosemid aus Lasix® in KRB pH 6.5 ging vergleichsweise schnell vonstatten, und die Wiederfindungsrate am Probennahmepunkt D war mit etwa 98 % ausreichend hoch. Am Probennahmepunkt B wurde jedoch eine zu hohe und bislang noch nicht zu erklärende Konzentration festgestellt. Mögliche Ursachen für dieses Verhalten könnten eine Sättigung des Effluxtransporters durch hohe Donorkonzentrationen oder reversible, durch osmotischen Druck vermittelte Effekte auf den Caco-2 Monolayer und seine Zell-Zell-Verbindungen sein. Dies wird in anschließenden Studien zu klären sein.

In Zukunft könnte die hier entwickelte Testapparatur wie folgt weiterentwickelt werden. Zum eine fehlt der Testapparatur noch die Möglichkeit den pH Wertverlauf, den eine Substanz nach oraler Applikation erfährt, zu simulieren. Zum anderen sollte das Dissolutionsmedium derart modifiziert werden, daß seine Eigenschaften näher an der

tatsächlichen *in vivo* Situation liegen und die Ergebnisse somit mehr *in vivo* Relevanz erlangen.

Zusammenfassend läßt sich sagen, daß erfolgreich ein vielseitiges und äußerst flexibles Werkzeug zur Bestimmung der Permeabilität fester, oraler Arzneiformen entwickelt wurde. Flußraten in den Modulen lassen sich weitestgehend frei einstellen; auch die Art der Pumpe im Dissolutionsmodul läßt sich frei wählen. Des weiteren weist die Apparatur einen hohen Grad an Automatisierung auf, was den Durchsatz erheblich steigert und mögliche Fehlerquellen minimiert. Hierbei stehen verschiedene Quantifizierungsmethoden zur Auswahl - so UV/VIS, Fluoreszenz oder HPLC- Messung - zur Wahl.

8 Annexes

8.1 List of abbreviations

BCS	biopharmaceutical classification system
CMC	critical micelle concentration
FIA	flow injection analysis
FTPC	flow through permeation cell
HEPES	N-2-hydroxyethylpiperazine- N'-2-ethane sulfonic acid
HPLC	high performance liquid chromatography
KRB	Krebs Ringer buffer
LOD	limit if detection
LOQ	limit of quantification
MES	morpholino ethane sulfonic acid
P_{app}	apparent permeability
$P_{app}(A\text{-}B)$	apparent permeability in absorptive direction (apical - basolateral)
$P_{app}(B\text{-}A)$	apparent permeability in secretory direction (basolateral - apical)
POM	polyoxythylene
RMSD	route mean square deviation
SIA	sequential injection analysis
s_{rel}	relative standard deviation
UV	ultra violet light
VIS	visible light

8.2 Standard operating procedure for the automated setup

8.2.1 Preparation:

8.2.1.1 Preparing the devices

- Turn on the UV lamp (burn in time: 45 min) and all other SIA devices. Manually log on all devices to the controlling computer.
- Heat the water bath to 37.0 ± 0.1 °C.
- Preheat all buffers prior to degassing to approximately 30 °C.
- Degas the carrier solvent for SIA (Millipore® water) by means of magnetically stirring for ten minutes in a 2 l feeding bottle (VWR 519-4125) under reduced pressure generated by a vacuum pump. Change the carrier water and its bottle at least once a weak.
- Degas all buffers by magnetically stirring for ten minutes in a 2 l feeding bottle (VWR 519-4125) under reduced pressure generated by a vacuum pump.
- Purge all tubing with the respective degassed buffers. Therefore, open the basolateral compartment and adjust flow rate of the SIA peristaltic pump to 40 arbitrary units (approx. 1.9 ml/min). Purge the dissolution module (> 6 $ml \cdot min^{-1}$) as well as the apical compartment (1 $ml \cdot min^{-1}$) for at least 30 min. Purge the basolateral compartment (1-2 $ml \cdot min^{-1}$) for at least 45 min.
- In the mean time, manually purge the interface tubing between the apparatus and the SIA eight port valve (sampling port D, A and B) and also the connecting tubing to the autosampler tip as well as the flow through detector cell (fluorescence and/or UV).
- UV detection: post washing the detector cell; perform a dark scan with the UV detector and subsequently a reference scan.
- Post purging the apparatus, close the basolateral compartment. Add sufficient volume of KRB (pH 7.4) in the basolateral vessel. Then, let the SIA peristaltic pump run until no more air bubble are visible in the tubing. Subsequently, turn off the SIA peristaltic pump.

- In order to exclude any air bubbles in the basolateral compartment press the “prime drain” button at the basolateral membrane dosage pump. Do not turn off the pump until any more air bubble escape out of the FPTC. Assure that during that procedure, the basolateral vessel does not run out of KRB.
- Add a "waste" Falcon® tube in standard tray position 10 of the autosampler.
- Open an appropriate SIA program for the experiment.

If analysis of the permeated compound by means of HPLC is planned, add sufficient HPLC vials with 200 µl inserts (CE Chromatographieservice, Langerwehe-Jüngersdorf, GE) into the autosampler tray (technical depiction given in Figure 8.7 and Figure 8.8).

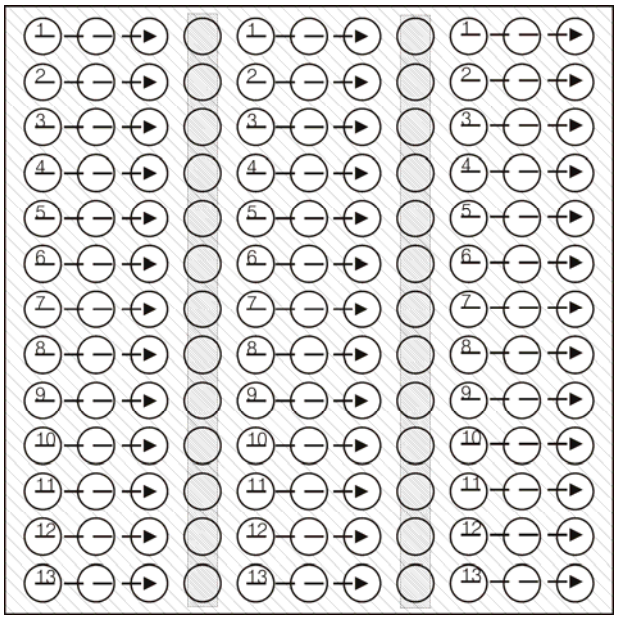

Figure 8.1. Allocation of the various positions on the autosampler tray. Numbers and arrow indicate the progression of the autosampler tip (first column sample tray 1; second column sample tray 2; ...).

8.2.1.2 Preparing the flow dissolution apparatus 4

- Add a ruby bead in the flow through cell
- Add approximately 1 g of glass beads into the flow cell
- Place the tablet onto the glass beads by means of tweezers
- Insert a filter sheet (type GF/D, Whatman International Ltd, Maidstone, UK) in the head of the apparatus 4 by means of tweezers.
- Connect the stainless steel bracket of the apparatus to the tubing of the dissolution pump (3 way valve). (this has to be done prior to assembling the apparatus 4)

- Turn on the dissolution pump in order to purge the “heating spiral” and the tubing between the apparatus 4 and the pump for 3 min with the respective KRB. Remove the buffer from the outlet by means of a Pasteur pipette. Then turn off the dissolution pump.
- Assemble the apparatus 4 completely, place it in the water bath, and connect also its outlet. Confirm that the 3-way valves are set correctly.

8.2.1.3 Preparing the Caco-2 cell monolayer

- Fill 50 ml of each KRB buffer in Falcon® tubes (Becton-Dickinson, Heidelberg, GE) and preheat those to 37 °C.
- Wash the Caco-2 cell monolayer twice with KRB.
- Equilibrate for at least 30 min. When assessing P-gp – surfactant interaction equilibrate for 60 min with the respective surfactant containing buffer.
- After the equilibration assess TEER value and microscopical appearance of the monolayer.

8.2.1.4 Inserting Caco-2 cell monolayer into the FTPC

- Prepare appropriate Falcon® tubes with preheated KRB buffer for primary filling of the FTPC
- Place the Transwell® plate with the Caco-2 monolayer in front of the water bath. Then, take the FTPC out the water bath, open it by means of an Allen key. Remove all KRB in the FTPC by means of a Pasteur pipette. After filling the basolateral cavity of the FTPC with the KRB ph 7.4, insert the Transwell® and finally add the respective apical KRB solution. Subsequently, close the FTPC cautiously in order to prevent deleterious pressure on the Caco-2 monolayer and submerse the FTPC in the water bath.
- Turn on all pumps (dissolution, apical and basolateral) except the SIA peristaltic pump. Assure that the basolateral vessel is not running out of KRB. Turn on the apical and basolateral pump simultaneously.
- Let the pumps run until basolaterally and apically no air bubbles are escaping the FTPC, but a least for 10 min. Then, turn off all pumps.
- In order to warrant a reproducible volume of KRB in the basolateral compartment, empty the basolateral vessel by means of a Pasteur pipette

completely. Subsequently, add 1.0 ml of KRB pH 7.4 into the vessel. Close the basolateral vessel by means of an Allen key.

8.2.1.5 Starting the analysis.

- Be sure, that all tubes are connected tightly and that all SIA devices are logged on.
- Control all three way valves for their correct position.
- Be sure that the buffer bottle prior to the dissolution pump is submersed in the water bath and is weighted down by means of a lead donut. (Otherwise, the bottle might afloat in the water bath when the water level in the bottle falls throughout the experiment)
- To start the real experiment, simultaneously turn on the dissolution pump and execute the SIA program. All other manually controlled pumps remain switched of.
- Observe the outlet of the flow through dissolution apparatus 4. After approximately 2 min (depending on the flow rate of the dissolution pump and the internal volume of the USP apparatus 4), the air will be completely driven out of the flow through dissolution cell and KRB will again fill the tubing.
- When KRB reaches the stream splitter, wait for another 2 seconds and subsequently turn on all other manually controlled pumps.
- Wait for the first sample aspirated and injected into the flow through absorption device. Be sure, that no air bubbles were allowed to enter the flow through absorption device. Check in the analysis window of the SIA software the shape and baseline of the first peak. If this peak is OK, check for another time all other devices for their proper function and all fill levels.

8.3 Programming codes for SIA for analysis of propranolol HCl in KRB

8.3.1 Main routine for propranolol HCl

```
Peristaltic Pump Clockwise(%) 20
Peristaltic Pump On

    Insert File C:\Programme\WINFIA 5.0\Programm September 2005\probenzug 50\Probenzug basolateral 1.fia

Delay (sec) 30

    Insert File C:\Programme\WINFIA 5.0\Programm September 2005\probenzug 25\Probenzug dissolution 25- neuer Propenzug.fia

    Insert File C:\Programme\WINFIA 5.0\Programm September 2005\probenzug 25\Probenzug apical 25- neuer Probenzug.fia

    Insert File C:\Programme\WINFIA 5.0\Programm September 2005\probenzug 25\Probenzug dissolution 25- neuer Propenzug.fia

    Insert File C:\Programme\WINFIA 5.0\Programm September 2005\probenzug 25\Probenzug apical 25- neuer Probenzug.fia

    Insert File C:\Programme\WINFIA 5.0\Programm September 2005\probenzug 25\Probenzug dissolution 25- neuer Propenzug.fia

    Insert File C:\Programme\WINFIA 5.0\Programm September 2005\probenzug 50\Probenzug basolateral 1.fia

     Insert File C:\Programme\WINFIA 5.0\Programm September 2005\probenzug 25\Probenzug dissolution 25- neuer Propenzug.fia

    Insert File C:\Programme\WINFIA 5.0\Programm September 2005\probenzug 25\Probenzug apical 25- neuer Probenzug.fia

Loop Start (#) 20

    Insert File C:\Programme\WINFIA 5.0\Programm September 2005\probenzug 25\Probenzug dissolution 25- neuer Propenzug.fia

    Insert File C:\Programme\WINFIA 5.0\Programm September 2005\probenzug 25\Probenzug apical 25- neuer Probenzug.fia

    Insert File C:\Programme\WINFIA 5.0\Programm September 2005\probenzug 25\Probenzug dissolution 25- neuer Propenzug.fia

    Insert File C:\Programme\WINFIA 5.0\Programm September 2005\probenzug 25\Probenzug apical 25- neuer Probenzug.fia

    Insert File C:\Programme\WINFIA 5.0\Programm September 2005\probenzug 25\Probenzug dissolution 25- neuer Propenzug.fia

    Insert File C:\Programme\WINFIA 5.0\Programm September 2005\probenzug 25\Probenzug apical 25- neuer Probenzug.fia

    Insert File C:\Programme\WINFIA 5.0\Programm September 2005\probenzug 50\Probenzug basolateral 1.fia

      Delay (sec) 15

Loop End
```

8.3.2 Aspiration and analysis of propranolol HCl at sampling port D (dissolution)

Syringe Pump Valve In

Syringe Pump Flowrate (microliter/sec) 250
Syringe Pump Aspirate (microliter) 1000

Multiposition Valve dissolution

Syringe Pump Delay Until Done

Syringe Pump Valve Out

Syringe Pump Flowrate (microliter/sec) 100
Syringe Pump Aspirate (microliter) 50
Syringe Pump Delay Until Done

Multiposition Valve waste

Syringe Pump Flowrate (microliter/sec) 200
Syringe Pump Dispense (microliter) 100
Syringe Pump Delay Until Done

Multiposition Valve dissolution

Syringe Pump Flowrate (microliter/sec) 25
Syringe Pump Aspirate (microliter) 25
Syringe Pump Delay Until Done

Multiposition Valve PMT-FL

Syringe Pump Flowrate (microliter/sec) 50
Syringe Pump Empty

Analyte New Sample
Analyte Name dissolution

PMT Start Scans

Syringe Pump Delay Until Done

PMT Stop Scans

8.3.3 Aspiration and analysis of propranolol HCl at sampling port A (apical)

Syringe Pump Valve In

Syringe Pump Flowrate (microliter/sec) 500
Syringe Pump Aspirate (microliter) 1000
Syringe Pump Delay Until Done

Syringe Pump Valve Out

Multiposition Valve apical

Syringe Pump Flowrate (microliter/sec) 15
Syringe Pump Aspirate (microliter) 100
Syringe Pump Delay Until Done

Multiposition Valve waste

Syringe Pump Flowrate (microliter/sec) 200
Syringe Pump Dispense (microliter) 200
Syringe Pump Delay Until Done

Multiposition Valve apical

Syringe Pump Flowrate (microliter/sec) 15
Syringe Pump Aspirate (microliter) 25
Syringe Pump Delay Until Done

Multiposition Valve PMT-FL

Syringe Pump Flowrate (microliter/sec) 50
Syringe Pump Empty

Analyte New Sample
Analyte Name apical

PMT Start Scans

Syringe Pump Delay Until Done

PMT Stop Scans

8.3.4 Aspiration and analysis at of propranolol HCl sampling port B (basolateral)

Syringe Pump Valve In

Syringe Pump Flowrate (microliter/sec) 500
Syringe Pump Aspirate (microliter) 1500
Multiposition Valve basolateral
Syringe Pump Delay Until Done

Syringe Pump Valve Out

Syringe Pump Flowrate (microliter/sec) 25
Syringe Pump Aspirate (microliter) 25
Syringe Pump Delay Until Done

Multiposition Valve waste

Syringe Pump Flowrate (microliter/sec) 100
Syringe Pump Dispense (microliter) 50
Syringe Pump Delay Until Done

Multiposition Valve basolateral

Syringe Pump Flowrate (microliter/sec) 25
Syringe Pump Aspirate (microliter) 50
Syringe Pump Delay Until Done

Multiposition Valve PMT-FL

Analyte New Sample
Analyte Name basolateral

Syringe Pump Flowrate (microliter/sec) 50
Syringe Pump Dispense (microliter) 1000

PMT Start Scans

Syringe Pump Delay Until Done

PMT Stop Scans

Multiposition Valve replenishing

Syringe Pump Flowrate (microliter/sec) 25
Syringe Pump Aspirate (microliter) 100
Syringe Pump Delay Until Done

Multiposition Valve basolateral

Syringe Pump Dispense (microliter) 75
Syringe Pump Delay Until Done

Multiposition Valve waste

Syringe Pump Flowrate (microliter/sec) 500
Syringe Pump Empty
Syringe Pump Delay Until Done

8.4 Programming codes for SIA for analysis of furosemide in KRB

8.4.1 Main routine for furosemide

```
Hardware Settings Wavelength 1 (nm) 275
Hardware Settings Wavelength 2 (nm) 276
Hardware Settings Wavelength 3 (nm) 344
Hardware Settings Wavelength 4 (nm) 360


Spectrometer Reference Scan

Variable Define New sampos

sampos = 1

Insert File C:\Programme\WINFIA 5.0\Furosemid dissolution measurement\Subroutinen DisPer measurement\basolateral-offen Kompartiment.fia

Delay (sec) 55

Insert File C:\Programme\WINFIA 5.0\Furosemid dissolution measurement\Subroutinen DisPer measurement\dissolution.fia

Insert File C:\Programme\WINFIA 5.0\Furosemid dissolution measurement\Subroutinen DisPer measurement\dissolution.fia

Insert File C:\Programme\WINFIA 5.0\Furosemid dissolution measurement\Subroutinen DisPer measurement\apical.fia

Insert File C:\Programme\WINFIA 5.0\Furosemid dissolution measurement\Subroutinen DisPer measurement\dissolution.fia

Insert File C:\Programme\WINFIA 5.0\Furosemid dissolution measurement\Subroutinen DisPer measurement\apical.fia

sampos += 1

Insert File C:\Programme\WINFIA 5.0\Furosemid dissolution measurement\Subroutinen DisPer measurement\basolateral-offen Kompartiment.fia

Loop Start (#) 40

sampos += 1

Insert File C:\Programme\WINFIA 5.0\Furosemid dissolution measurement\Subroutinen DisPer measurement\dissolution.fia

Insert File C:\Programme\WINFIA 5.0\Furosemid dissolution measurement\Subroutinen DisPer measurement\apical.fia

Insert File C:\Programme\WINFIA 5.0\Furosemid dissolution measurement\Subroutinen DisPer measurement\dissolution.fia

Insert File C:\Programme\WINFIA 5.0\Furosemid dissolution measurement\Subroutinen DisPer measurement\apical.fia

Insert File C:\Programme\WINFIA 5.0\Furosemid dissolution measurement\Subroutinen DisPer measurement\dissolution.fia

Insert File C:\Programme\WINFIA 5.0\Furosemid dissolution measurement\Subroutinen DisPer measurement\apical.fia

Insert File C:\Programme\WINFIA 5.0\Furosemid dissolution measurement\Subroutinen DisPer measurement\basolateral-offen Kompartiment.fia

Loop End
```

8.4.2 Aspiration and analysis of furosemide at sampling port D (dissolution)

Syringe Pump Valve In

Syringe Pump Flowrate (microliter/sec) 500
Syringe Pump Aspirate (microliter) 750
Multiposition Valve dissolution
Syringe Pump Delay Until Done

Syringe Pump Valve Out

Syringe Pump Flowrate (microliter/sec) 100
Syringe Pump Aspirate (microliter) 50
Syringe Pump Delay Until Done

Multiposition Valve Waste

Syringe Pump Flowrate (microliter/sec) 250
Syringe Pump Dispense (microliter) 300
Syringe Pump Delay Until Done

Multiposition Valve dissolution

Syringe Pump Flowrate (microliter/sec) 15
Syringe Pump Aspirate (microliter) 100
Syringe Pump Delay Until Done

Delay (sec) 2

Multiposition Valve UV- detector

Syringe Pump Flowrate (microliter/sec) 30

Analyte New Sample
Analyte Name Dis

Spectrometer Absorbance Scanning

Delay (sec) 3
Syringe Pump Empty
Syringe Pump Delay Until Done

Spectrometer Stop Scanning

8.4.3 Aspiration and analysis of furosemide at sampling port A (apical)

Syringe Pump Valve In

Syringe Pump Flowrate (microliter/sec) 500
Syringe Pump Aspirate (microliter) 750
Multiposition Valve apical
Syringe Pump Delay Until Done

Syringe Pump Valve Out

Syringe Pump Flowrate (microliter/sec) 15
Syringe Pump Aspirate (microliter) 100
Syringe Pump Delay Until Done

Multiposition Valve Waste

Syringe Pump Flowrate (microliter/sec) 250
Syringe Pump Dispense (microliter) 350
Syringe Pump Delay Until Done

Multiposition Valve apical

Syringe Pump Flowrate (microliter/sec) 15
Syringe Pump Aspirate (microliter) 100
Syringe Pump Delay Until Done

Delay (sec) 2

Multiposition Valve UV- detector

Syringe Pump Flowrate (microliter/sec) 30

Analyte New Sample
Analyte Name Api

Spectrometer Absorbance Scanning

Delay (sec) 3
Syringe Pump Empty
Syringe Pump Delay Until Done

Spectrometer Stop Scanning

8.4.4 Aspiration and analysis of furosemide at sampling port B (basolateral)

Syringe Pump Valve In

Syringe Pump Flowrate (microliter/sec) 500
Syringe Pump Aspirate (microliter) 750
Multiposition Valve basolateral
Syringe Pump Delay Until Done

Syringe Pump Valve Out

Syringe Pump Flowrate (microliter/sec) 15
Syringe Pump Aspirate (microliter) 100
Syringe Pump Delay Until Done

Multiposition Valve Waste

Syringe Pump Flowrate (microliter/sec) 250
Syringe Pump Dispense (microliter) 350
Syringe Pump Delay Until Done

Multiposition Valve PMT-FL

Syringe Pump Flowrate (microliter/sec) 25
Syringe Pump Aspirate (microliter) 25
Syringe Pump Delay Until Done

Multiposition Valve basolateral

Syringe Pump Flowrate (microliter/sec) 15
Syringe Pump Aspirate (microliter) 100

autosampler Wash
autosampler standard rack (sample #) 10

Syringe Pump Delay Until Done

Multiposition Valve PMT-FL

Syringe Pump Flowrate (microliter/sec) 25
Syringe Pump Aspirate (microliter) 25
Syringe Pump Delay Until Done

Multiposition Valve autosampler

Syringe Pump Flowrate (microliter/sec) 25
Syringe Pump Dispense (microliter) 210
Syringe Pump Delay Until Done

autosampler RACK 2 (sample #) sampos

Delay (sec) 0,2

Syringe Pump Flowrate (microliter/sec) 25
Syringe Pump Dispense (microliter) 110
Syringe Pump Delay Until Done

autosampler standard rack (sample #) 10

Syringe Pump Flowrate (microliter/sec) 250
Syringe Pump Dispense (microliter) 350
Syringe Pump Delay Until Done

8.4.5 Configuration of the autosampler rack

8.4.5.1 Configuration of the autosampler rack for the 10 standard falcon tubes

name of rack :	standard rack
number of rows:	5
number of columns:	2
X position of Sample #1 [mm]:	1
Y position of Sample #1 [mm]:	53
Delta X position of samples in rack [mm]:	30
Delta Y position of samples in rack [mm]:	36
Up position [mm]:	50
Down position [mm]:	70

Table 8.1. Standard tray autosampler configuration

8.4.5.2 Configuration of the autosampler rack for HPLC vial filling

name of rack :	standard rack
number of rows:	5
number of columns:	2
X position of Sample #1 [mm]:	1
Y position of Sample #1 [mm]:	53
Delta X position of samples in rack [mm]:	30
Delta Y position of samples in rack [mm]:	36
Up position [mm]:	50
Down position [mm]:	70

Table 8.2. HPLC vials tray autosampler configuration

8.4.6 Configuration of the UV spectrometer (USB 2000)

parameter	setting
integration time [ms] :	80
detectors to average :	1
samples to average :	3
sample rate [Hz] :	4
plotting threshold [counts] :	0
offset absorbance :	0
scale voltage :	10
first coefficient :	0.3832872
second coefficient :	$-1.45952 \cdot 10^{-5}$
third coefficient :	$-2.31592 \cdot 10^{-9}$
intercept :	177.4774

Table 8.3. Setting of the spectrometer for furosemide UV - SIA analysis.

8.4.7 Port allocation of the multiposition valve for propranolol HCl

allocation	port position
waste	1
autosampler	2
KRB for replenishing	3
basolateral	4
apical	5
dissolution	6
--	7
PMT-FI	8

Table 8.4. SIA port allocation for propranolol HCl.

8.4.8 Port allocation of the multiposition valve for furosemide

allocation	port position
waste	1
autosampler	2
--	3
basolateral	4
apical	5
dissolution	6
"air"	7
UV detector	8

Table 8.5. SIA port allocation for furosemide.

8.5 Engineering detail drawings

In the following, the gauges of the custom made parts of the apparatus for permeability assessment of solid oral dosage formulations based on a Caco-2 monolayer and a flow through dissolution cell are given. Gauges are given where necessary in millimetre.

8.5.1 Technical depiction of the stream splitter

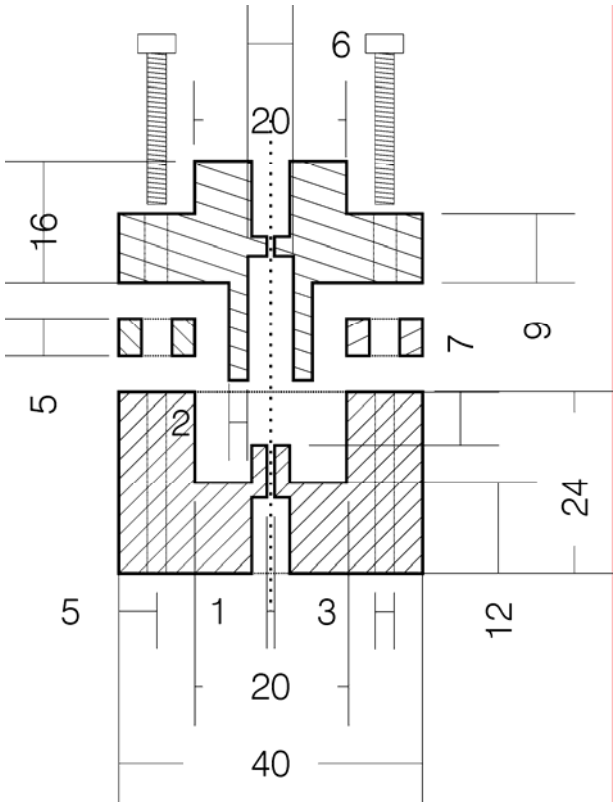

Figure 8.2. Stream splitter, material PEEK

8.5.2 Technical depiction of the FTPC

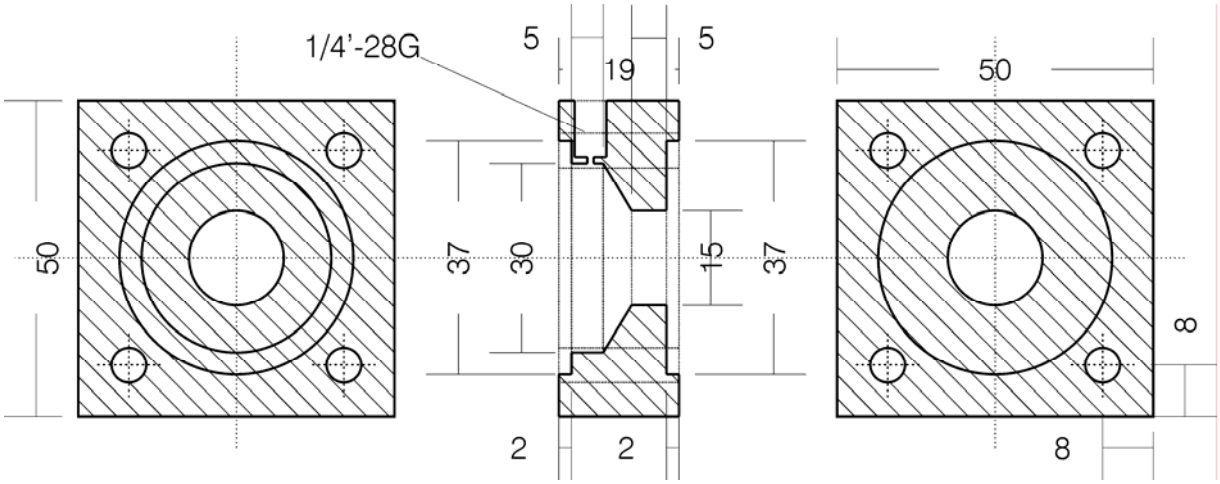

Figure 8.3. Middle part of the FTPC, material PEEK

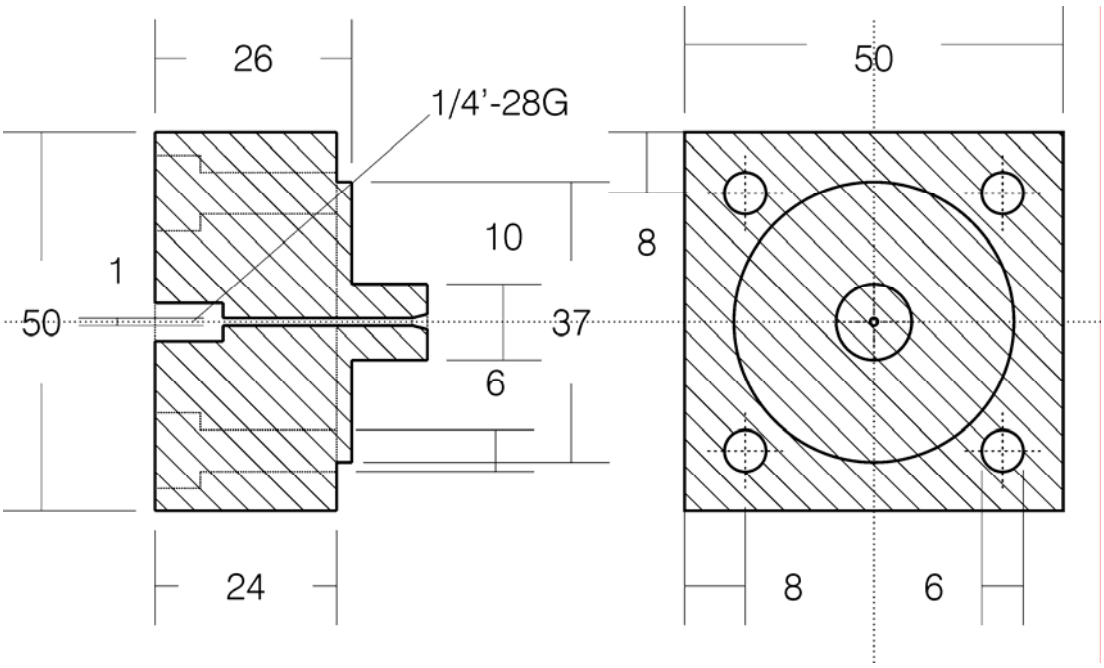

Figure 8.4. Apical part of the FTPC, material PEEK

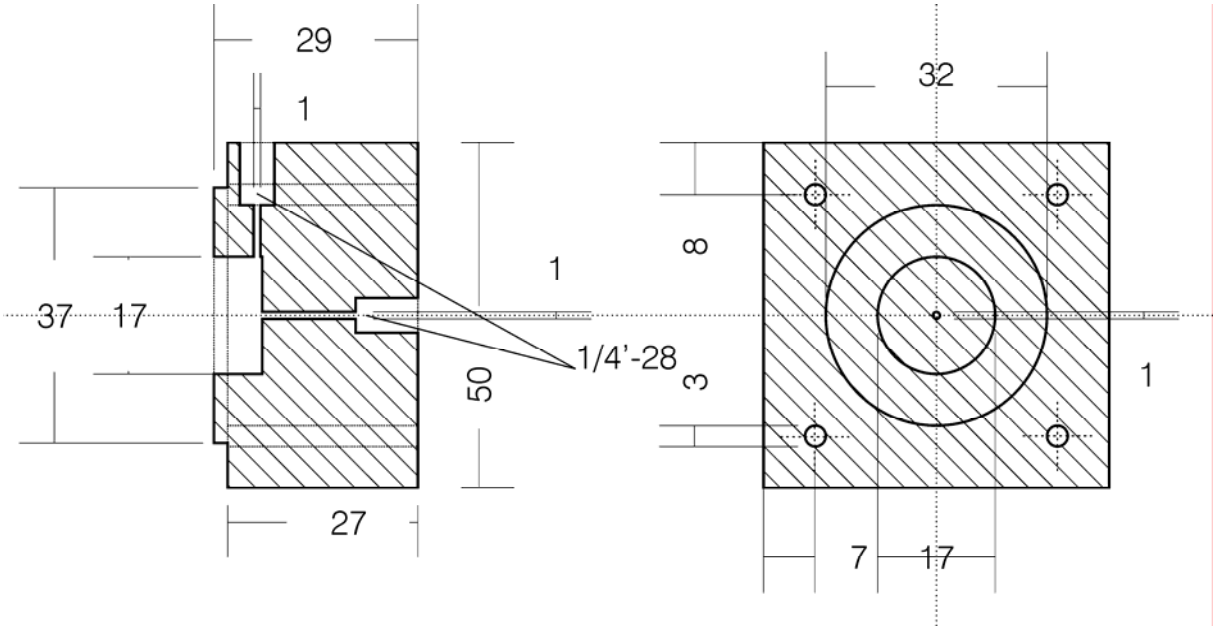

Figure 8.5. Basolateral part of the FTPC, material PEEK

8.5.3 Technical depiction of the basolateral vessel

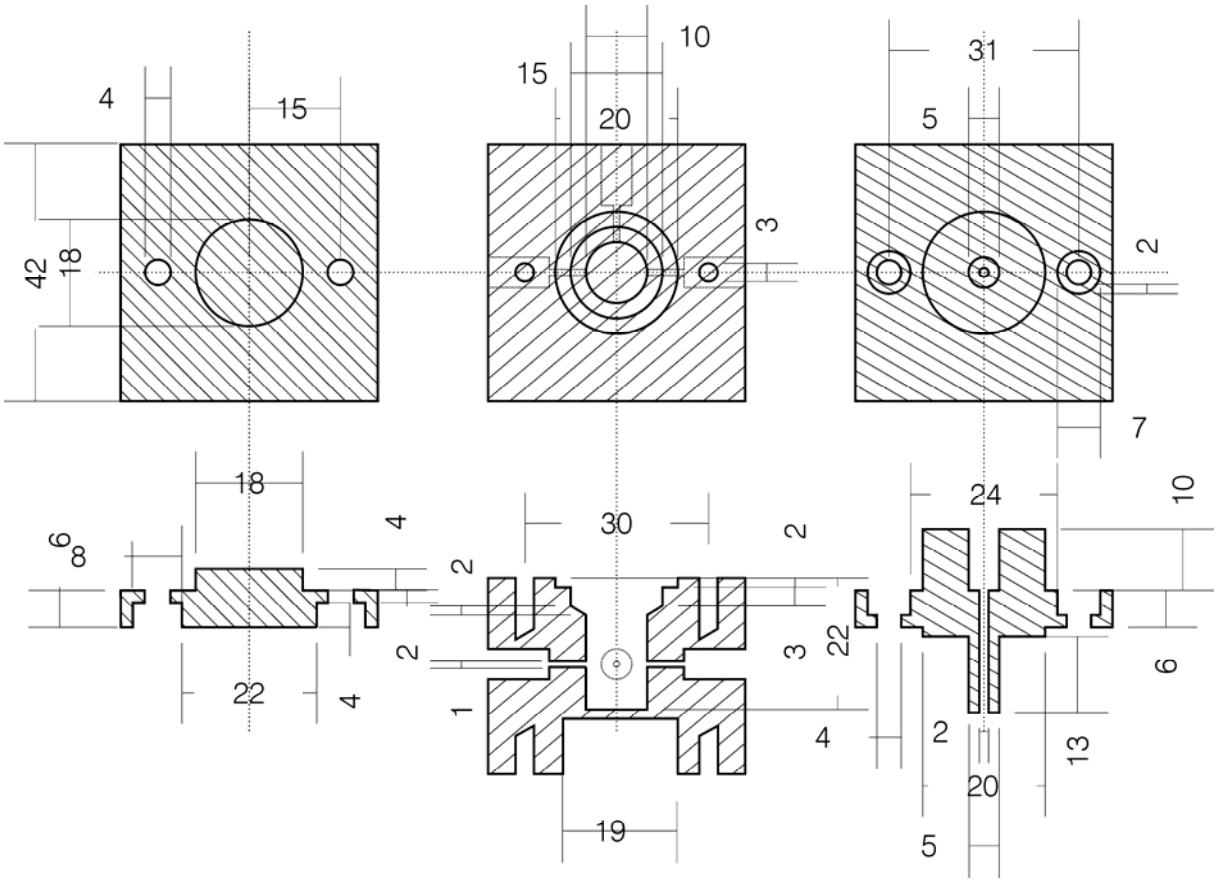

Figure 8.6. Basolateral vessel, material PEEK.

8.5.4 Technical depiction of the autosampler tray

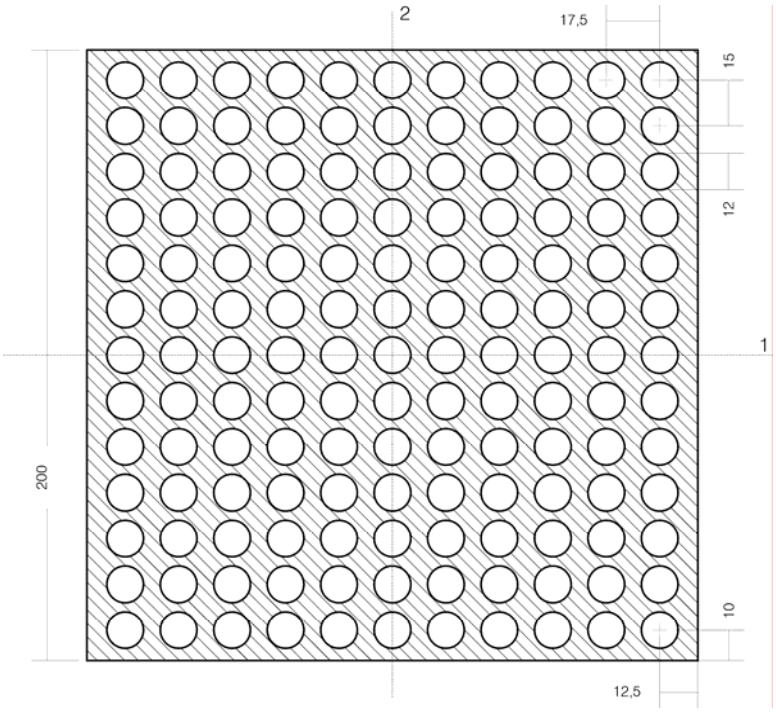

Figure 8.7. Top view on the autosampler tray, material POM

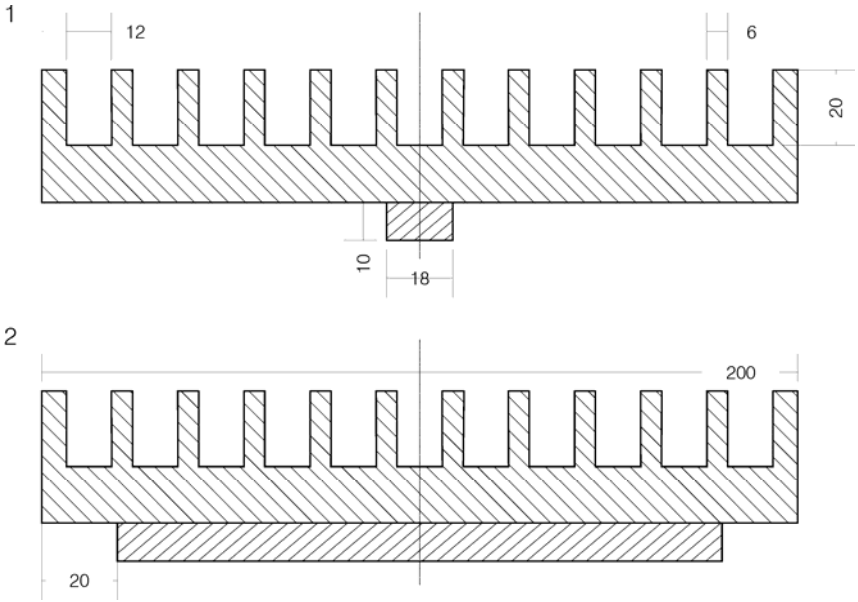

Figure 8.8. Lateral view on the autosampler tray, material POM

8.6 Publication list

publications:

Motz SA, Schaefer UF, Balbach S, Eichinger T, Lehr CM. Permeability assessment for solid oral drug formulations based on Caco-2 monolayer in combination with a flow through dissolution cell, Eur. J. Pharm. Biopharm. (2007), doi:10.1016/j.ejpb.2006.10.015

Motz SA, Klimundová J, Schäfer U, Balbach S, Eichinger T, Solich P, Lehr CM. Automated measurement of dissolution and permeation of propranolol HCl tablets using sequential injection analysis, Analytica Chimica Acta, Acta 581 (2007) pp. 174–180

Motz SA, Bur M, Schäfer UF, Lehr CM. Instrumented approaches to assess epithelia permeability of drugs from pharmaceutical formulations, Springer, Ed. Kim KJ, Ehrhardt C, 2007

awards:

CRS Capsugel/Pfizer Innovative Aspect of Oral Drug Delivery and Absorption Graduate/ Post-Doc award, June 2005, Miami, FL, USA

conferences:

posters:

Motz SA, Schäfer UF, Balbach S, Eichinger T, Lehr CM. Development of a flow through system with combined dissolution and permeation device for drug formulations, Pharmaceutical Sciences World Congress (PSWC), May/June 30-03, Kyoto, Japan.

Motz SA, Schäfer UF, Balbach S, Eichinger T, Lehr CM. Combined measurement of dissolution and permeation through a Caco-2 monolayer of propranolol HCl immediate release tablets, 6th International Conference and Workshop on Cell Culture and In-Vitro Models for Drug Absorption and Delivery, March 1-10, 2006, Saarbrücken, Germany

Motz SA, Schäfer UF, Balbach S, Eichinger T, Lehr CM. Combined measurement of dissolution and permeation through a Caco-2 monolayer of propranolol HCl extended release tablets, 33rd annual meeting of the controlled release society (CRS), June 22-26, 2006, Vienna, Austria

Motz SA, Klimundová J, Schäfer UF, Balbach S, Eichinger T, Solich P, Lehr CM. Automated measurement of dissolution and permeation of propranolol HCl tablets using sequential injection analysis, 2006 AAPS Annual Meeting and Exposition, October 29. – November 02., 2006, San Antonio, TX, USA *and* GPEN 2006, October 24-27, 2006, Lawrence, KS, USA

oral presentations:

Motz SA, Schäfer UF, Balbach S, Eichinger T, Lehr CM. Development of a flow through system with combined dissolution and permeation device for drug formulations, Global Pharmaceutical Education Network (GPEN), May 26-28, 2004, Kyoto, Japan.

Motz SA, Schäfer UF, Balbach S, Eichinger T, Lehr CM. Combined measurement of dissolution and permeation through a Caco-2 monolayer of propranolol HCl immediate release tablets, 32nd annual meeting of the controlled release society (CRS), June 20-24, 2005, Miami Beach, FL, USA.

8.7 Curriculum vitae

personal information

name	Stephan Alexander Motz
date of birth	16.11.1976
place of birth:	Lahr, Germany

PhD thesis

September 2004 – December 2006	Department of Biopharmaceutics and pharmaceutical Technology, Saarland University under supervision of Prof. Dr. Claus- Michael Lehr

undergraduate study

WS 1997/98 – WS 2001/02	Pharmacy, Albert-Ludwigs-Universität, Freiburg Certification as Pharmacist in May 2004

civilian service

1996 –1997	Intensive care unit, Herzzentrum Lahr.

school

1987 – 1996	Secondary High School “Max- Planck- Gymnasium” Lahr. University entrance requirement
1983 – 1987	Friedrich-Grundschule, Lahr

internships

August 1999	Department of regulatory affairs, former Gödecke, -Parke/Davis, Freiburg (Famulatur).
May 2002 – October 2002	Galenic research and development, Hoffman-La Roche, Basel, Switzerland (first part of the practical training for pharmacists).
November 2002 – April 2003	„City Apotheke“, Freiburg (second part of the practical training for pharmacists).

9 References

[1] Kim KJ, Ehrhard C (2007) Preclinical Biopharmaceutics - In situ, in vitro, and in silico tools for drug absorption studies. Springer,

[2] Galia E, Nicolaides E, Horter D, Löbenberg R, Reppas C, Dressman JB (1998) Evaluation of various dissolution media for predicting in vivo performance of class I and II drugs. Pharm Res 15: 698-705

[3] Artursson P, Karlsson J (1991) Correlation between oral drug absorption in humans and apparent drug permeability coefficients in human intestinal epithelial (Caco-2) cells. Biochem Biophys Res Commun 175: 880-885

[4] Nicolaides E, Galia E, Efthymiopoulos C, Dressman JB, Reppas C (1999) Forecasting the in vivo performance of four low solubility drugs from their in vitro dissolution data. Pharm Res 16: 1876-82

[5] Löbenberg R, Krämer J, Shah VP, Amidon GL, Dressman JB (2000) Dissolution testing as a prognostic tool for oral drug absorption: dissolution behavior of glibenclamide. Pharm Res 17: 439-44

[6] Aungst BJ (2000) Intestinal permeation enhancers. J Pharm Sci 89: 429-42

[7] Swenson EC, Curatolo WJ (1992) Intestinal permeability enhancement for proteins, peptides and other polar drugs: Mechanisms and potential toxicity. Adv Drug Del Rev 8: 39-92

[8] Terao T, Matsuda K, Shouji H (2001) Improvement in site-specific intestinal absorption of furosemide by Eudragit L100-55. J Pharm Pharmacol 53: 433-40

[9] Nozawa T, Toyobuku H, Kobayashi D, Kuruma K, Tsuji A, Tamai I (2003) Enhanced intestinal Absorption of drugs by activation of peptide transporter PEPT1 using proton releasing polymer. J Pharm Sci 92: 2208-2216

[10] Lindmark T, Kimura Y, Artursson P (1998) Absorption enhancement through intracellular regulation of tight junction permeability by medium chain fatty acids in Caco-2 cells. J Pharmacol Exp Ther 284: 362-369

[11] Sakai M, Imai T, Ohtake H, Azuma H, Otagiri M (1997) Effects of absorption enhancers on the transport of model compounds in Caco-2 cell monolayers: Assessment by confocal laser scanning microscopy. J Pharm Sci 86: 779-785

[12] Borchard G, Lueßen HL, De Boer AG, Verhoef JC, Lehr C-M, Junginger HE (1996) The potential of mucoadhesive polymers in enhancing intestinal peptide drug absorption. III: Effects of chito and carbomer on epithelial tight junctions in vitro. J Controlled Release 39: 131-138

[13] Ranaldi G, Marigliano I, Vespignani I, Perozzi G, Sambuy Y (2002) The effect of chitosan and other polycations on tight junction permeability in the human intestinal Caco-2 cell line. Journal of Nutritional Biochemistry 13: 157-167

[14] Thanou M, Verhoef JC, Junginger HE (2001) Oral drug absorption enhancement by chitosan and its derivatives. Adv Drug Del Rev 52: 117-126

[15] Wagner D, Spahn-Langguth H, Hanafy A, Koggel A, Langguth P (2001) Intestinal drug efflux: formulation and food effects. Adv Drug Del Rev 50 Suppl 1: S13-31Pflügers Archiv European Journal of Physiology

[16] Shen Q, Lin Y, Handa T, Doi M, Sugie M, Wakayama K, Okada N, Fujita T, Yamamoto A (2006) Modulation of intestinal P-glycoprotein function by polyethylene glycols and their derivatives by in vitro transport and in situ absorption studies. Int J Pharm 313: 49-56

[17] Collnot E-M, Baldes C, Wempe MF, Hyatt J, Navarro L, Edgar KJ, Schaefer UF, Lehr C-M (2006) Influence of vitamin E TPGS poly(ethylene glycol) chain length on apical efflux transporters in Caco-2 cell monolayers. J Controlled Release 111: 35-40

[18] Seeballuck F, Ashford MB, O'Driscoll CM (2003) The effects of Pluronic® block copolymers and Cremophor® EL on intestinal lipoprotein processing and the potential link with P-glycoprotein in Caco-2 cells. Pharm Res 20: 1085-1092

[19] Lo Y-L (2003) Relationships between the hydrophilic-lipophilic balance values of pharmaceutical excipients and their multidrug resistance modulating effect in Caco-2 cells and rat intestines. J Controlled Release 90: 37-48

[20] Shah P, Jogani V, Bagchi T, Misra A (2006) Role of Caco-2 cell monolayers in prediction of intestinal drug absorption. Biotechnol Prog 22: 186-198

[21] Nerurkar MM, Burton PS, Borchardt RT (1996) The use of surfactants to enhance the permeability of peptides through caco-2 cells by inhibition of an apically polarized efflux system. Pharm Res 13: 528-534

[22] Brouwers J, Tack J, Lammert F, Augustijns P (2006) Intraluminal drug and formulation behavior and integration in in vitro permeability estimation: A case study with amprenavir. J Pharm Sci 95: 372-383

[23] Ramsay-Olocco K, Alexandrova L, Nellore R, Killion R, Li L, Coen P, Ho Q, Jung D, Rocha C (2004) Pre-clinical and clinical evaluation of solution and soft gelatin capsule formulations for a BCS class 3 compound with atypical physicochemical properties. J Pharm Sci 93: 2214-2221

[24] Bogman K, Zysset Y, Degen L, Hopfgartner G, Gutmann H, Alsenz J, Drewe J (2005) P-glycoprotein and surfactants: Effect on intestinal talinolol absorption. Clin Pharmacol Ther 77: 24-32

[25] Lin JH, Yamazaki M (2003) Role of P-glycoprotein in pharmacokinetics: Clinical implications. Clin Pharmacokinet 42: 59-98

[26] Abrahamsson B, Albery T, Eriksson A, Gustafsson I, Sjöberg M (2004) Food effects on tablet disintegration. Eur J Pharm Sci 22: 165-172

[27] Wonnemann M, Schug B, Schmücker K, Brendel E, van Zwieten PA, Blume H (2006) Significant food interactions observed with a nifedipine modified-release formulation marketed in the European Union. Int J Clin Pharmacol Ther 44: 38-48

[28] Welling PG (1996) Effects of food on drug absorption. Annu Rev Nutr 16: 383-415

[29] Singh BN, Malhotra BK (2004) Effects of food on the clinical pharmacokinetics of anticancer agents: underlying mechanisms and implications for oral chemotherapy. Clin Pharmacokinet 43: 1127-56

[30] Persson EM, Gustafsson A-S, Carlsson AS, Nilsson RG, Knutson L, Forsell P, Hanisch G, Lennernäs H, Abrahamsson B (2005) The effects of food on the dissolution of poorly soluble drugs in human and in model small intestinal fluids. Pharm Res 22: 2141-2151

[31] Charman WN, Porter CJ, Mithani S, Dressman JB (1997) Physiochemical and physiological mechanisms for the effects of food on drug absorption: the role of lipids and pH. J Pharm Sci 86: 269-82

[32] Fleisher D, Li C, Zhou Y, Pao LH, Karim A (1999) Drug, meal and formulation interactions influencing drug absorption after oral administration. Clinical implications. Clin Pharmacokinet 36: 233-54

[33] Wu C-Y, Benet LZ (2005) Predicting Drug Disposition via Application of BCS: Transport/Absorption/Elimination Interplay and Development of a Biopharmaceutics Drug Disposition Classification System. Pharm Res 22: 11-23

[34] Ingels F, Oth M, Beck B, Augustijns P (2004) Effect of simulated intestinal fluid on drug permeability estimation across Caco-2 monolayers. Int J Pharm 274: 221-232

[35] Neuhoff S, Ungell AL, Zamora I, Artursson P (2003) pH-dependent bidirectional transport of weakly basic drugs across Caco-2 monolayers: implications for drug-drug interactions. Pharm Res 20: 1141-8

[36] Ingels FM, Augustijns PF (2003) Biological, pharmaceutical, and analytical considerations with respect to the transport media used in the absorption screening system, Caco-2. J Pharm Sci 92: 1545-58

[37] Ingels F, Deferme S, Destexhe E, Oth M, Van den Mooter G, Augustijns P (2002) Simulated intestinal fluid as transport medium in the Caco-2 cell culture model. Int J Pharm 232: 183-92

[38] Patel N, Forbes B, Eskola S, Murray J (2006) Use of simulated intestinal fluids with Caco-2 cells and rat ileum. Drug Dev Ind Pharm 32: 151-61

[39] Motz SA, Schaefer UF, Balbach S, Eichinger T, Lehr C-M (2007) Permeability assessment of solid oral drug formulations based on a Caco-2 monolayer in combination with a flow through dissolution cell. Eur J Pharm Biopharm doi:10.1016/j.ejpb.2006.10.015:

[40] Dibbern HW (1966) [On the resorption profile of drugs. 2. On studies with the resorption model]. Arzneimittelforschung 16: 1304-6

[41] Dibbern HW, Scholz GH (1969) [Resorption model experiments with artificial lipoid membranes. 3. Model experiments for gastroenteral resorption]. Arzneimittelforschung 19: 1140-5

[42] Koch HP (1980) The Resotest Apparatus. A universally applicable biopharmaceutical experimental tool. Methods Find Exp Clin Pharmacol 2: 97-102

[43] Dressman J, Krämer J (2005) Pharmaceutical Dissolution Testing. Taylor & Francis Group,

[44] Artursson P, Palm K, Luthman K (1996) Caco-2 monolayers in experimental and theoretical predictions of drug transport. Adv Drug Del Rev 22: 67-84

[45] Artursson P, Palm K, Luthman K (2001) Caco-2 monolayers in experimental and theoretical predictions of drug transport. Adv Drug Del Rev 46: 27-43

[46] Amidon GL, Lennernas H, Shah VP, Crison JR (1995) A theoretical basis for a biopharmaceutic drug classification: the correlation of in vitro drug product dissolution and in vivo bioavailability. Pharm Res 12: 413-420

[47] FDA (August 2000) Guidance for industry: Waiver of In Vivo Bioavailability and Bioequivalence Studies for Immediate-Release Solid Oral Dosage Forms Based on a Biopharmaceutics Classification System

[48] FDA (August 1997) Guidance for industry: Dissolution Testing of Immediate Release Solid Oral Dosage Forms

[49] Souliman S, Blanquet S, Beyssac E, Cardot J-M (2006) A level a in vitro/in vivo correlation in fasted and fed states using different methods: Applied to solid immediate release oral dosage form. Eur J Pharm Sci 27: 72-79

[50] Ginski MJ, Taneja R, Polli JE (1999) Prediction of dissolution-absorption relationships from a continuous dissolution/Caco-2 system. AAPS PharmSci 1: E3

[51] Polli JE, Crison JR, Amidon GL (1996) Novel approach to the analysis of in vitro-in vivo relationships. J Pharm Sci 85: 753-60

[52] Kobayashi M, Sada N, Sugawara M, Iseki K, Miyazaki K (2001) Development of a new system for prediction of drug absorption that takes into account drug dissolution and pH change in the gastro-intestinal tract. Int J Pharm 221: 87-94

[53] He X, Sugawara M, Kobayashi M, Takekuma Y, Miyazaki K (2003) An in vitro system for prediction of oral absorption of relatively water-soluble drugs and ester prodrugs. Int J Pharm 263: 35-44

[54] He X, Kadomura S, Takekuma Y, Sugawara M, Miyazaki K (2004) A new system for the prediction of drug absorption using a pH-controlled Caco-2 model: evaluation of pH-dependent soluble drug absorption and pH-related changes in absorption. J Pharm Sci 93: 71-77

[55] Sugawara M, Takekuma Y, Miyazaki K, Kadomura S, He X, Kohri N (2005) The use of an in vitro dissolution and absorption system to evaluate oral absorption of two weak bases in pH-independent controlled-release formulations. Eur J Pharm Sci 26: 1-8

[56] Kataoka M, Masaoka Y, Yamazaki Y, Sakane T, Sezaki H, Yamashita S (2003) In vitro system to evaluate oral absorption of poorly water-soluble drugs: simultaneous analysis on dissolution and permeation of drugs. Pharm Res 20: 1674-1680

[57] Kataoka M, Masaoka Y, Sakuma S, Yamashita S (2006) Effect of food intake on the oral absorption of poorly water-soluble drugs: in vitro assessment of drug dissolution and permeation assay system. J Pharm Sci 95: 2051-61

[58] (2004) USP. United States Pharmacopoeial Convention Inc., Rockville, USA,

[59] Vogelpoel H, Welink J, Amidon GL, Junginger HE, Midha KK, Moller H, Olling M, Shah VP, Barends DM (2004) Biowaiver monographs for immediate release solid oral dosage forms based on biopharmaceutics classification system (BCS) literature data: verapamil hydrochloride, propranolol hydrochloride, and atenolol. J Pharm Sci 93: 1945-1956

[60] Takamatsu N, Welage LS, Idkaidek NM, Liu D-Y, Lee PI-D, Hayashi Y, Rhie JK, Lennernas H, Barnett JL, Shah VP, Lesko L, Amidon GL (1997) Human Intestinal Permeability of Piroxicam, Propranolol, Phenylalanine, and PEG 400 Determined by Jejunal Perfusion. Pharm Res 14: 1127-1132

[61] Pade V, Stavchansky S (1998) Link between drug absorption solubility and permeability measurements in Caco-2 cells. J Pharm Sci 87: 1604-7

[62] Pade V, Stavchansky S (1997) Estimation of the relative contribution of the transcellular and paracellular pathway to the transport of passively absorbed drugs in the Caco-2 cell culture model. Pharm Res 14: 1210-5

[63] Takka S, Rajbhandari S, Sakr A (2001) Effect of anionic polymers on the release of propranolol hydrochloride from matrix tablets. Eur J Pharm Biopharm 52: 75-82

[64] Lindenberg M, Kopp S, Dressman JB (2004) Classification of orally administered drugs on the World Health Organization Model list of Essential Medicines according to the biopharmaceutics classification system. Eur J Pharm Biopharm 58: 265-278

[65] Dillard RL, Eastman H, Fordtran JS (1965) Volume-flow relationship during the transport of fluid through the human small intestine. Gastroenterology 49: 58,66

[66] Fordtran JS, Locklear TW (1966) Ionic constituents and osmolality of gastric and small-intestinal fluids after eating. Am J Dig Dis 11: 503-21

[67] Sunesen VH, Pedersen BL, Kristensen HG, Müllertz A (2005) In vivo in vitro correlations for a poorly soluble drug, danazol, using the flow-through dissolution method with biorelevant dissolution media. Eur J Pharm Sci 24: 305-313

[68] Karlsson J, Artursson P (1991) A method for the determination of cellular permeability coefficients and aqueous boundary layer thickness in monolayers of intestinal epithelial (Caco-2) cells grown in permeable filter chambers. Int J Pharm 71: 55-64

[69] Duizer E, Penninks AH, Stenhuis WH, Groten JP (1997) Comparison of permeability characteristics of the human colonic Caco-2 and rat small intestinal IEC-18 cell lines. J Controlled Release 49: 39-49

[70] Imai T, Sakai M, Ohtake H, Azuma H, Otagiri M (1999) In vitro and in vivo evaluation of the enhancing activity of glycyrrhizin on the intestinal absorption of drugs. Pharm Res 16: 80-86

[71] Yu LX, Amidon GL, Crison JR (1996) Compartmental transit and dispersion model analysis of small intestinal transit flow in humans. Int J Pharm 140: 111-118

[72] Peterson MD, Mooseker MS (1993) An in vitro model for the analysis of intestinal brush border assembly. I. Ultrastructural analysis of cell contact-induced brush border assembly in Caco-2(BBe) cells. J Cell Sci 105: 445-460

[73] Costa P, Sousa Lobo JM (2001) Modeling and comparison of dissolution profiles. Eur J Pharm Sci 13: 123-33

[74] Higuchi T (1961) Rate of release of medicaments from ointment bases containing drugs in suspension. J Pharm Sci 50: 874-5

[75] Motz SA, Klimundová J, Schaefer UF, Balbach S, Eichinger T, Solich P, Lehr C-M (2007) Automated measurement of permeation and dissolution of propranolol HCl tablets using sequential injection analysis. Anal Chim Acta 581: 174-180

[76] Ginski MJ, Polli JE (1999) Prediction of dissolution-absorption relationships from a dissolution/Caco-2 system. Int J Pharm 177: 117-125

[77] Ruzicka J, Hansen EH (1975) Flow injection analyses. Part I. A new concept of fast continuous flow analysis. Anal Chim Acta 78: 145-157

[78] Lenehan CE, Barnett NW, Lewis SW (2002) Sequential injection analysis. Analyst 127: 997-1020

[79] Solich P, Polásek M, Klimundová J, Ruzicka J (2004) Sequential injection technique applied to pharmaceutical analysis. TrAC - Trends in Analytical Chemistry 23: 116-126

[80] Pimenta AM, Montenegro MCBSM, Araújo AN, Calatayud JM (2006) Application of sequential injection analysis to pharmaceutical analysis. Journal of Pharmaceutical and Biomedical Analysis 40: 16-34

[81] Economou A (2005) Sequential-injection analysis (SIA): A useful tool for on-line sample-handling and pre-treatment. TrAC - Trends in Analytical Chemistry 24: 416-425

[82] Legnerová Z, Huclová J, Thun R, Solich P (2004) Sensitive fluorimetric method based on sequential injection analysis technique used for dissolution studies and quality control of prazosin hydrochloride in tablets. Journal of Pharmaceutical and Biomedical Analysis 34: 115-121

[83] Legnerová Z, Sklenárová H, Solich P (2002) Automated sequential injection fluorimetric determination and dissolution studies of Ergotamine Tartrate in pharmaceuticals. Talanta 58: 1151-1155

[84] Pinto PCAG, Saraiva MLMFS, Santos JLM, Lima JLFC (2006) Fluorimetric determination of aminocaproic acid in pharmaceutical formulations using a sequential injection analysis system. Talanta 68: 857-862

[85] Liu X-Z, Fang Z-L (1998) Sequential-injection system for drug-dissolution studies of ibuprofen tablets and sustained-release formulations. Anal Chim Acta 358: 103-110

[86] Liu X-Z, Fang Z-L, Liu S-S, Wu J-F (1999) Simultaneous monitoring of aspirin, phenacetin and caffeine in compound aspirin tablets using a sequential injection drug-dissolution testing system with partial least squares calibration. Anal Chim Acta 392: 273-281

[87] Pasamontes A, Callao MP (2006) Sequential injection analysis for the simultaneous determination of clavulanic acid and amoxicillin in pharmaceuticals using second-order calibration. Anal Sci 22: 131-135

[88] Ponto LL, Schoenwald RD (1990) Furosemide (frusemide). A pharmacokinetic/ pharmacodynamic review (Part I). Clin Pharmacokinet 18: 381-408

[89] Rege BD, Yu LX, Hussain AS, Polli JE (2001) Effect of common excipients on Caco-2 transport of low-permeability drugs. J Pharm Sci 90: 1776-86

[90] Hilgendorf C, Spahn-Langguth H, Regardh CG, Lipka E, Amidon GL, Langguth P (2000) Caco-2 versus Caco-2/HT29-MTX co-cultured cell lines: permeabilities via diffusion, inside- and outside-directed carrier-mediated transport. J Pharm Sci 89: 63-75

[91] Ponto LL, Schoenwald RD (1990) Furosemide (frusemide). A pharmacokinetic/ pharmacodynamic review (Part II). Clin Pharmacokinet 18: 460-71

[92] Hammarlund MM, Paalzow LK, Odlind B (1984) Pharmacokinetics of furosemide in man after intravenous and oral administration. Application of moment analysis. Eur J Clin Pharmacol 26: 197-207